IONIC COMPOSITION OF PRECIPITATION IN MARMARIS STATION

A THESIS SUBMITTED TO
THE GRADUATE SCHOOL OF NATURAL AND APPLIED SCIENCES
OF
MIDDLE EAST TECHNICAL UNIVERSITY

BY

GİZEM YÜCEL

IN PARTIAL FULLFILLMENT OF THE REQUIREMENTS
FOR
THE DEGREE OF MASTER OF SCIENCE
IN
ENVIRONMENTAL ENGINEERING

MAY 2019

Approval of the thesis:

IONIC COMPOSITION OF PRECIPITATION IN MARMARIS STATION

submitted by **GİZEM YÜCEL** in partial fulfillment of the requirements for the degree of **Master of Science in Environmental Engineering Department, Middle East Technical University** by,

Prof. Dr. Halil Kalıpçılar
Dean, Graduate School of **Natural and Applied Sciences** _____

Prof. Dr. Bülent İçgen
Head of Department, **Environmental Eng.** _____

Prof. Dr. Gürdal Tuncel
Supervisor, **Environmental Eng., METU** _____

Examining Committee Members:

Prof. Dr. İpek İmamoğlu
Environmental Engineering, METU _____

Prof. Dr. Gürdal Tuncel
Environmental Engineering, METU _____

Assoc. Prof. Dr. Tuba Hande Ergüder Bayramoğlu
Environmental Engineering, METU _____

Assist. Prof. Dr. Zöhre Kurt
Environmental Engineering, METU _____

Assist. Prof. Dr. Ebru Koçak
Environmental Engineering, Aksaray University _____

Date: 08.05.2019

I hereby declare that all information in this document has been obtained and presented in accordance with academic rules and ethical conduct. I also declare that, as required by these rules and conduct, I have fully cited and referenced all material and results that are not original to this work.

Name, Surname: Gizem Yücel

Signature:

ABSTRACT

IONIC COMPOSITION OF PRECIPITATION IN MARMARIS STATION

Yücel, Gizem
Master of Science, Environmental Engineering
Supervisor: Prof. Dr. Gürdal Tuncel

May, 2019, 124 pages

In this study, wet-only rain samples were collected at a high-altitude rural site, by General Directorate of Meteorology, between July 2011 and November 2016. The sampling station was located at Marmaris Meteorological Radar, which has an altitude of 1000 m from sea level and located 15 km to the North of Marmaris. Collected samples were analyzed for major ions (SO_4^{2-}, NO_3^-, NH_4^+, H^+, Ca^{2+}, Mg^{2+}, K^+ and Na^+) by ion chromatography. Approximately 300 samples were collected and analyzed during study period. Residence time calculations showed that the station is under the influence of emissions at western Turkey and Balkan countries. Average pH of rainwater is 6.0 indicating extensive neutralization, which can be attributed to $CaCO_3$, which is an abundant component in alkaline soil on the Mediterranean coast of Turkey. Neutralization of rainwater acidity is almost complete during summer period and decreases in winter, owing to limited resuspension of soil in winter. Trajectories of the station are grouped into 5 clusters, residence time analysis of trajectory segments with altitudes less than 500 m indicated that western parts of Turkey, Balkan countries, Ukraine and the Black Sea coast of Russia are potential source regions affecting composition of rainwater at Eastern Mediterranean. Most of the ions measured in this work have higher concentrations during summer season. The positive matrix factorization model revealed four factors, which were identified as two anthropogenic, one marine and one crustal factors. Potential source regions for the anthropogenic

components in rainwater were identified as to be western Ukraine, Western Black Sea coast of the Turkey, Balkan Countries, North Africa and Georgia.

Keywords: Eastern Mediterranean, Wet Deposition, Rainwater Composition, Acid Rain, Back Trajectory

ÖZ

MARMARIS İSTASYONUNDA YAĞIŞIN İYONİK KOMPOZİSYONU

Yücel, Gizem
Yüksek Lisans, Çevre Mühendisliği
Tez Danışmanı: Prof. Dr. Gürdal Tuncel

Mayıs, 2019, 124 sayfa

Yağmur suyunun kimyasal bileşimi bir bölgeden diğerine kirletici taşınımının önemli bir göstergesidir. Kıyı alanlarında daha da önemlidir, çünkü ıslak kirleticilerin birikmesi deniz ortamında önemli bir kirlilik kaynağı olabilir. Bu çalışmada, Temmuz 2011 - Kasım 2016 tarihleri arasında Meteoroloji Genel Müdürlüğü tarafından yüksek rakımlı bir kırsal alanda yağmur örnekleri toplanmıştır. Örnekleme istasyonu, Marmaris Meteoroloji Radarı'na 1000 m. deniz seviyesi ve Marmaris'in 15 km kuzeyine bulunmaktadır. Toplanan örnekler, iyon kromatografisi ile ana iyonlar (SO_4^{2-}, NO_3^-, NH_4^+, H^+, Ca^{2+}, Mg^{2+}, K^+ ve Na^+) için analiz edildi. Çalışma süresi boyunca yaklaşık 300 örnek toplanmış ve analiz edilmiştir. Kalma süresi hesaplamaları, istasyonun batı Türkiye ve Balkan ülkelerindeki emisyonların etkisinde olduğunu gösterdi. Ortalama yağış suyu pH'ı, Türkiye'nin Akdeniz kıyılarındaki alkali topraklarda bol miktarda bulunan $CaCO_3$'a atfedilebilecek olan, geniş nötrleşme olduğunu gösteren 6.0'dır. Yağmur suyunun asitliğinin nötralizasyonu yaz döneminde neredeyse tamamlanmakta ve kışın toprağın yeniden süspansiyon haline gelmesi nedeniyle kışın azalmaktadır. İstasyonun yörüngeleri 5 kümeye ayrılır, 500 m'den daha düşük rakımlı yörünge bölümlerinin oturma süresi analizi, Türkiye'nin batı bölgelerinin, Balkan ülkelerinin, Ukrayna'nın ve Rusya'nın Karadeniz kıyılarının, Doğu Akdeniz'de yağmur suyunun bileşimini etkileyen potansiyel kaynak bölgeler olduğunu göstermiştir. Bu çalışmada ölçülen iyonların çoğu yaz mevsiminde daha

yüksek konsantrasyonlara sahiptir. Pozitif matris faktoring modeli, iki antropojenik, bir deniz ve bir kabuksal faktör olarak tanımlanan dört faktör ortaya koydu. Yağmur suyundaki antropojenik bileşenlerin potansiyel kaynak bölgelerinin batı Ukrayna, Türkiye'nin Batı Karadeniz kıyıları, Balkan Ülkeleri, Kuzey Afrika ve Gürcistan olduğu tespit edildi.

Anahtar Kelimeler: Doğu Akdeniz, Yaş Çökelme, Yağmur Suyu Kompozisyonu, Asit Yağmuru, Geri Yörünge

“There's a point, around age twenty, when you have to choose whether to be like everybody else the rest of your life, or to make a virtue of your peculiarities. Those who build walls are their own prisoners. I'm going to go fulfil my proper function in the social organism. I'm going to go unbuild walls.”

— Ursula K. Le Guin

ACKNOWLEDGEMENTS

I would like to express my gratitude to my supervisor Prof. Dr. Gürdal Tuncel for his advice, guidance and insight throughout the research. I would also like to thank Ali İhsan İlhan, Tülay Balta and Yalçın Ün from the General Directorate of Meteorology for providing us the rainwater data without which this work will not be possible.

I would like to thank my committee members Prof. Dr. İpek İmamoğlu, Assoc. Prof. Dr. Tuba Hande Ergüder Bayramoğlu, Assist. Prof. Dr. Zöhre Kurt, Assist. Prof. Dr. Ebru Koçak for their contributions.

I would like to especially thank Dr. İlker Balcılar for teaching me about the modeling programs that I am supposed to use and guiding in the times when I needed. I also would like to thank old and current members of our Air Pollution and Quality Research Group Elif Sena Uzunpınar and Pınar Tuncer for their supports.

I also would like to thank my dear friends Elif Begüm Gökerküçük, Selin Özkul, Hazal Aksu Bahçeci, Nazlı Barçın Doğan, Melike Kiraz, Ceren Ayyıldız for their endless support and friendship.

Finally, I would like to express my deepest gratitude and love to my father, mother and sister for their unconditional love and everything that they have done for me throughout my life.

I gratefully acknowledge the financial support provided by The Scientific and Technological Research Council of Turkey (TÜBİTAK) under project grant no: 115Y252.

TABLE OF CONTENTS

LIST OF TABLES

TABLES

LIST OF FIGURES

FIGURES

LIST OF ABBREVIATIONS

ABBREVIATIONS

BDL	Below Detection Limit
CMB	Chemical Mass Balance
DL	Detection Limit
EMEP	European Monitoring and Evaluation Programme
EPA	Environmental Protection Agency
FA	Factor Analysis
FC	Flow Climatology
GIS	Geographical Information Systems
HYSPLIT	Hybrid Single Particle Lagrangian Integrated Trajectory
IC	Ion Chromatography
MGM	General Directorate of Meteorology
NOAA	National Oceanic and Atmospheric Administration
PCA	Principle Componen Analysis
PMF	Positive Matrix Factorization
PSCF	Potential Source Contribution Function
QA/QC	Quality Assurance/Quality Control
TRMSD	Total Root Mean Square Deviation
VWA	Volume Weighted Average

CHAPTER 1

INTRODUCTION

Acid deposition considered as one of the primary environmental concerns since in several regions large number of lakes were detected to be acidic and adverse effects on forests and aquatic environments were started to be a concern; in a number of conditions acid deposition can be harmful on human health (Watmoug, et al., 2016).

Acid rain, which can be identified as the precipitation with pH value under 5, is mainly caused by anthropogenic activities such as combustion (fossil fuel and biomass) where considerable amounts of SO_2 and NO_x is present. In atmosphere, SO_2 is going into reaction and gives the product of sulfuric acid (H_2SO_4) and from the reaction of NO_x and oxygen produces inorganic and organic nitrates. Due to their solubility these products dissolve in the water droplets in the atmosphere and may form acid rain (Liang, 2013).

By investigating the ionic composition of precipitation, possible sources for the pollutants and potential source areas can be identified. And by determining source locations it will be easier to recommend the solutions in order to decrease the pollution amount.

1.1. Aim of the Study

In this study, measurements of rainwater composition in the Marmaris Station of General Directorate of Meteorology, in the Mediterranean Region of Turkey, are used. The objectives of this study can be listed as:

- To analyze major ion composition in the rainwater at the West Mediterranean Part of the Turkey.
- To investigate the acidity and the neutralization of the rainwater in the study area.

- To determine the temporal variations of the measured ions.
- To study the flow climatology of the region.
- To determine the types of sources that are affecting the ion concentration in the region.
- To determine the source regions of the pollutants by using back trajectory statistics.

CHAPTER 2

LITERATURE REVIEW

2.1. Atmospheric Removal Mechanisms

Pollutants present in the atmosphere eventually removed by several methods such as dry deposition, wet deposition, sedimentation or reaction, apart from the fine particulate matter, which can stay in the atmosphere remaining airborne for a long time period (Vallero, 2008).

Process that transfers trace chemicals, which are present in the atmosphere, to the surface of the Earth via movement of air is called dry deposition (Toyota, et al. 2016; Wesely & Hicks, 2000). Dry deposition is dependent on the particle size, density, terrain, vegetation, meteorological conditions and chemical species (Giardina & Buffa, 2018).

Wet deposition process can be defined as the transfer of the airborne species to the surface of the Earth in aqueous form (Seinfeld & Pandis, 1997). Wet deposition is divided into two different processes: rainout and washout. Rainout is the process when the gas molecule or the particle is removed via incorporation inside cloud droplets which later transform to raindrops. Washout is the removal of pollutant by the raindrops which are precipitating to the surface (Colls, 2002)

2.2. Acid Deposition

Acid deposition, which is defined as the precipitation with pH value below 5, generally occurs as acid rain but may also refer to snow or fog. In recent years, unpolluted precipitation has a pH value of 5.6, which is caused by the CO_2 concentration in the atmosphere (Jacob, 1999).

Drop in the pH of precipitation is caused generally by oxidation of sulphur and nitrogen, coming from anthropogenic sources such as domestic and industrial combustion of sulphur dioxide, SO_2, and nitrogen oxides, NO_x. These chemicals later form H_2SO_4 and HNO_3 in the atmosphere (Chmielewski, 2011).

Acid rain is considered as an environmental pollution, which affects human health, harms forestry, causes corrosion on metal structures and monuments and results in acidification of aquatic and terrestrial ecosystems (Al-Khashman, 2005; Al-Momani, et al., 1995).

2.2.1. Chemical Composition of Acid Precipitation

Pure water has pH value of 7, yet unpolluted rainwater has a pH of 5.6, which is acidic. This acidity of the rainwater is caused by presence of substances such as CO_2, NO and SO_2 in the troposphere, which are considered as acid precursors (Casiday & Frey, 1998; Bricker & Rice, 1993).

The reaction pure water goes through is as follows (Jacob, 1999):

$$H_2O \leftrightarrow H^+ + OH^- \quad (2.1)$$

The reactions carbon dioxide, which is the highest in concentration in the above three substance, go through is shown in the following equations (Casiday & Frey, 1998):

$$CO_2 + H_2O \leftrightarrow H_2CO_3 \quad (2.2)$$

$$H_2CO_3 \leftrightarrow H^+ + HCO_3^- \quad (2.3)$$

The decrease in the pH of rainwater is mainly caused by the nitric oxide and sulfur dioxide. These oxides are mainly the end product of combustion processes and the reactions of sulfuric acid, which is the source of the most of the acidity of rainwater, are as follows (Casiday & Frey, 1998; Hartley, Jr, 1973):

$$SO_{2(aq)} + \frac{1}{2}O_{2(aq)} + H_2O_{(l)} \leftrightarrow H_2SO_{4(aq)} \quad (2.4)$$

$$H_2SO_4 \rightarrow HSO_4^- + H^+ \quad (2.5)$$

$$HSO_4^- \rightarrow SO_4^{2-} + H^+ \quad (2.6)$$

The acidity of the precipitation can also be neutralized by the basic components present in the atmosphere such as ammonia, NH_3, or calcium carbonate, $CaCO_3$. Reactions of these components are (Jacob, 1999):

$$NH_3 + H^+ \leftrightarrow NH_4^+ \quad (2.7)$$

$$CaCO_3 + H^+ \rightarrow Ca^{2+} + HCO_3^- \quad (2.8)$$

Chemical composition of the rainwater is both influenced by acids and the neutralizers existing in the atmosphere which will be discussed in detail in following sections.

2.2.1.1.Principle Precursors of Acidification

The main source for emission of sulfur dioxide is the combustion of fossil fuel, primarily coal and oil. Also metal smelting and pulp and paper processing are considered as important sources for sulfur (Bricker & Rice, 1993; Smith, et al., 2011). Natural processes that release sulfur compounds to the atmosphere are volcanic emissions, forest fires and biogenic sources (Bricker & Rice, 1993). Also, over the oceans, considerable amounts of sulfur is being emitted as a consequence of sea spray (Committee on Public Works, 1975).

The sum nitrogen dioxide and nitrogen oxide is called nitrogen oxides, NO_x, which is another precursor for acid rain additionally causes other environmental problems such as smog and eutrophication. Nitrogen oxides are again similar to the sulfur: exhaust emissions from vehicles (cars, trucks and planes), application of agricultural fertilizer to the soil; lightning and decomposition of animal wastes and wildfires (Lu, et al., 2015; Bricker & Rice, 1993).

These sulfur and nitrogen compounds can be transported tens to thousands of kilometers from their sources, before they can reach back to the earth as acid deposition. Throughout their transportation, these compounds interact with water vapor, be oxidized and generate sulfuric acid and nitric acid, sulfate aerosols and particulate sulfate. Since the NO_x is generally emitted from the sources closer to the

ground with respect to SO_2, it is generally oxidized faster than the SO_2, which results as deposition of NO_x is mostly closer to its source (Bricker & Rice, 1993).

2.2.1.2.Principle Precursors of Neutralization

The acid-base status of the precipitation is a result of balance between acidifying compounds and alkaline compounds, where acidifying compounds are generally sulfur and nitrogen; alkaline compounds are ammonia and alkaline matter in the windblown soil dust (Rodhe, et al., 2002).

Ca^{2+} is the main element that is involved with the neutralization of acidic components (Sicard, et al., 2007). Also other cations such as Mg^{2+}, K^+ and Na^+ play important role on the chemical processes of acid deposition, because both the acidic and basic content affects the acidity of the materials (van Leeuwen, et al., 1996).

Neutralization of acidity via $CaCO_3$, calcium carbonate, which is present in the airborne dust, is a common precursor, especially in the western part of Mediterranean region due to soil properties in the area and transportation of Saharan dust, which is also rich in terms of $CaCO_3$ (Al-Khashman, 2005).

2.2.2. Studies of Acid Precipitation

Composition of precipitation is an important area of study, since the chemicals present in the precipitation is an indicator of air pollution of the area and especially acidity of the precipitation negatively affects not only human health but also damages environmental ecosystems (Vazquez, et al., 2003). Also, in order to observe the buffering effect, neutralization of the acidity in area of interest is a significant process. Furthermore, studies on precipitation chemistry helps decision makers in the process of policy implementations in order to reduce emissions.

2.2.2.1.Studies of Chemical Precipitation

On a global scale study made in 2014, 3 year averages of precipitation between 2000-2002 and 2005-2007 are measured and the results obtained gave the information of global patterns of pH are generally showed parallel trend to SO_2 and NO_x emissions.

North America, Europe, East Asia and central Africa showed the lowest pH values and highest acidity. Areas that had low SO_2 and NO_x emissions and relatively acidic precipitation due to long range transport of S and N compounds are parts of northeast Canada and northern Scandinavia, where the transport of high emissions are believed to be coming from the south. Northern Mediterranean, central Africa and south Asia are the regions that show high pH values with low SO_2 and NO_x emissions and high dust emissions (Vet, et al., 2014).

For Europe, a study shows that, non-marine sulphate concentrations in wet deposition are highest in eastern and central Europe, border between Germany-Poland-Czech Republic, also known as the Black Triangle, Ukraine and former Yugoslavia. These large concentrations are told to be caused by SO_2 emissions from industries and power stations, where fossil fuel burning occurs. Also raise in nitrate concentrations are due to NO_x emissions from motor vehicle exhausts and again from industries and power stations where burning processes are present (van Leeuwen, et al., 1996). As it comes to base cations in Europe, a separation can be made as marine origin elements and others (that mainly originate from calcareous soils, agricultural practices, and Saharan dust). Marine originated elements (sodium, chloride and some extent magnesium) showed a pattern that as distances from the sea increase elemental concentrations decrease. Other base cations (potassium and calcium), showed little spatial variation throughout the Europe continent (van Leeuwen, et al., 1996)

In a more recent study, in which the pH and some chemicals in wet deposition are compared in 7 different locations in Europe, it was found that lowest pH is observed in Poland and Greece whereas the highest SO_4^{2-} concentrations are measured in Romania (Arsene, 2007).

The eastern Mediterranean region is an important area in terms of precipitation chemistry since the neutralization of acidity is commonly occurring in the area due to airborne $CaCO_3$ particles present in the soil (Al-Momani, et al., 1998). In a study conducted in Athens, Greece, neutralization of acids in the rainwater is determined to be the main process occurring in the rain, where the neutralization is originating

mainly from the ammonia that is coming from the fertilizers, marine water and dust rising from the ground and the dust containing calcium carbonate is not only carried from the urban area but also transported by the global atmospheric events (Nastos, et al.,2007). Similar studies on rainwater that performed on West Bank, Jordan and Turkey in areas close Mediterranean coasts showed the similarities on acidity of the precipitation and neutralization patterns. In these studies of eastern Mediterranean common conclusion is that the Saharan dust transported from North Africa is one of the main reasons of acid neutralization of rainwater (Al-Khashman, 2005; Özsoy, et al., 2008; Ghanem, et al. 2010).

Furthermore, for the studies made for Asia, a study sampled in North-Western Himalayan Region of India, where volume average pH value was obtained higher than 5.6 (unpolluted rainwater pH), alkalinity of the precipitation was determined to be caused mostly by Ca^{2+} and NH_4^+ and acidic compounds were specified to be transported from power plants and other man made activities via wind (Tiwari, et al. 2012). In south China, one of the regions in the world which suffers from acid rain problem, where rainwater pH reached the lowest value 3.6 in urban areas, a 5-year study was conducted. After measurements, SO_4^{2-} was found to be the most abundant ion in the rainwater samples, which is the end-product of the coal burning, which is stated as the primary energy source of the China. Sulphate is followed by Ca^{2+} and NH_4^+ which indicates that the mineral particles such as $CaCO_3$, $CaCO_3.MgCO_3$ and $CaSO_4.2H_2O$ which derived from the crust and the gaseous ammonia released from the fertilizers, biomass burning and livestock breeding were all critical component in terms of neutralizing in the sampling area atmosphere (Huang, et al., 2010).

2.3. Source Apportionment

For the management of air quality, determination of the sources of the pollution materials, quantifications of the emission rates of the pollutants identification of the transportation of the substances and the physical and chemical processes that substances go through during transportation is essential (Hopke, 2009). Source

apportionment is a method for identifying the air pollution sources and the quantification of their contribution to the pollution levels that has been measured. This can be accomplished by different approaches such as emission inventories, source-oriented models and receptor oriented models (Belis, et al., 2014).

2.3.1. Source Oriented Models

The source-oriented air quality models relies mainly on predicting the meteorological properties of air pollution or air pollution concentrations using mathematical descriptions of influential physical and chemical processes (Pitchford, et al., 2004). Source-oriented models are confirmed with the help of comparison with the predicted and measured spatial and temporal distribution of the pollutant concentrations (Schauer, et al., 1996).

2.3.2. Receptor Oriented Models

Receptor-oriented models function by apportion measured mass of an atmospheric pollutant at a given site to its emission sources by solving mass balance equation. This models generally used for estimating the source contribution at local and regional levels. Some examples for receptor models can be listed as: Positive Matrix Factorization (PMF), Potential Source Contribution Function (PSCF), UNIMIX and Chemical Mass Balance (CMB) (Hopke, 2009; Belis, et al., 2014; Karagulian, et al., 2015).

Receptor models gives advantage on procuring the information that had been derived from real-world measurements, which also means that a data set is required for the model. This data set is used for determination of large number of chemical species, for instance elemental concentrations of the samples, which is assumed to be result of the summation of the mass contributions of a number of independent sources or source types (Hopke, 2009; Karagulian, et al., 2015).

The general mass balance equation used for receptor models for a specie *m* in the *n* samples as contributions from *p*-independent sources is as follows (Hopke, 2009):

$$x_{ij} = \sum_{p=1}^{p} g_{ip} f_{pj} + e_{ij} \qquad (2.9)$$

Where x_{ij} is the measured concentration of the *j*th specie in the *i*th sample, f_{pj} is the concentration of the *j*th specie in the material emitted by source *p*, g_{ip} is the contribution of the *p*th source to the *i*th sample and e_{ij} is the portion measurement that cannot fit to the model (Hopke, 2009).

For this study, both PSCF and PMF models has been used in order to determine sources of the measured pollutants.

2.3.2.1.Trajectory Statistics

Trajectory can be simply defined as the path that air parcels take until it reaches to the receptor site. Trajectory models are used for numerous purposes in meteorology to environmental sciences; such as identifying the pathways of water vapors, determining the transportation of desert dust and appointing the source-receptor relationships for pollutants in the atmosphere (Stohl, 1998). For the determination of pollution sources, calculated back trajectories of air parcels are combined with measured pollutant concentrations, which give information on the source regions of the pollutants.

The recent trajectory models, that has been developed, takes into account winds, which have been observed, as horizontal component. As for vertical component calculations, air parcels one of the isobaric, isentropic or kinematic properties are used; in which constant surface pressure, constant temperature potential or movement with vertical velocity wind fields are assumed respectively (Işıkdemir, 2006).

Two back-trajectory based calculations, trajectory statistics methods, flow climatology and potential source contribution function are used in this study to estimate and compare the regions contributing to the pollutants.

2.3.2.2.Potential Source Contribution Function

Potential Source Contribution Function (PSCF) is a model used for estimating the probability of contribution of a given region to the pollutant concentration of a receptor site (Petroselli, et al., 2018). PSCF receptor model is mostly used with trajectory ensemble methods. Back trajectories of an air parcel which is ending at the receptor site are used for representing segment endpoints. These endpoints have both latitude and longitude which is the representative of the central location of the air parcel for the specific time. Geographic region, which is covered with the back trajectories, should be covered by the grid cells completely for the calculation of the PSCF (Hopke, 2009).

Let the cell indices of the grid locations are defined as *i* and *j*, *N* is defined as the total number of endpoints of the trajectory segments during the study period *T*, *n* is the endpoints of the trajectory segments that are located in the *ij*th cell (shown as n_{ij}), the probability of the event is defined as *A* and $P[A_{ij}]$ is the measurement of the residence time of a randomly selected air parcel in the *ij*th cell in the time period *T*, formula giving $P[A_{ij}]$ is as follows (Hopke, 2009):

$$P\left[A_{ij}\right] = \frac{n_{ij}}{N} \qquad (2.10)$$

Also for the same *ij*th cell, a subset m_{ij} is defined which corresponds to trajectories passing from the segment and reaching to the receptor site with concentration values higher than a specified value. The probability of this high concentration event, which is defined as B_{ij}, is given by the following formula of $P[B_{ij}]$ (Hopke, 2009):

$$P\left[B_{ij}\right] = \frac{m_{ij}}{N} \qquad (2.11)$$

Like $P[A_{ij}]$ this subset probability is related to the residence time of air parcel in the *ij*th cell but the probability *B* is for the contaminated air parcels. The PSCF is formulized as follows:

$$P_{ij} = \frac{P\left[B_{ij}\right]}{P\left[A_{ij}\right]} = \frac{m_{ij}}{n_{ij}} \qquad (2.12)$$

P_{ij} is the conditional probability of the *ij*th cell, which air parcel with high concentration passed through before arriving to the receptor point. Despite the endpoints of the trajectory segments are matter to uncertainty, which can be ensured to be accurate by adequate number of endpoints of the source locations, only if the location errors are not systematic but random. Cells that are containing emission sources can be defined with conditional probabilities close to one, if the trajectories passing through these cells, are transporting the emitted pollutants to the receptor site effectively. Hereby, the PSCF model procures geographic areas as potential of the sources. The model does not provide the distribution of the sources for the measured data from the receptor site (Hopke, 2009).

2.3.2.3.Positive Matrix Factorization

Positive Matrix Factorization is a multivariate factor analysis tool that distributes a matrix of speciated sample data into two matrices as factor contributions and factor profiles, which has been firstly developed by Paatero and Tapper in 1994. The obtained factor profiles are needed to be interpreted by the user, using the measured source profile information and emissions/discharge inventories, in order to identify the source type which is contributing to the sample (Norris, et al. 2014).

PMF takes into consideration both sample concentration and uncertainty that has been provided by the user associated with the sample data to weight individual points; this raises the confidence of the measurements. Data below the detection limit can be retained from the model and with the adjusted uncertainty data points below the detection limit have less effect on the result than the ones above the detection limit (Norris, et al. 2014).

PMF uses weighted least-squares fit with the known estimates of the elements of the data matrix used to derive the weights. Quantitative non-negative solutions that is derived from PMF can be written as:

$$X = GF + E \qquad (2.13)$$

In this equation, *X* is the matrix of the measured chemical species. *G* (Factor Contributions) and *F* (Factor Profiles) are the factor matrices that is aimed to be determined. *E* is defined as a residual matrix. In PMF, known standard deviations for each value of *X* are used to determine the matrix *E* (Rose, 2006).

At the beginning of the analysis the elements of the *E* which is defined as residual matrix is defined as (Hopke, 2000):

$$e_{ij} = x_{ij} - \sum_{k=1}^{p} f_{ik} * g_{kj} \qquad (2.14)$$

Where, i is number of samples,j is chemical specie measured and k is the source

An object function *Q*, which is minimized as a function of matrices *G* and *F* can be formulized as (Hopke, 2000):

$$Q(E) = \sum_{i=1}^{m} \sum_{j=1}^{n} \left[\frac{e_{ij}}{s_{ij}}\right]^2 \qquad (2.15)$$

Where s_{ij} is an estimate of uncertainty in the ith variable measured in the jth sample. The factor analysis problem become minimizing the Q(E) with respect to matrices G and F with the limitation of G and F elements should be non-negative (Hopke, 2000). The problem is used to be solved iteratively using alternating least squares at first. In alternating least-squares, one of the matrices, G or F, is taken as known and the chi-squared (test that is used for comparing the observed data with obtained data) is minimized with respect to the other matrix as a weighted linear-least-squares problem. Then the roles of G and F are reversed so that the matrix that has just been calculated is fixed and the other is calculated by minimizing Q. The process then continues until convergence (Hopke, 2000; Fisher & Yates, 1963).

PMF can be applied to wide range of data, including particulate matter, size-resolved aerosols, deposition, air toxics, high time resolution measurements and volatile organic carbons (Norris, et al. 2014). Some of the studies are: Lee et al. measured trace metals in Hong Kong between 1992 and 1994, source profiles obtained with

PMF; Lestari et al. used PMF to determine the sources on several trace metals and some ions such as NO_3^-, SO_4^{2-} and NH_4^+ for both dry and wet seasons where data obtained is 6-year long and measured in an urban site in Indonesia; Emami et al. used PMF for analyzing the particulate matter data measured between 2008 and 2010 in Rochester, New York; Lu et al. combined PMF method with molecular marker chemical mass balance (MM-CMB) for a source apportionment study that has been conducted in early 2010 in Wuhan, China to obtain the sources of the organic carbon and particulates with aerodynamic diameter of 2.5 μm or less ($PM_{2.5}$) (Lee, et al, 1999, Lestari & Mauliadi, 2009, Emami & Hopke, 2007; Lu, et al., 2018).

2.4. Geography and Climatology of Study Area

The Mediterranean Sea is located between three big land masses which are Europe, Africa and Asia, excluding Black Sea its surface area is 2.5 million km^2. The Strait of Gibraltar is the barrier between Atlantic Ocean. The Mediterranean Sea is considered as tha larges inland sea in the world (Lionello, 2012; Blondel, et al.2010). Some of the countries that have boundaty to the Mediterranean Sea are France, Spain, Italy, Tunusia, Libya, Syria and Turkey (Bottenberg, et al., 2006).

Mediterranean Climate is defined as soft winters and warm to hot summers. The land-sea pattern of the Mediterranean is specified by islands, peninsulas and several regional seas. These characteristics results as circulations on both sea and atmosphere, which determine large spatial variability and availability of several subregional and mesoscale attributes. Atmospheric circulation occurring is mostly influenced by the topography, which plays an important role in terms of directing the air flow (Lionello, et al., 2006)

Atmosphere of the Eastern Mediterranean is determined to be under the influence of the following types of sources: anthropogenic sources located in the north and northwest of the area; strong crustal sources from North Africa and the marine source of the Mediterranean Sea (Işıkdemir, 2006).

CHAPTER 3

MATERIALS AND METHODS

3.1. Sampling Site

There are 10 rainwater collection stations located in different parts of Turkey established by General Directorate of Meteorology (MGM). These stations are generally in the coastal areas. Locations of stations in this network are: Amasra, Antalya, Balıkesir, Çamkoru, Çatalca, Hatay, İzmir, Marmaris, Trabzon and Yatağan. Stations except for Yatağan, are located away from urban areas. Data used in this work is generated in Marmaris station in the network.

Study area is located at the Aegean Region, southwest corner of Turkey. The station is located in the premises of the Meteorological Doppler radar which is on Toros mountains, 10 km from town of Marmaris and at an altitude of 948 m. Coordinates of the station is: 36°53'9.05" N and 28°19"57.04" E. The location of the station is shown in Figure 3.1.

Figure 3.1 Location of Marmaris MGM station from Google Earth

Climate of the study area is similar to the general Mediterranean Climate with hot summer and warm winters. Long term meteorological data, which are measured at Muğla meteorological station between 1926 and 2017 are given in Table 3.1.

Table 3.1 Historical Temperature and Precipitation Data for the City of Muğla (MGM, 2017)

	Average Temp. (°C)	**Max Average Temp. (°C)**	**Min Average Temp. (°C)**	**Monthly Average Precipitation (mm)**	**Max Temp. (°C)**	**Min Temp. (°C)**
January	5.4	9.7	1.5	241.9	20.9	-12.6
February	6.1	10.8	1.8	178.4	25.5	-9.9
March	8.5	14.0	3.5	124.7	28.8	-8.5
April	12.6	18.7	6.9	64.7	31.2	-3.6
May	17.6	24.1	11.3	49.5	36.0	1.0
June	22.8	29.5	16.0	21.3	40.8	6.7
July	26.2	33.3	19.6	8.4	42.1	10.5
August	26.0	33.4	19.5	9.4	41.2	9.0
September	21.6	29.1	15.2	19.0	38.8	5.6
October	16.0	23.0	10.2	72.8	36.1	0.1
November	10.7	16.5	5.8	138.3	29.0	-7.0
December	7.1	11.4	3.1	265.7	21.0	-9.0
Annual	15.0	21.1	9.5	1194.1	42.1	-12.6

Coldest month in Muğla is January with average temperature of 5.4ºC and the hottest month is July with the average temperature of 26.2 ºC. Also for Muğla, December has been the month with the highest wet deposition amount, between the measurement years, with average monthly precipitation of 295.7 mm (MGM, 2017).

Station is located 10 km away from the county of Marmaris and the nearest road to the station is 5 km away, which indicates that anthropogenic sources are not affecting the sampling. Station is in the premises of a Meteorological radar. The sampling platform is shown in Figure 3.2.

Sample collection in the station started in June 2011 and still continuing; however, samples collected between July 2011 and November 2016 are used in this study. During this time period approximately 300 wet deposition samples are collected and measured by the MGM for the major ion concentration.

3.2. Collection of Wet Deposition Samples

In all the stations established by MGM, samples are collected using the same procedure. In stations samples are collected with a home-made automated wet and dry sampler. The samplıng system have the same characteristics of the well-documented Andersen wet-and dry sampler. Sampler that was used in this work can be seen in Figure 3.2.

Figure 3.2 Precipitation Sampler of Marmaris Station

Sampler is consisting of two 30 cm-diameter buckets, one for dry deposition and one for wet deposition. An automated cover, which receiver sıgnal from a rain sensor moves to cover dry bucket when rain starts and the same cover moves to cover wet bucket when rain ends. In this way, during the rain bucket is left open, but dry bucket is closed and during non-rain period, dry bucket is left open and rain bucket is kept closed.

Both buckets are lined with 10 L capacity polyethylene bags, which makes it easier to collect the samples when the collection period is finished. Collection period for dry deposition samples are one week, at the end of each week a new polyethylene bag is

replaced and the old one is taken for analyze. For wet deposition, bags containing rainwater are replaced with fresh ones at the end of every rain event.

3.3. Sample Handling

3.3.1. Determination of Volume and pH

Volume and pH of collected samples were measured in the laboratory. Volume measurement is done by the calibrated sampling bottles. The volume of the sample and calibrated bottle height are compared at 25ºC, and the volume of the precipitation is determined. Radiometer PHM 80 portable pH meter with a glass electrode is used to measure pH. Before measuring, pH meter is calibrated with standard buffer solutions at pH 4.0 and pH 7.0.

3.3.2. Preparation of Samples for Ion Chromatography

Ionic and trace element composition of samples were determined in MGM laboratory at the central MGM campus at Keçiören, Trace element data were not used in this work. For measurement of ion concentration, extensive sample treatment is not required, but the fine particulate matter must be removed from the sample. To remove the particulate matter samples are filtrated through 0.2 µm pore sized cellulose acetate membrane filters. Filtration avoids the Ion Chromatography to clog with particles. Sulphate, NO_3^-, NH_4^+, Na^+ and Cl^- are 100% soluble in the rainwater samples, therefore these ions are not affected from the filtration process. Nevertheless, Ca^{2+}, K^+ and Mg^{2+} ions are not dissolving in the rainwater samples completely, their solubility's are dependent on the acidity of the precipitation. In this study, only the soluble part of these ions are taken into consideration. This approach of measuring soluble fraction of ions is common in rain water research. Genç (2013) analyzed ions in aerosol samples collected at Kırklareli station, first by IC after dissolving them with water, then by ICMS after acid digestion with HNO_3 – HF mixture which dissolves alumina silicate matrix as well. The ICPMS-to-IC median ratio was 1.4 for Na, 3.5 for Mg, 2.2 for K and 1.5 for Ca. Although the difference between water soluble and insoluble fractions of these ions is significant, please note that insoluble fraction which

can be measured only after strong acid digestion is not bioavailable and cannot be picked up by plants and animals. This is the rationale behind analysis of soluble fractions of ions in most monitoring networks.

3.4. Analysis of Samples

Soluble fractions of ions were analyzed using Ion Chromatography (IC). IC is a technique used to identify the ionic composition of liquid samples. With IC, common anions (such as fluoride, chloride, nitrite, nitrate and sulfate), common cations (such as lithium, sodium, ammonium and potassium), transition metals and low molecular-weight organic acids can be measured within a liquid sample, in parts-per-million (ppm) or parts-per-billion (ppb) quantities (Burke, 2006). Working principle of an IC is as follows: sample to be analyzed (analyte) is injected to the carrier fluid (eluent); the combination is passed through a column that contains a stationary adsorbent; compounds, that are contained in the analyte, are partitioned between the adsorbent and the moving eluent/analyte mixture; as the eluent flows through the column, the components of the analyte will move down the column at different speeds and therefore separate from one another; a detector is used to analyze the output at the end of the column; each ion that exits from the column generates a peak on the chromatogram (Stute, 2009).

For the samples in Marmaris Station, soluble fractions of the ions were analyzed in MGM laboratory with a Dionex 120 Ion Chromatograph. Different columns were used for anions and cations. The columns used for anion and cation measurements are Dionex model AS9-HC and Dionex model CS12A, respectively. In addition to these analytical columns, suppressor columns ASRS-ULTRA for anions and CSRS-ULTRA for cations were also used. Eluent was 10 mM sodium carbonate (Na_2CO_3) solution for anions and 18 mM methane sulfonic acid (MSA) solution for cations.

3.5. Data Quality Assurance

3.5.1. Field Blanks

Contamination of the collected rainwater samples is a problem that must not be ignored. For the elimination of the possible effects of contamination, field blanks and laboratory blanks must be collected. The field and laboratory blanks should be collected using the same collection procedures and also should be analyzed the same way with the collected rainwater samples (U.S. Geological Survey Techniques of Water-Resources Investigation, 2006).

Field blanks are collected by pouring distilled water in the polyethylene bags which are placed in the sampler, which then collected and analyzed as the same way with the rainwater samples. Laboratory blanks are used in order to detect the potential contamination from lab procedures. Neither field, nor lab blanks were significant for any of the ions measured in this work.

3.5.2. Calculation of Detection Limits

Limit of detection is an analytical method simply defined as the lowest detectable amount of analyte in a sample (Ogen, et al., 2018). The definition of limit of detection adopted in this study is the “concentration that corresponds to three times the standard deviation of ten replicate measurements at blank level”. Detection limits of major ions calculated with this definition are given in Table 3.2. Figures in the table clearly demonstrate that, measured average concentrations of ions are several orders of magnitude than their corresponding detection limits and thus detection limits of ions is not an important source of uncertainty in conclusions.

Table 3.2 Detection Limits of the Ions (Ayaklı, 2014)

Ion	Detection Limit (µg/L)	Average conc. in rainwater (µg/L)
SO_4^{2-}	0.021454	2000
NO_3^-	0.022668	890
Cl^-	0.076439	3500
NH_4^+	0.081163	390
Ca^{2+}	0.044752	1600
Na^+	0.018494	2000
K^+	0.020703	170
Mg^{2+}	0.007738	450

3.5.3. Quality Assurance

Quality Assurance/Quality Control (QA/QC) Programs are developed in order to assure the accuracy, precision and, representativeness and completeness of the data used in the studies. Quality control term is defined as "the routine application of the procedures designed to achieve and sustain a determined level quality for a measurement system" and quality assurance is defined as "a set of coordinated actions that are used to ensure the measurement program can be quantifiable and procedure data of known quality" (Acid Deposition Monitoring Network in East Asia, 2000).

For the purposes of this study, Dionex-120 Ion Chromatograph, was calibrated using standards that are commercially available; Dionex Seven Anion Standard-II was used for anions and Dionex Six Cation Standard-II for cations. For checking the accuracy of the calibration, Standards prepared using high purity salts of measured ions (Merck, suprapure NaCl, K_2SO_4, $NaNO_3$, KCl, $CaCl_2$ and NH_4Cl) were used. Solutions prepared were used to test the calibration occasionally. Results of one of the calibration checks are given in Table 3.3. By comparing the measurements and calculations, it was agreed that the calibration of the instrument is reliable.

Table 3.3 Calculated and Measured Concentrations of the High Purity Salts (Genç Tokgöz D. , 2013)

Ion	Calculated Concentration (mg/L)	Measured Concentration (mg/L)
SO_4^{2-}	6.0 ± 0.3	6.25 ± 0.1
NO_3^-	6.0 ± 0.3	6.36 ± 0.12
Cl^-	6.0 ± 0.3	6.26 ± 0.05
NH_4^+	2.94 ± 0.15	3.1 ± 0.28
Ca^{2+}	3.1 ± 0.16	3.04 ± 0.24
K^+	3.05 ± 0.15	2.93 ± 0.3
Na^+	3.01 ± 0.15	2.96 ± 0.27

3.6. Computation of Back Trajectories

Trajectories are defined as the path a particle/air parcel will go, likewise the back trajectory (also called backward trajectory) can be defined as the path it came from, so back trajectories are often used in order to determine the relationships between the sources and receptors (Stohl, et al., 2002).

Backtrajectories were calculated using HYSPLIT (Hybrid Single Particle Lagrangian Integrated Trajectory), which is a 3D isentropic model developed by the National Oceanic and Atmospheric Administration (NOAA). This model is integrated into TrajStat, which is a GIS (Geographical Information System) based software that is available in NOAA website.

Back trajectories of each sampling days were calculated using TrajStat. Calculations were performed for 120 hours (five days) backward in time, starting at Marmaris Station. Trajectories were calculated starting at 100 m, 500 m and 1500 m. altitudes. All trajectory calculations were started at 12:00 UTC (Universal Time Coordinate). The model is set to be isentropic trajectory type, in which air parcel is assumed to be travel at potential temperature. Latitude and longitude of the receptor location is converted from degree-minute-second format to decimal degree format. Also the necessary monthly meteorological data for the software is downloaded from the database of NOAA.

The screenshot from the trajectory calculation interface of the software TrajStat is shown in Figure 3.3.

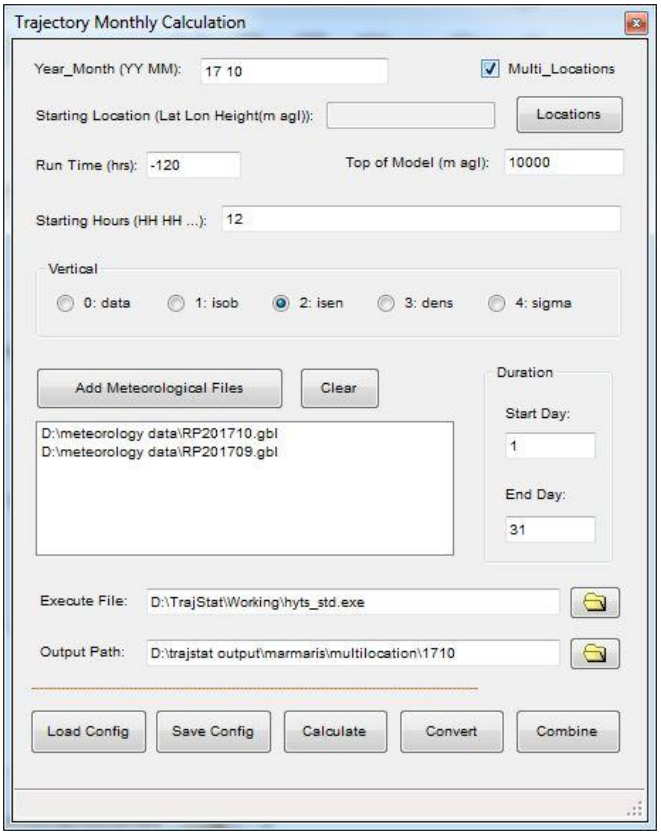

Figure 3.3 Trajectory Calculation Window of TrajStat

3.6.1. Flow Climatology

Flow climatology refers to air-flow patterns affecting the receptor. In our case it is Marmaris station, or Marmaris region in general. When this information is combined with concentrations of ions, it can provide some preliminary information about source regions affecting chemical composition of precipitation in the Eastern Mediterranean.

Two different approaches were used to calculate flow patterns of upper atmospheric air masses, before they were intercepted at our station. One of them is “residence time analysis”, which is a method developed in our group. The second approach is more conventional and bases on calculating time air masses spent in each wind sector. The second approach can be seen frequently in literature.

In the first approach study domain, which extends from west of UK to East of Caspian Sea in East –West direction and from North of Scandinavia almost to equator in North – South direction, were divided to 1ºx1º grids. The study domain and grid system superimposed to it is depicted in Figure 3.4. In the second step, number of trajectory segments in each grid were counted and results were interpolated using MAPINFO software to generate residence time distributions. Since back trajectories calculated by HYSPLIT consisted of hourly segments which are characterized by x, y, z coordinates and time, they were suitable for mapping. Consequently, number of segments in each grid indicate number of hours air masses spent in that grid during study period (or during the time interval for which flow climatology calculations are done). Residence time distribution-maps were prepared for each starting altitude and for summer and winter separately.

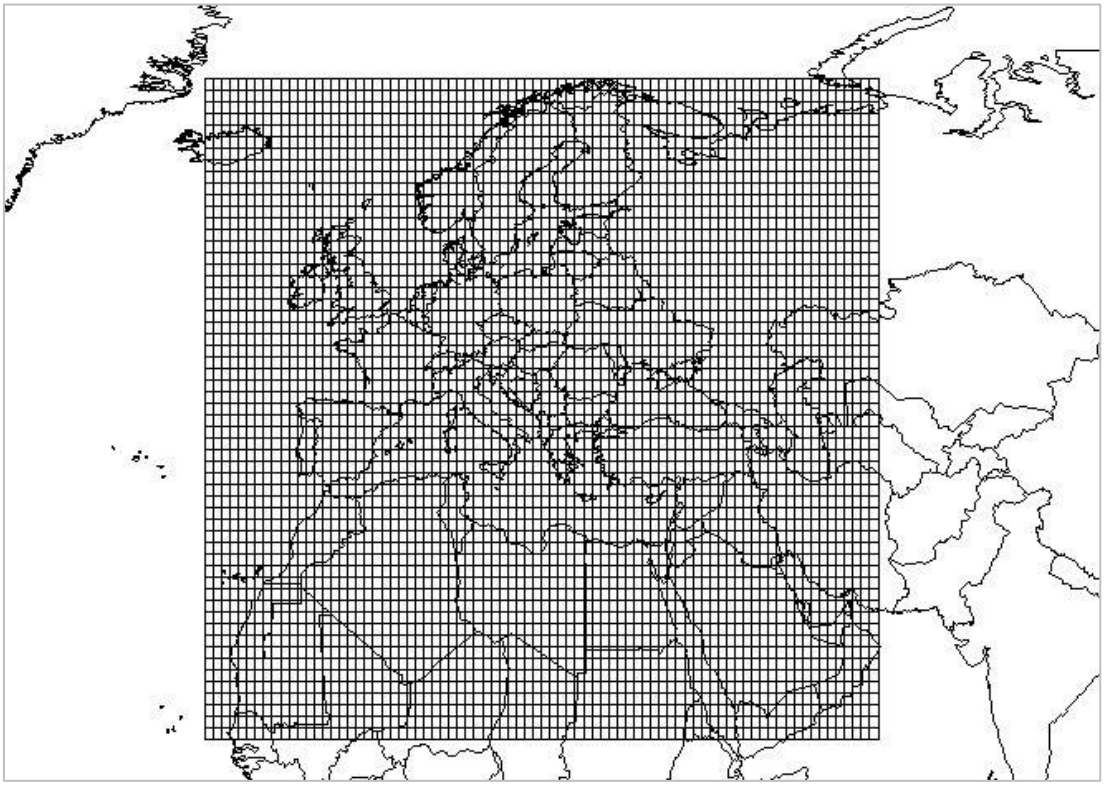

Figure 3.4 Study Domain for the Residence Time Analysis

As pointed out before residence time distribution was developed in our group and used in a number of projects and thesis. However, unfortunately it does not allow us to compare flow patterns calculated in this work with similar patterns reported in other studies. To avoid this difficulty, flow climatology was also calculated in conventional way, which can be found in literature, as well.

The study domain is divided into 8 wind sectors (N, NE, E, SE, S, SW, W, NW), number of trajectory segments in each sector is counted. It should be noted that in conventional approach assigning trajectories to a sector is always a problem, because trajectories pass through two or more sectors, before they end up at our station. This issue was bypassed by counting number of segments (hours air parcels spent) at each sector.

3.7. Potential Source Contribution Function

For determining the potential source regions of the pollutants, Potential Source Contribution Function (PSCF), which is a statistical tool in trajectory statistics was used. PSCF shows the areas that contributed to high concentrations of pollutants at the receptor, thus pointing to source areas of pollutants.

As in the approach used in flow climatology, PSCF calculations also include counting trajectory segments in the grid system, described in previous section.

Trajectory files of the measured days are selected and the trajectories that correspond to the highest 40% of pollutant concentration is grouped as "polluted" trajectories and segments in these polluted trajectories are categorized as "polluted segments". Polluted and all (polluted + unpolluted) segments in each grid were counted and PSCF value for that grid was calculated using Equation 3.1.

$$PSCF_{ij} = \frac{m_{ij}}{n_{ij}} \tag{3.1}$$

Where Σm_{ij} refers to the total number polluted trajectories in gird "i" and Σn_{ij} refers to total number of all (polluted + unpolluted) segments in the same grid. "j" is a trajectory counter.

One of the problems associated with PSCF approach is the small number of segments at the peripheral grids in the domain. Trajectories calculated in this study is 5 days long, which means there is 120 hourly segments in each back trajectory. Since there is 302 samples (day), and 3 trajectories with different starting altitudes in day, total number of segments used is 108720. However, a large majority of these segments are in grids that are close to our station. There are few segments in grids that are located at the boundaries of our grid system. PSCF values assigned with few trajectories can have very large uncertainties and can lead to misleading conclusions. To avoid this, a weighting approach, which was developed by Zhao ve Hopke (2006) and shown in Equation 3.2 was used.

$$W(n_{ij}) = \begin{cases} 0.15 & n_{ij} \leq {}^{n_{avg}}/_{2} \\ 0.5 & {}^{n_{avg}}/_{2} < n_{ij} \leq n_{avg} \\ 0.75 & n_{avg} < n_{ij} \leq 2 * n_{avg} \\ 1.0 & n_{ij} > 2 * n_{avg} \end{cases} \quad (3.2)$$

where $W(n_{ij})$ is the weighting function,

n_{avg} is the average number of the segments in all grids

The equation implies that if total number of grids in a particular grid is at least twice higher than average number of segments in all grids at the domain, then PSCF value for that grid was multiplied by 1.0. If the number of segment is between avg number of segments and 2 times average number, PSCF value of the grid was grids were multiplied with 0,75. PSCF is multiplied by 0,5 if the number of segments in that grid is between one-half of the average number of segments and average number of segments. Finally PSCF value for a grid was multiplied by 0.15 if number of segments in that grid I less than half of the average number. As can be seen from the equation, importance of peripheral grids with few segments are significantly reduced in PSCF distributions.

3.8. Positive Matrix Factorization

EPA PMF version 5.0 was for source apportionment part of the study. In order to insert the measured data to the software, missing data and data below the detection limit (given in Table 3.2), should be replaced. For missing data geometric mean of that ion is used; for the data below detection limit (BDL) half of the detection limit is used, but uncertainties of such data are increased so that this data do not affect the "fit".

Software also requires the uncertainty data referring to each measurement calculated as (Norris, et al., 2014; Reff, et al, 2007):

$$\sigma_{ij} = \begin{cases} Real\ Concentration, & x_{ij} * 0.05 + \dfrac{DL}{2} \\ Below\ Detection\ Limit, & \dfrac{5}{6} * DL \\ Missing\ Data, & 4 * Geometric\ Mean \end{cases} \quad (3.3)$$

Where σ_{ij} is analytical uncertainty, x_{ij} is the concentration of the specie j measured on sample i, DL is the detection limit.

Object function that had been explained in Section 2.3.2.3. PMF software calculates 2 different Q values for each run: Q_{robust} and Q_{true}. Also a theoretical Q value should be calculated by following equation:

$$Q_{theoretical} = (k * m) - t(k + m) \quad (3.4)$$

Where k is the number of elements, m is the number of days and t is the number of factors. While trying to determine the number of factors, several runs should be made by the software and for each run software gives: Q_{robust} and Q_{true} values which also shoul be compared with: $Q_{theoretical}$. : Q_{true} / $Q_{theoretical}$ value should be around 1-1.5 for the factor number to be accurate.

After the factor number is selected, by analyzing the correlation between species and the factor profiles, it can be determined that which factor refers to which source.

CHAPTER 4

RESULTS AND DISCUSSION

4.1. General Characteristics of the Data

In this study, 302 rainwater samples collected by MGM between 2011 and 2016 were analyzed. In these 302 samples, concentrations of nine major ions, including H^+, SO_4^{2-}, NO_3^-, Cl^-, NH_4^+, Ca^{2+}, Mg^{2+}, K^+ and Na^+ were determined. General characteristics of data are given in Table 4.1.

Table 4.1 Statistical Summary of Ionic Composition (concentrations are in mg L-1)

	Volume Weighted Average	Mean	Standard Deviation	Median	Range	Number of Samples
pH	5.12	5.91	0.89	6.01	3.69 – 7.9	302
H^+	0.0076	0.0094	0.025	0.0009	$1.26 * 10^{-5}$ – 0.20	302
SO_4^{2-}	2.03	3.11	4.63	1.76	0.06 – 47.69	296
NO_3^-	0.89	1.45	2.08	0.79	0.04 – 20.40	287
Cl^-	3.49	4.05	7.37	2.00	0.02 – 105.04	300
NH_4^+	0.39	1.09	4.82	0.19	0.002 – 56.06	259
Ca^{2+}	1.63	2.34	4.02	0.86	0.01 – 25.77	302
Mg^{2+}	0.45	0.57	1.48	0.28	0.01 – 20.44	297
K^+	0.17	0.34	1.08	0.12	0.01 – 11.68	289
Na^+	2.00	2.24	2.62	1.51	0.02 – 22.75	299

Volume weighted concentrations of constituents are used instead of regular averages in studies aiming to determine rainwater composition, to avoid dilution effect. Concentrations of elements and ions (and other constituents also) in rainwater is inversely related with rainfall amount. Concentrations are lower in intense rains and

higher in rain with low precipitation amount, obviously due to dilution. This dilution effect is avoided in volume weighted average concentrations of elements and ions, as concentrations are normalized with rainfall amount.

Volume weighted averages (VWA) of the sample concentrations are calculated using the following formula:

$$C_{xp} = \frac{\sum(C_x * V_p)}{\sum V_p} \quad (4.1)$$

Where C_{xp} stands for the volume weighted concentration of the specie x,

C_x stands for the concentration of the specie x in the given sample,

V_p stands for the precipitation volume of the sample.

The ratio of average concentrations of elements to their volume-weighted averages vary between 1.1 and 2.7, for Na for NH_4^+, respectively. It is interesting to note that the ratio for crustal and marine elements are low (the average-to-VWA ratio for Cl^- is 1.2, for Na^+ is 1.1, for Mg^{2+} is 1.3, for Ca^{2+} is 1.4) and ratios are high for pollution-derived ions (for SO_4^{2-} is 1.5, for NO_3^- 1.6 and for NH_4^+ 2.7). This systematic difference between crustal, marine and anthropogenic elements is probably due to the way they are deposited to the surface. Crustal and marine ions that we measured in our rainwater samples are from local sources and washed out by rain from the atmosphere during very early phases of the rain event (10 – 30 min) (Al-Momani, et al., 1998; Kaya & Tuncel, 1997). Pollution derived ions that we measure in rain samples, on the other hand, are brought to Marmaris in clouds and when clouds rain, they are deposited to the surface where we sample them. Their concentrations do not change significantly throughout the rain (Al-Momani, et al., 1998; Kaya & Tuncel, 1997). A slight decrease is observed in the beginning of the rain event due to their washed-out fraction. However the decrease is not as large as the concentration decrease in crustal and marine ions and elements (Al-Momani, et al., 1998; Kaya & Tuncel, 1997). This scenario suggests that concentrations of crustal and marine elements in rainwater samples depends on how much seawater and crustal particles

exists in the atmosphere when rain starts. Their concentrations are independent of rainfall amount, because they are washed out in first 10 – 15 minutes of rain and thus do not depend on how long rain continues (rainfall amount). Concentrations of pollution derived ions on the other hand, depends strongly on dilution of these ions with rainfall amount. This scenario can explain observed polarity in AVG-to-VWA concentration ratios of anthropogenic, crustal and sea salt ions. Volume weighted average concentrations of ions vary between 0.4 mg L^{-1} for NH_4^+ ion and 3.5 mg L^{-1} for Cl^- ion. Median concentrations of ions are approximately a factor 2 lower than their average values. Lower median values together with high standard deviations are indications of right skewed data as will be discussed in the next section of this manuscript.

4.1.1. Distribution Characteristics of the Data

Distribution characteristics (frequency histograms) of anions and cations measured in this study are given in Figure 4.1 and Figure 4.2, respectively. Atmospheric data have always right skewed distributions, as depicted in these figures. There are many different right-skewed distributions, but log-normal distribution is the most common distribution observed in environmental data. The distribution characteristics of data for each ion was tested using Chi-square goodness of the fit test with null hypothesis that distributions are "log-normal". The results showed that distributions are log normal with > 95% statistical significance for H^+, NO_3^-, NH_4^+ Ca^{2+}, Mg^{2+}, K^+ and Cl^-. However, null hypothesis was rejected for SO_4^{2-} and Na^{2+} ions. Apparently, these two ions have histograms that represent another right-skewed distribution. We did not further investigate to find type distribution followed by these two ions.

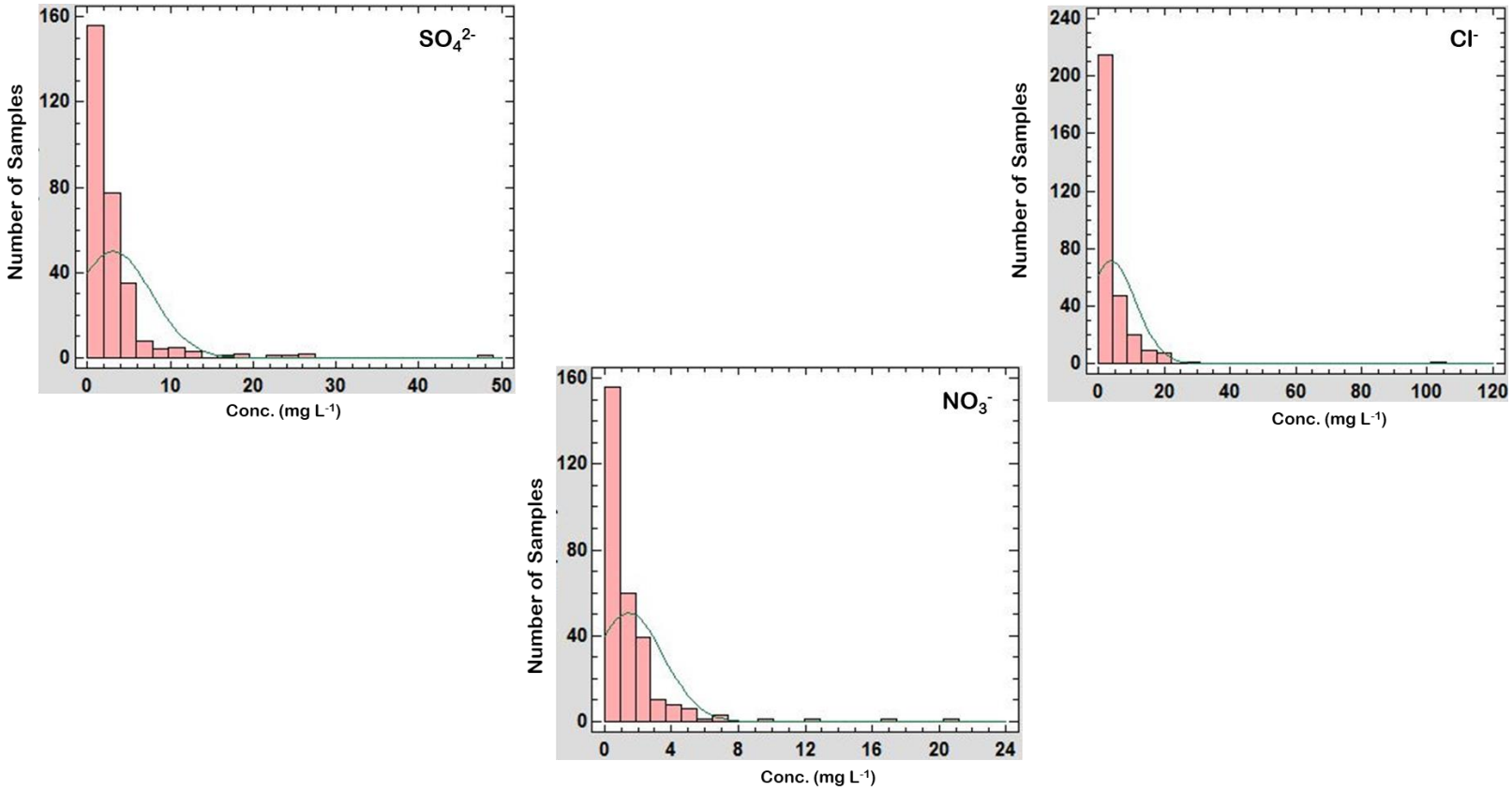

Figure 4.1 Frequency Distribution of Anions Measured in this Study

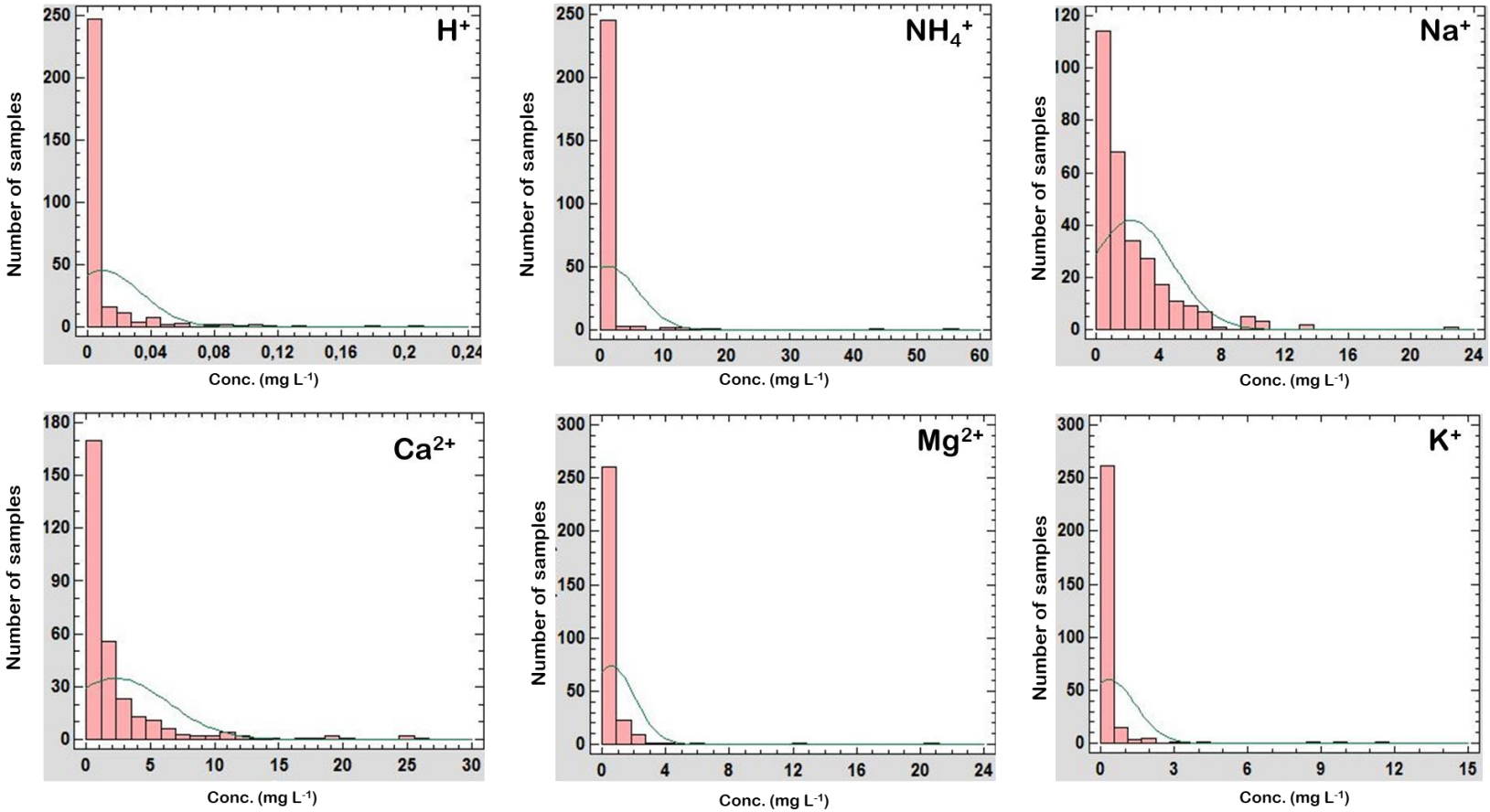

Figure 4.2 Frequency Distribution of Cations Measured in this Study

4.1.2. Comparison of the Data with Literature

Air quality in urban and industrial areas is assessed by comparing measured concentrations of pollutants with air quality standards. Situation is more complicated in air quality at rural airshed. Concentrations of pollutants are always lower than their corresponding concentrations measured at urban or industrial areas, because rural areas are not under direct influence of industrial, residential and traffic emissions. However, standards are designed for human health, but at rural airshed, concern is the health of ecosystem, which can be more vulnerable than humans due to very long-term exposure to pollutants. For example, since forests are exposed to pollutants for hundreds of years, they can be affected from fairly concentrations, which are safe for humans. Since regulatory standards are useless in evaluating rural air quality, the only way for such an assessment is to compare pollutant concentrations measured at the rural station with corresponding data from rural areas reported in literature. Furthermore, such a comparison can also provide information about transport mechanisms of pollutants to the rural station.

In this study, generated data are compared with corresponding concentrations, which are measured in two comparable networks. Data is first compared with similar data generated in rain monitoring stations in Turkey. In the second step data generated in this work are compared with similar ion data measured in EMEP network.

Rural rainwater data generated in Turkey is unexpectedly extensive. 13 rural rain monitoring stations operated in Turkey up today. Among these 10 stations, namely, Yatağan, Trabzon, Izmir, Hatay, Çatalca, Çamkoru, Balıkesir, Antalya 3, Marmaris and Amasra were established and operated by General Directorate of Meteorology, Research division (MGM network). These stations are strategically very important, because MGM can operate them for long periods of time. Some of them are now in operation more than 15 years. The network was initiated in 2004 by establishing a bulk sampling station at Çamkoru. Çamkoru was the only station equipped with bulk samplers. All other stations in the network were equipped with automated wet-and-dry samplers. However, an automated wet-and-dry sampler was also installed to

Çamkoru station in 2014. Two additional stations also became operational in 2004. One at Amasra and the other one at Balıkesir. Two additional stations, namely Antalya and Çatalca were activated in 2005. These are followed by a station at Izmir and Marmaris in 2011, at Yatağan in 2012, at Hatay 2013 and Trabzon in 2014. Stations are named with cities to describe their geographical locations, but none of them, except for Amasra station, are located in urban areas, most of them (Hatay, Marmaris, Trabzon, Çatalca, İzmir, Balıkesir, Hatay) are located at Meteorological Doppler radar sites, which are >10 km away from the urban area. Data set evaluated in this thesis is the one generated at Marmaris station between 2011 and 2016. In all these stations, samples are collected in polyethylene bags and shipped to MGM central laboratory at Ankara, where they are analyzed for ions and trace elements.

The Çubuk station used in comparison is the only EMEP station in Turkey. It was established in 1993 by the Ministry of Health, with financial assistance of the German Government. It was successfully operated by the Refik Saydam Hıfzıssıhha Merkezi between 1993 and 2006. In 2006, the station was transferred to Ministry of Environment. It is not operating since then. Other stations. Namely Antalya 1, Antalya 2, Ankara, Bartın were operated in the past by our group.

EMEP network is the monitoring component in LRTAP (Long Range Transboundary Air Pollution) convention. Operations in the network started in 1977 and it is still operational. EMEP network consisted of approximately 180 stations (all of these stations were not operational all time). Variety of parameters in aerosol, gas phase and rainwater are being measure on an hourly and daily basis. Main objective of the network is to generate data with high spatial coverage for model validation and monitor long term trends in concentrations of pollutants.

Rain composition data was downloaded from EMEP database (EMEP, 2017). Data included event-based concentrations of major ions from 176 stations in 37 countries, between 1977 and 2015, locations of the stations are given in Appendix A. EMEP data for each ion were then separated into seven categories, including All, Eastern Europe, Western Europe, Northern Europe, Central Europe, Southern Europe and Islands.

Such division was necessary, because EMEP data depicted categorical differences geographically. For example, stations in Southern Parts of EMEP network report Ca^{2+} concentrations that are significantly higher than corresponding concentrations reported in other parts of the EMEP network. Eastern Europe, in this section, refers to former USSR countries. Anthropogenic emissions and hence concentrations of pollutıon-derived elements and ions in these countries was very high before their unification with EU, then gradually decreased owing to EU-supported action taken to reduce emissions. This long-term pattern is not the same with the patterns observed western European countries.

Average concentrations of pollution-derived ions measured in EMEP network and at Marmaris are given in Figure 4.3. Concentrations of SO_4^{2-} and NH_4^+ measured in this work are higher than SO_4^{2-} and NH_4^+ concentrations measured anywhere in Europe. High SO_4^{2-} concentrations in Mediterranean region, particularly at the Eastern Mediterranean is well documented in aerosol studies (Hacısalihoğlu, et al. 1992; Güllü, et al., 1998; 2005; Luria, et al., 1996; Koulouri, et al., 2008; Im, et al., 2013). High NH_4^+ concentration in particles is also reported in a number of studies for the Eastern Mediterranean (Al-Momani, et al., 1998; Güllü, et al., 2005, Im, et al., 2013) and attributed to evaporation of NH_3 from fertilizer use and its subsequent oxidation to NH_4^+ ion in atmosphere. High concentrations of SO_4^{2-} and NH_4^+ in EMEP stations in Southern European countries ("Southern" in the figure) demonstrate that high concentrations of these two ions is a regional phenomenon and not specific to Marmaris Station. Nitrate concentrations measured at our station is not significantly different from NO_3^- concentrations measured in other European sites. Unlike SO_4^{2-} and NH_4^+, NO_3^- concentrations do not change significantly throughout Europe, including the Mediterranean region.

Spatial variation of H^+ concentration is very different. It is high in Northern Europe and in Eastern European countries and low at Southern European countries (countries in the Mediterranean region) and very low at Marmaris. A number of points needs to be highlighted in this pattern. Please note that countries that has high H^+ concentration are the ones that suffered most from acid rain in 70's and 80's. Also, concentration of

SO_4^{2-} is highest in Marmaris and Mediterranean countries ("Southern" in figure), but these sites reported have the lowest H^+ concentration. This peculiar spatial variation in H^+ concentration in Europe is due to neutralization of rainwater acidity and will be extensively discussed later in the manuscript.

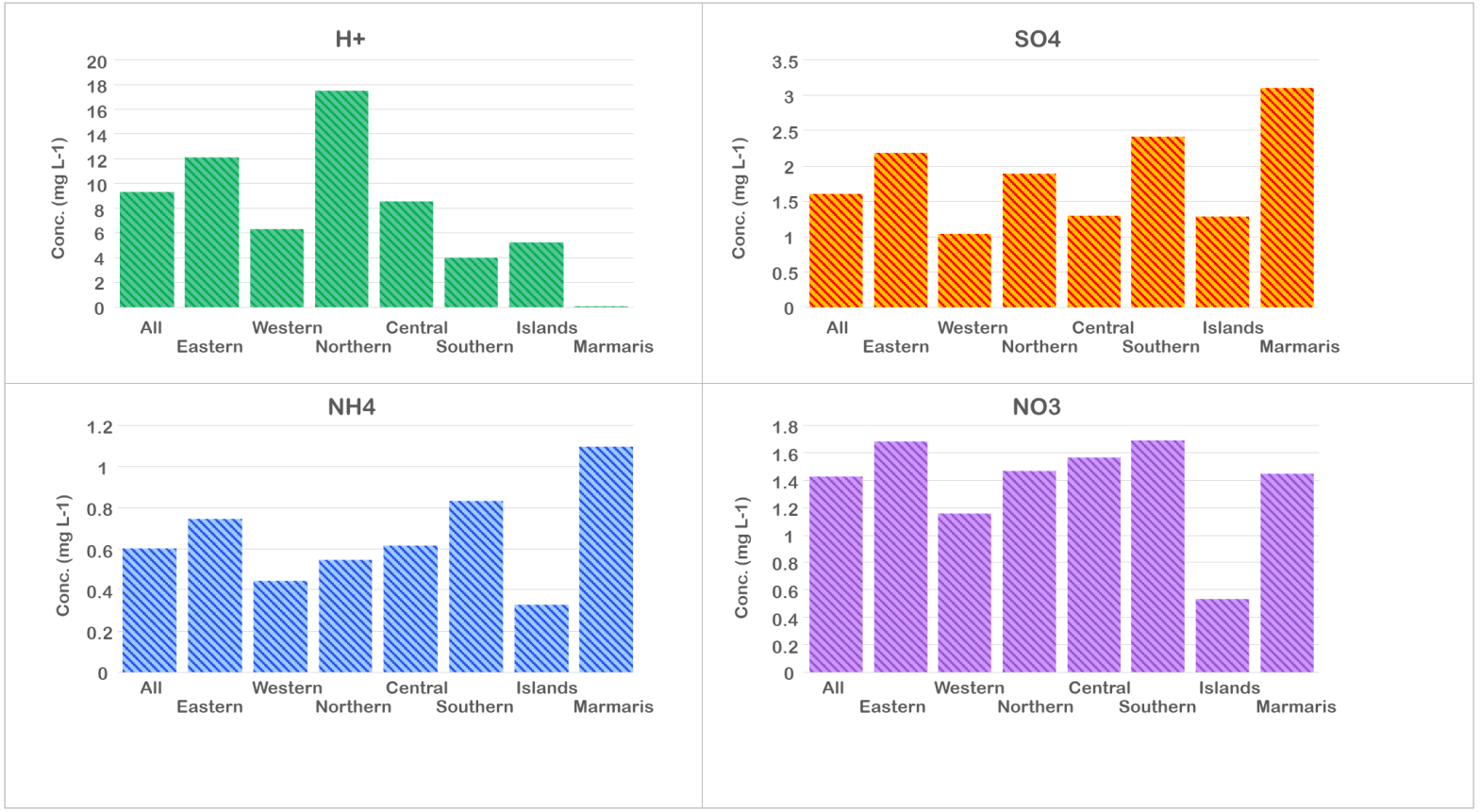

Figure 4.3 Comparison of pollution-derived ions measured in this study with corresponding data from EMEP network. Different median values were generated from EMEP stations depending on their location in Europe

Concentrations of ions with natural sources in EMEP stations and in Marmaris are given in Figure 4.4. Calcium concentration measured at Marmaris are the highest in all data groups, which is followed by the Ca^{2+} concentration reported at "Southern" European countries, indicating that high Ca^{2+} concentration is a regional process. High Ca^{2+} in southern part of Europe is due to highly alkaline nature of the soil in the Mediterranean region and will be discussed later in the manuscript in relation to neutralization of rainwater acidity.

Na^{+} and Cl^{-} are sea salt ions and their concentrations are high at "Island" station group, as expected. Since concentrations of Na^{+} and Cl^{-} are high in stations close to the sea, higher concentration of these ions in "Northern" station group can be due to close proximity of measurement stations to the sea in this station group. This is reasonable explanation, because most of the stations in "Northern" group are located in Norway and Sweden. Wherever a station is located, it will not be too far from the sea in these countries. Concentrations of sea salt ions measured at Marmaris is higher than those reported for "Eastern", "Central" and "Southern" station groups, but not as high as concentrations reported for "Island" and "Western" station groups. Marmaris station is approximately 10 km from the sea. Low concentrations are probably due to high altitude of the station.

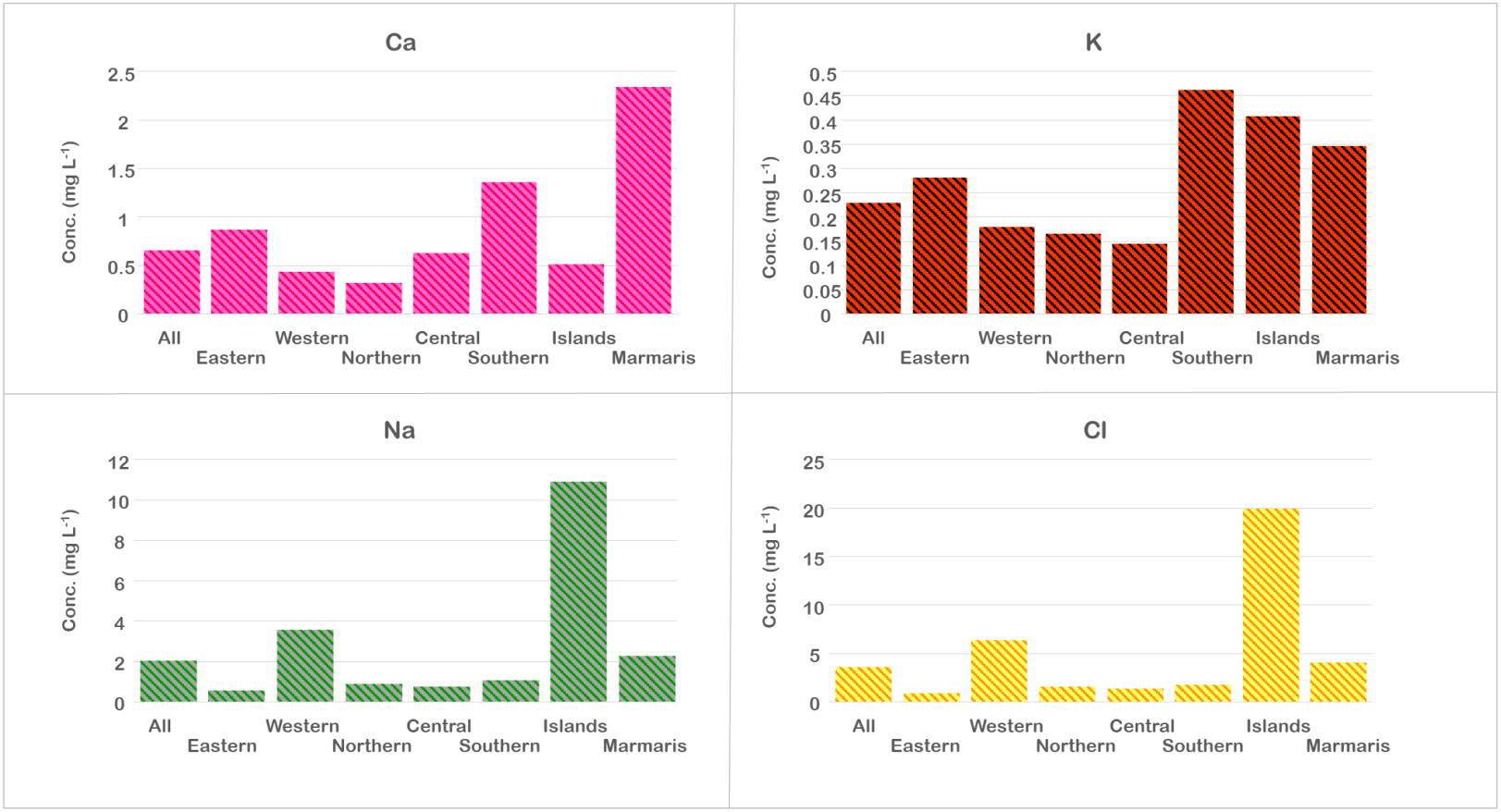

Figure 4.4 Comparison of crustal and marine ions measured in this study with corresponding data from EMEP network.. Different median values were generated from EMEP stations depending on their location in Europe

Average concentrations of pollution-derived ions at Marmaris and other stations in Turkey are given in Figure 4.5. Levels of anthropogenic ions measured at Marmaris station is not significantly different from their levels reported for other stations in Turkey, with few exceptions. Average SO_4^{2-} concentration at Marmaris station is smaller than those measured Yatağan and Antalya. SO_4^{2-} concentration reported for Yatağan is significantly higher than SO_4^{2-} concentrations measured at all stations. This probably reflects presence of the Yatağan thermal power plant in the close proximity of the station. High SO_4^{2-} concentration reported for Antalya is an artifact. Concentration reported for Antalya station is an average value from samples collected between 1992 and 2001. In those years SO_4^{2-} concentration in all Eastern Mediterranean basin was were high. Average SO_4^{2-} concentration measured at Antalya 3 station are more representative for the SO_4^{2-} levels in the region today.

Concentrations of NO_3^- ion are high at Antalya station for the same reason. Average NO_3^- concentration measured at Marmaris station is not significantly different from NO_3^- concentrations reported in most of the stations in Turkey. Average concentration of NH_4^+ measured in this work are also comparable to similar concentrations reported in other parts of Turkey. However, higher NH_4^+ concentrations are reported for Hatay, Izmir, Trabzon and Yatağan stations. Discussion of the reasons for these high concentrations is beyond the scope of this study.

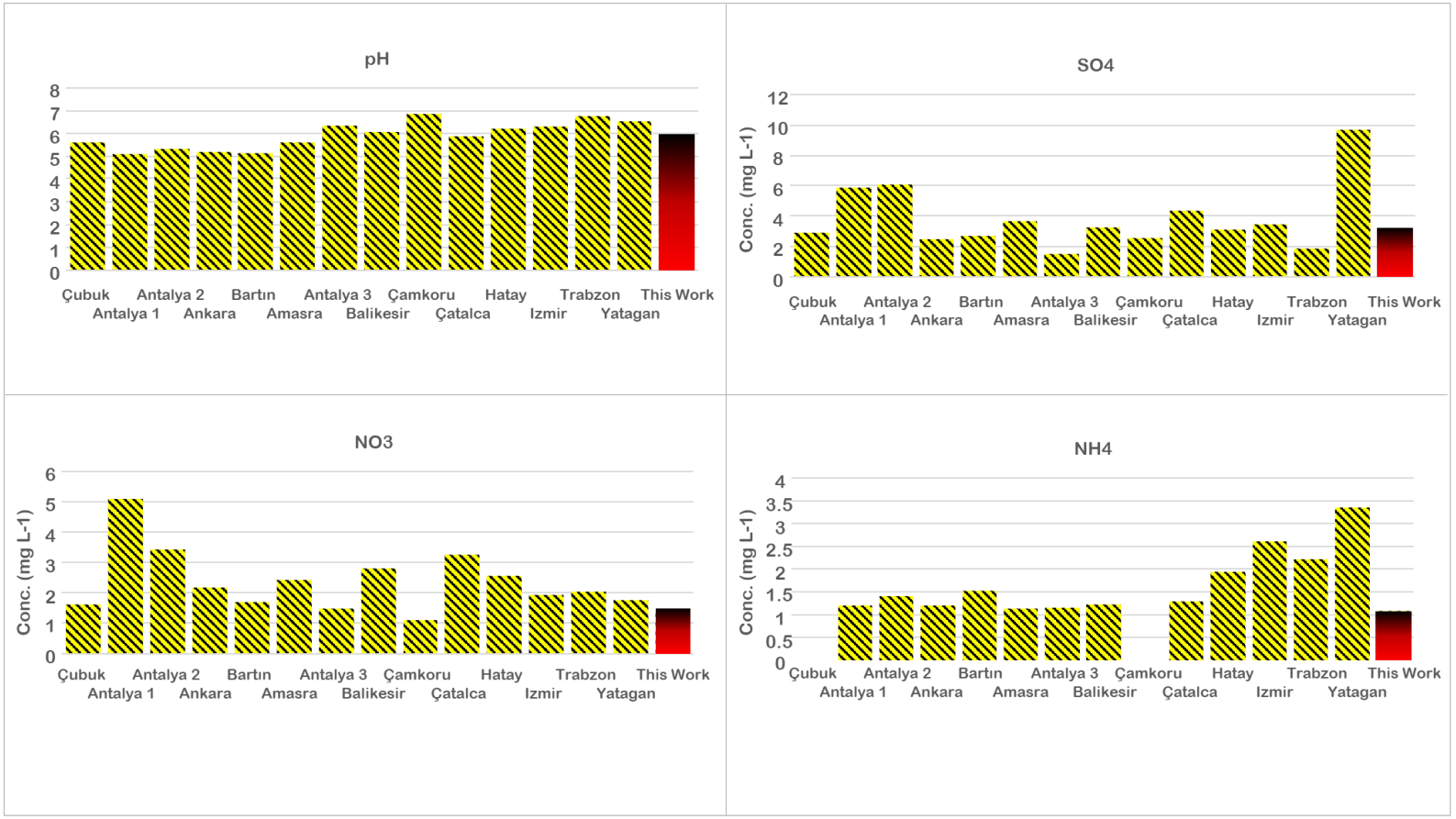

Figure 4.5 Comparison of ionic composition determined in this study with corresponding data generated in other locations in Turkey: Ions with anthropogenic sources

Concentrations of sea salt and crustal elements measured at Marmaris and elsewhere in Turkey are given in Figure 4.6. Concentrations of Na^+ and Cl^- are the highest at Antalya station, because at Antalya station was located at the coast. Concentrations of these sea salt ions are not equally high at Marmaris because (1) station is approximately 10 km from the coastline and (2) station was 1000 m above sea level. Calcium concentration measured at Marmaris is comparable to concentrations measured in other rainwater monitoring stations. The reason for unusually high Ca^{2+} concentration reported for Yatağan station is not known. Potassium concentration; however, is high at Antalya, Bartin and Amasra stations, which are located on at the coast. Please note that K^+ concentration at coastal stations are also contributed by sea salt. Please also note that concentrations of Na^+ and Cl^- are also high in these stations.

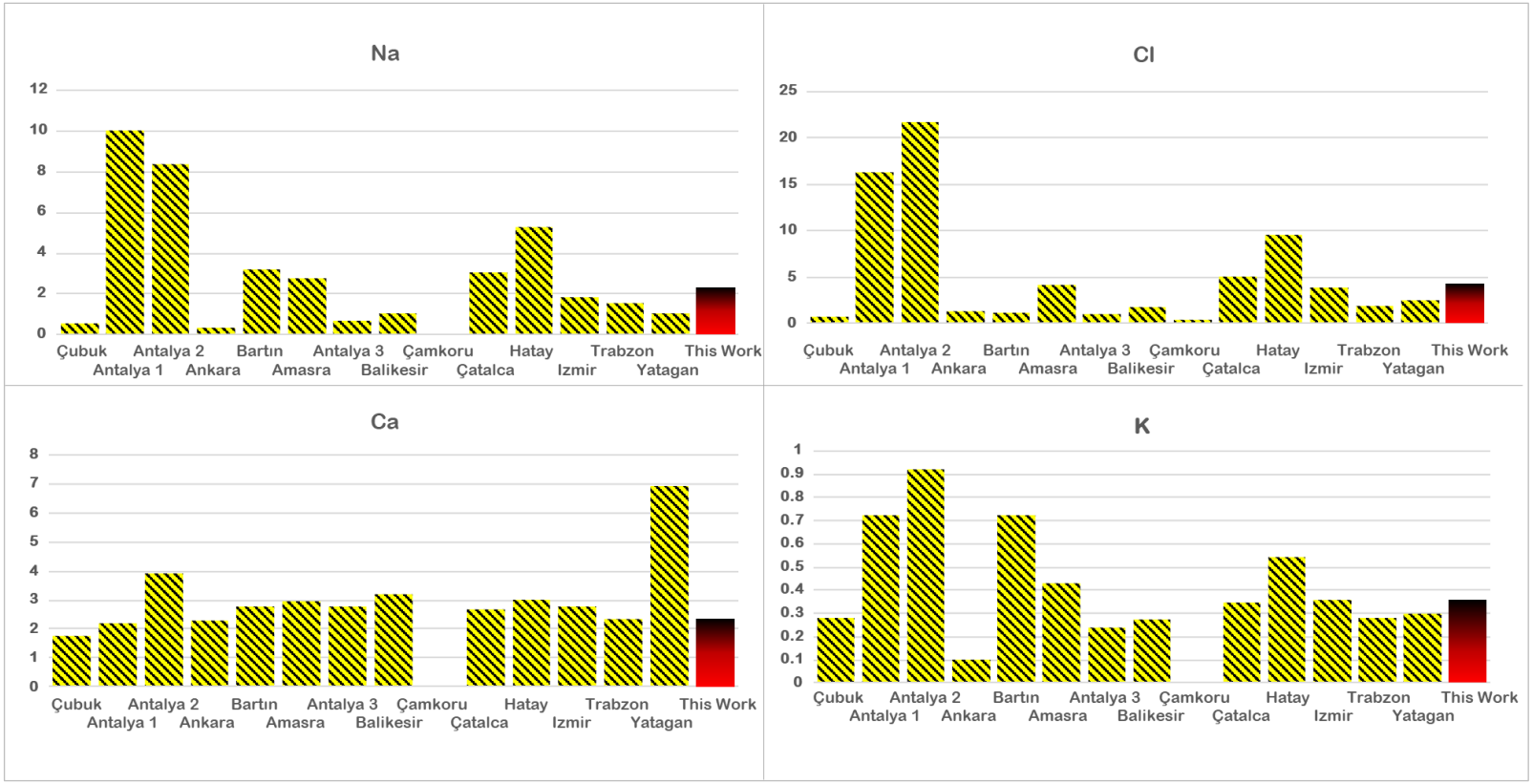

Figure 4.6 Comparison of ionic composition determined in this study with corresponding data generated in other locations in Turkey: Marine and crustal ions

4.2. Flow Climatology

Flow climatology is an important approach used in this study, as it signifies areas where air masses spent most of their time before they arrive to our station. Such data can provide information about source areas of pollutants that are intercepted at the sampling point. Two different approaches were used in this study. In the first method, hours spent by air masses at each grid of our study domain were computed. In the second method, number of hours spent by air masses in wind sectors was computed. Since trajectory information is necessary in both methods, 5-day long back trajectories were calculated every day for 13 years, which is longer than our sampling period at Marmaris station. For each day three different trajectories with starting altitudes 100 m, 500 m and 1500 m were calculated. Trajectories were consisted of 1-hour segments. These segments were counted in grids and in wind sectors. Trajectories were computed for a period longer than sampling period to reduce uncertainties in calculated residence times and clusters. Please note that, since flow climatology and cluster analysis do not depend on ion concentrations, trajectory calculations are not limited with our sampling period in Marmaris station. Back trajectories for were calculated for 13 years to minimize statistical uncertainty in residence time and cluster calculations.

4.2.1. Residence Time Analysis

For residence time analysis, segment counts in grids are transformed to distribution maps showing the time spent by air masses in different parts of the study domain. Distribution of residence times of air masses in the study domain are given in Figure 4.7, (a), (b) and (c) in the figure are distributions for 100 m, 500 m and 1500 m starting altitudes, respectively. Figure 4.7 (d), on the other hand, are prepared by combining segments in all three starting altitudes. There are not substantial differences in residence time distributions between different starting altitudes. The effect areas appear to be expanded in Figure 4.7 (d), because it includes factor of three times more segments than segments in individual starting altitudes.

The areas, where air masses spent most of their time before they arrive to Marmaris are, western parts of Turkey, most of the Balkan countries (particularly Greece, Bulgaria, Romania), Ukraine and the Black Sea coast of Russia, indicating that sources in these areas have higher probability of contributing atmospheric composition at Marmaris.

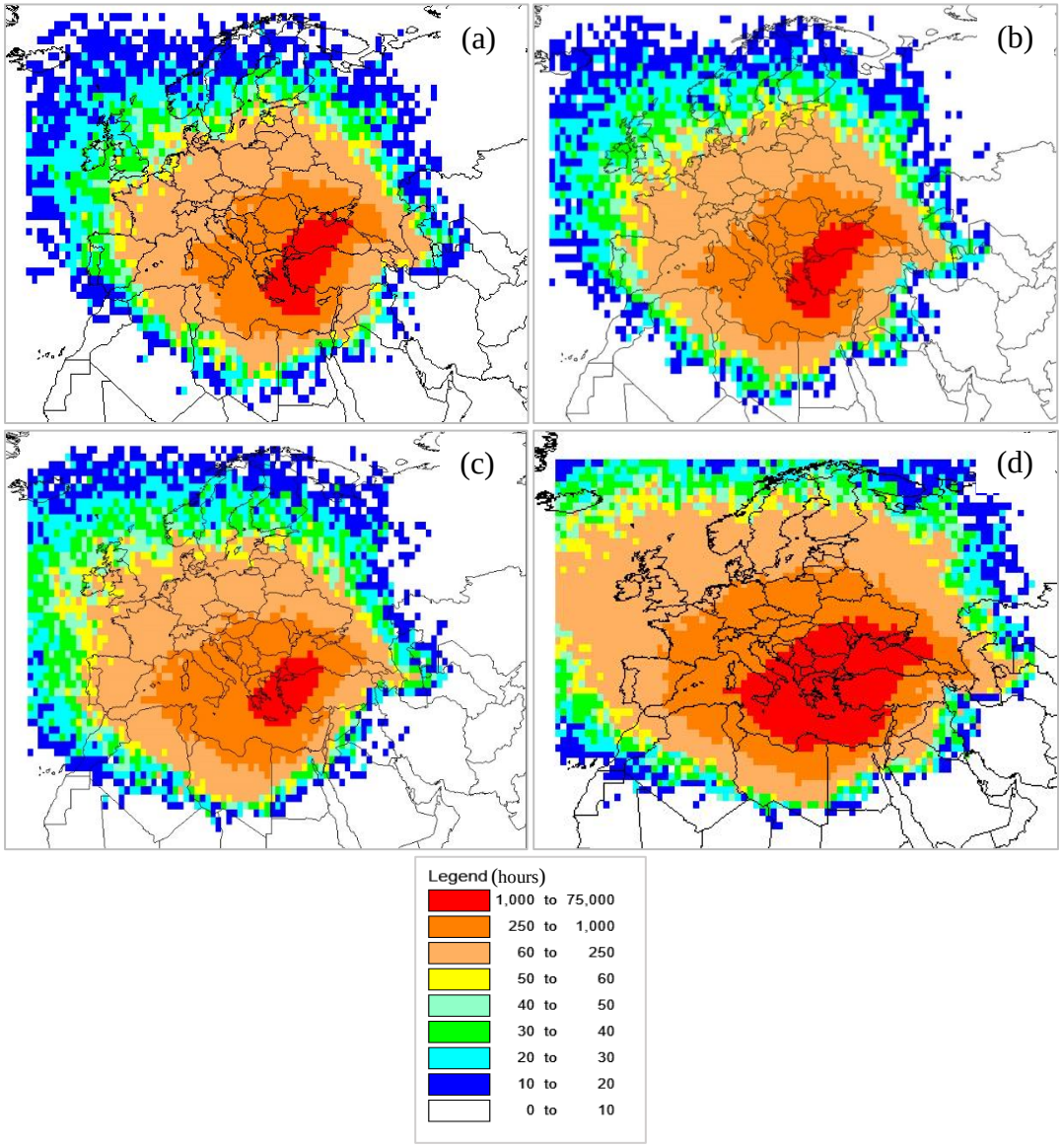

Figure 4.7 Distribution of Air Mass Residence Times in Study Domain
(a) 100 m starting altitude, **(b)** 500 m starting altitude,
(c) 1500 m starting altitude, **(d)** Segments in all starting altitudes

For the calculation of summer and winter residence times, trajectories in summer and winter months were separately counted. In this and in many other studies performed in our group, summer season was assumed to be between April and September and winter season was taken as the remaining part of the year. This summer-winter partitioning was based rainfall in the Mediterranean area. In the Eastern Mediterranean area approximately 20% of the annual rainfall occurs between April and September (our summer season) and 80% of the rainfall occur in the remainder of the year (our winter). Since wet scavenging is an important factor in temporal variations of atmospheric constituents in atmospheric particles and precipitation, such rainfall-based division of the year into seasons enhances summer winter differences in concentrations of elements and ions and makes them easier to detect.

Summer (a) and winter (b) season distributions are given in Figure 4.8 along with the distribution of summer - winter differences (c). In Figure 4.8 (c), positive numbers in the legend indicate grids where air masses spent longer time in summer and negative numbers indicate grids where air masses spent more time in winter. It is very clear from figure that air masses, which we intercept at our station spent more time in North and Northwestern parts of the study area in summer and spent more time in Western Europe, North Africa and Middle East in winter. This was considered in the source region apportionment part of the study.

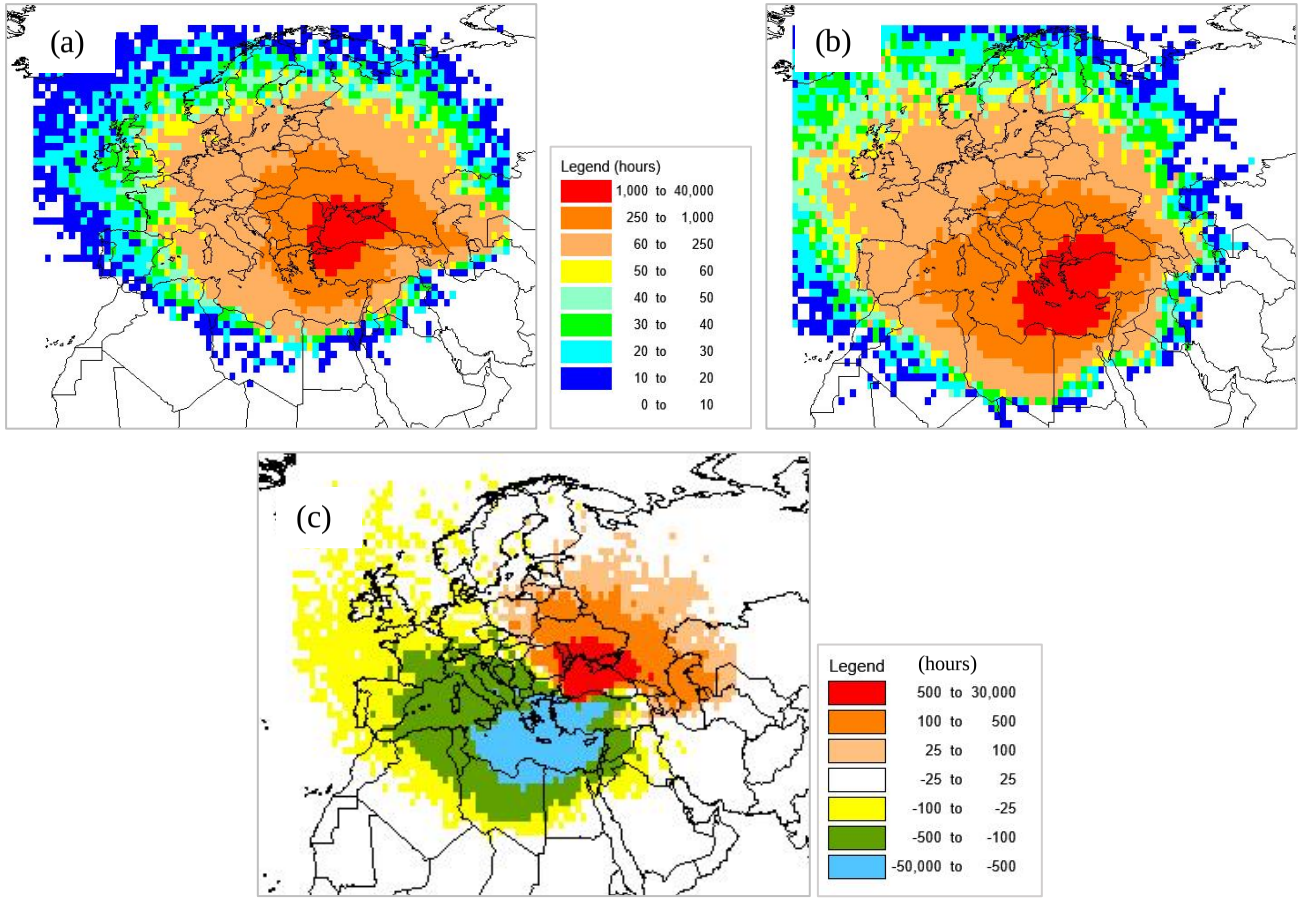

Figure 4.8 Seasonal Variation in Hourly Residence Times
(a) Summer Residence Times, **(b)** Winter Residence Times, **(c)** Summer-Winter Difference
["-" sign means longer residence time in winter and "+" sign indicates longer residence times in summer]

4.2.2. Sector-Based Flow Climatology

Grid-based climatology, which was discussed in previous section is not a conventional way of presenting flow climatology. We are using it for many years in our group and we are satisfied with the results we are getting. However, we also investigated the conventional way of presenting flow climatology. In this second approach, segments in each of the eight wind sectors were counted on an annual basis and in different seasons. Results are given in Figure 4.9. Results of sector-based approach are not significantly different from results obtained in grid-based climatology. Grid-based approach is more informative about potential source areas that can affect composition of particles, gases and rainwater at Eastern Mediterranean basin.

Upper atmospheric air masses spent significantly longer times at N, NE, W and NW sectors. Residence times are longer in summer at N and NE sectors and longer in winter E, SE, S and SW sectors. They are comparable in W and NW sectors. This conclusion is similar to conclusions reached in grid-based approach. This more frequent flow from N, NE, W and NW sectors and seasonal differences discussed in this section is a general characteristic of Eastern Mediterranean region, because it is observed in a number of studies performed in the region (Güllü, et al., 1998; Zodiatis, et al., 2003; Dayan, et al., 2017; Erel, et al., 2007).

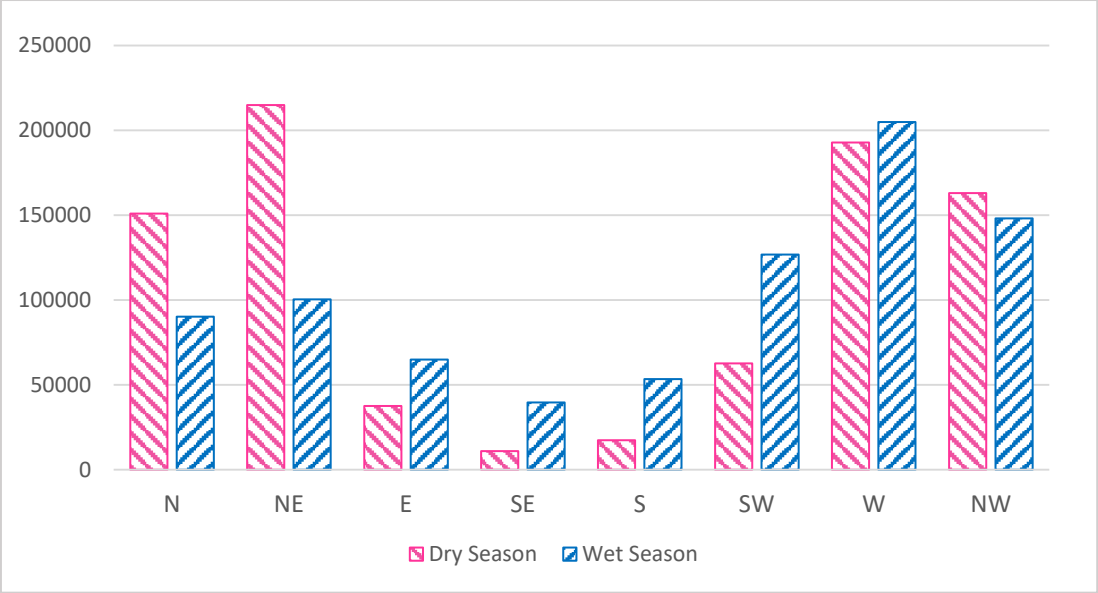

Figure 4.9 Hourly Residence Times of Air Masses in Wind Sectors

4.2.3. Cluster Analysis

If they are properly associated with concentrations, back trajectories adds geographical information to concentration data. As pointed before trajectories are the paths followed by air masses before they are intercepted at our station. Back trajectory calculations involve sophisticated modeling and include data from every single rawinsonde station in Europe, parts of Africa and Asia. Because of such high input data requirement, it was not practical to run the model in our own computers. Thus, the model was run at NOAA computer system and only outputs were transferred to our computers. The model used for this purpose is HYSPLIT, which is a three-dimensional model developed at Air Resources Laboratory in National Oceanic and Atmospheric Administration (NOAA) (Draxler & Hess, 1997; 1998). In this study trajectories were calculated for five days backwards in time. Every day three separate trajectories were calculated at three starting altitudes (at 100 m, 500 m and 1500 m). Starting time of every trajectory was 12:00 noon and they were calculated for 5 days backward in time. Trajectories were consisted of 120 hourly segments and each segment consisted of x, y and z (latitude, longitude and altitude) coordinates. Every day 3 back trajectories (at three starting altitudes) and 120x3 = 360 trajectory segments

are computed. Since trajectory calculation continued for 13 years, a total of 14000 back trajectories and $1.7x10^6$ trajectory segments are generated.

All of these trajectory and segment data were used in flow pattern studies, such as flow climatology and cluster analysis, which are independent of measured concentrations. However, only trajectories and segments computed in sampling days were used in trajectory statistics, such as potential source contribution function calculations, because trajectory segments are linked to measured concentrations in PSCF. That group included 302 days, 906 trajectories and 108000 trajectory segments.

When there are few trajectories, they can be visually inspected to relate geographical information with concentrations. However visual inspection is out of question when there are approximately 14 000 trajectories. In such a case one uses statistics to group trajectories with similar characteristics. In this study cluster analysis, which is a multivariate technique that separates trajectories into groups (clusters) depending on their curvature characteristics (Kumar & Verma, 2016; Anil, et al., 2017; Brankov, et al., 1998, Bruno, et al., 2011, Cheng, et al., 2013) was used. TrajStat software was used to form the clusters from the calculated trajectories. The software uses a hierarchical method (Ward, 1963) to combine the closest trajectories. An Euclidean distance formula, which is given in Equation 4.2, was used to calculate the distance between two back trajectories (Wang, 2008);

$$d_{12} = \sqrt{\sum_{i=1}^{n} \left(\left(X_1(i) - X_2(i) \right)^2 + \left(Y_1(i) - Y_2(i) \right)^2 \right)} \tag{4.2}$$

Where d_{12} distance between trajectories 1 and 2, X_1 (Y_1) and X_2 (Y_2) are reference back trajectories 1 and 2, respectively. Trajectories with all three starting altitudes were included in cluster analysis (Dorling, et al., 1992; Brankov, et al., 1998).

A two-step approach was used to determine optimum number of clusters. First, number of clusters were incremented from 3 to 20 and root-means-square-deviation was calculated for each case. Variation of RMSD with number of clusters is depicted in Figure 4.10. Five percent was chosen to be the threshold value for TRMSD (Brankov, et al., 1998). The cluster number that is before exceeding the 5% threshold value is suggested to be chosen as the optimum number of clusters, which in this study corresponds to either 6 or 10 clusters. In the second step cluster centroids were inspected, which indicated that in 6-cluster solution cluster 6 was generated by splitting cluster 5 and centroids of these two clusters were very close to each other. This split does not give more information than the 5-cluster case. Consequently, the 5-cluster solution was selected as optimum.

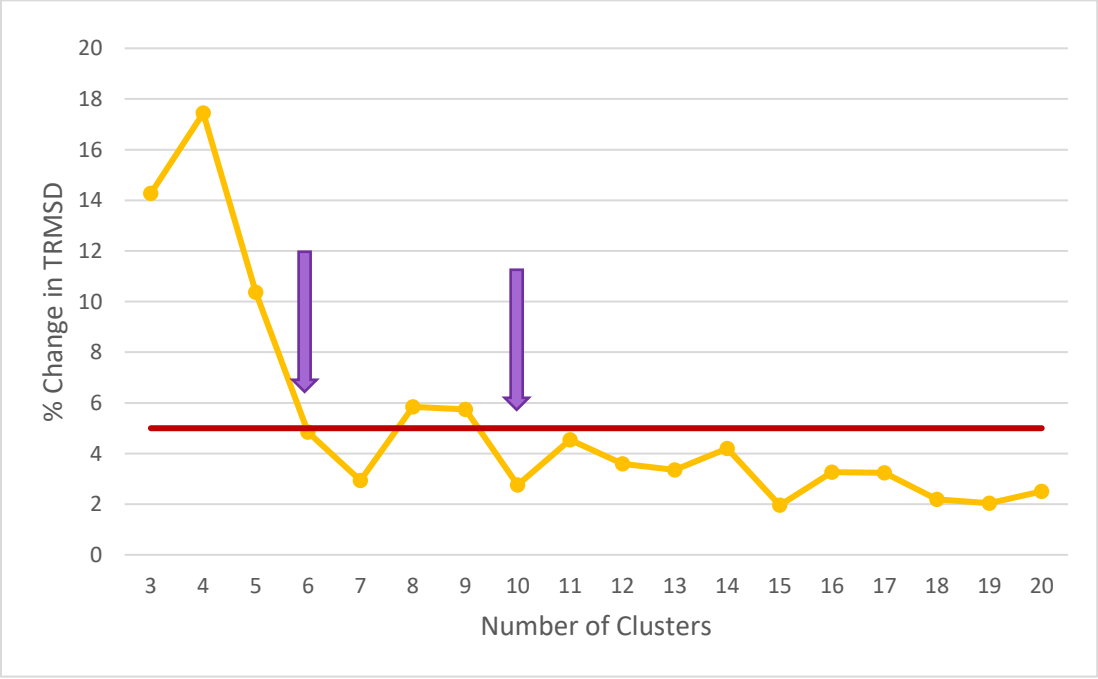

Figure 4.10 The Percentage Change in TRMSD to Cluster Numbers

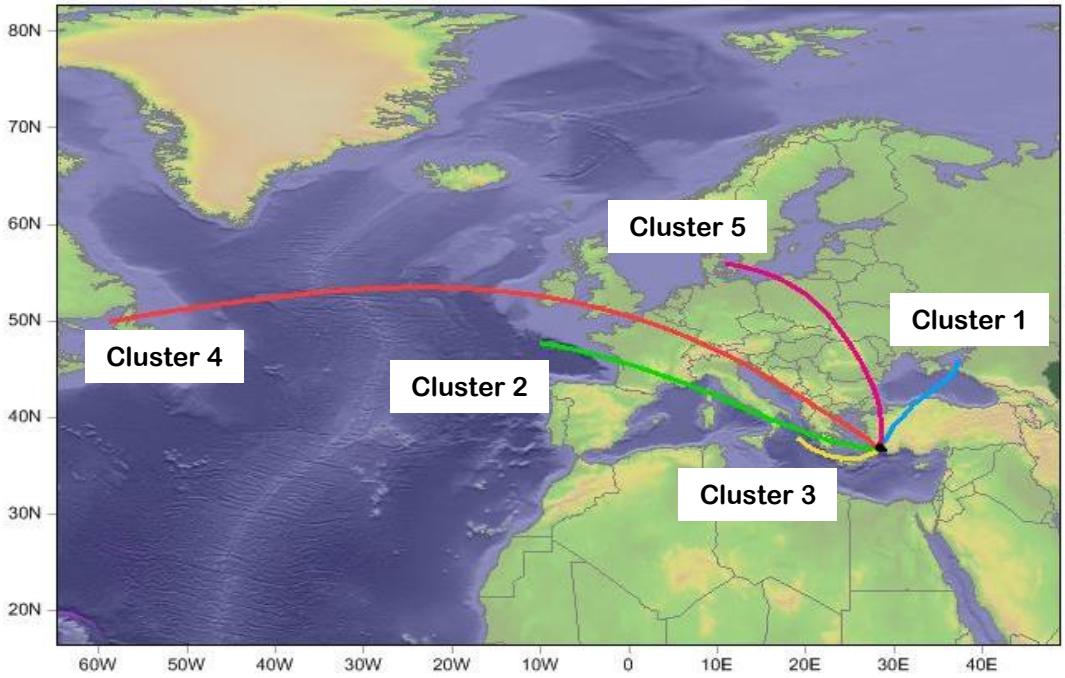

Figure 4.11 Cluster Centroids of Clusters Calculated for Combined Trajectories

Table 4.2 Number and Percentage of Trajectories Allocated in Each Cluster

Cluster	Trajectory Number	Ratio
1	4784	33.6 %
2	3031	21.3 %
3	3384	23.8 %
4	706	5.0 %
5	2342	16.4 %

The cluster centroids and trajectories associated with each cluster are given in Figure 4.11 and Table 4.2 respectively.

In this work, we also computed residence times of air masses with altitude lower than 500 m for each cluster. All trajectories that are intercepted and segments associated with them are assigned equal probability to pick up pollutants when they cross over a source area. However, this assumption is not entirely correct. Trajectory segments that cross a source area at 3000 m altitude cannot have the same probability of picking up of pollutants emitted at the surface with a segment crossing the same area at 200 m altitude. This is the logic behind computing residence times of low-lying ($z < 500$ m)

air masses (segments). In source apportionment part of this thesis we adopted a more sophisticated approach and weighted the influence of segments based on their altitudes. However, in clusters we only computed residence times of low-lying segments to obtain some information about potential source areas affecting clusters.

Distribution of residence times of segments with $z < 500$ m are given in Figure 4.13.

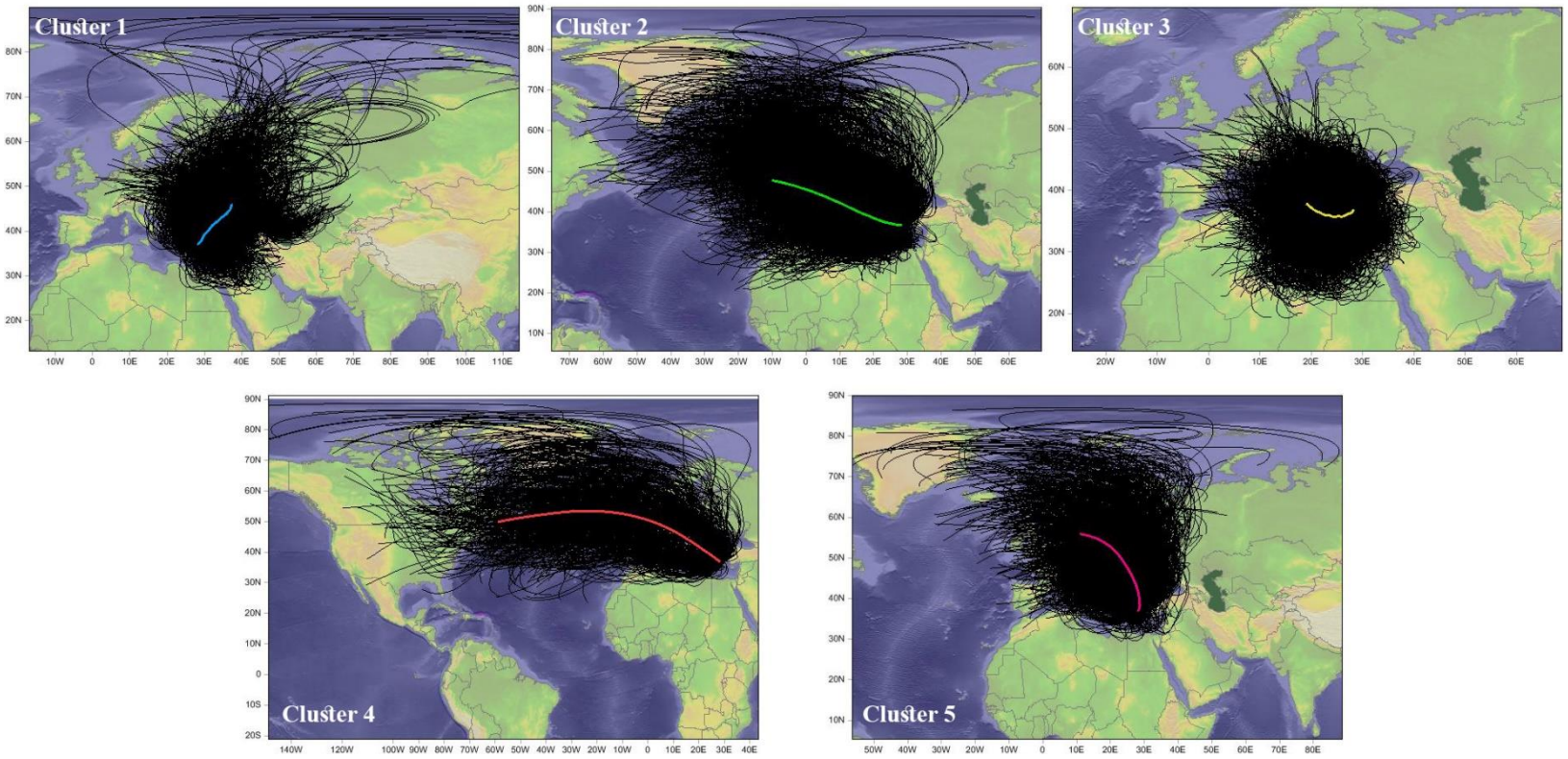

Figure 4.12 Trajectories Allocated to Different Clusters

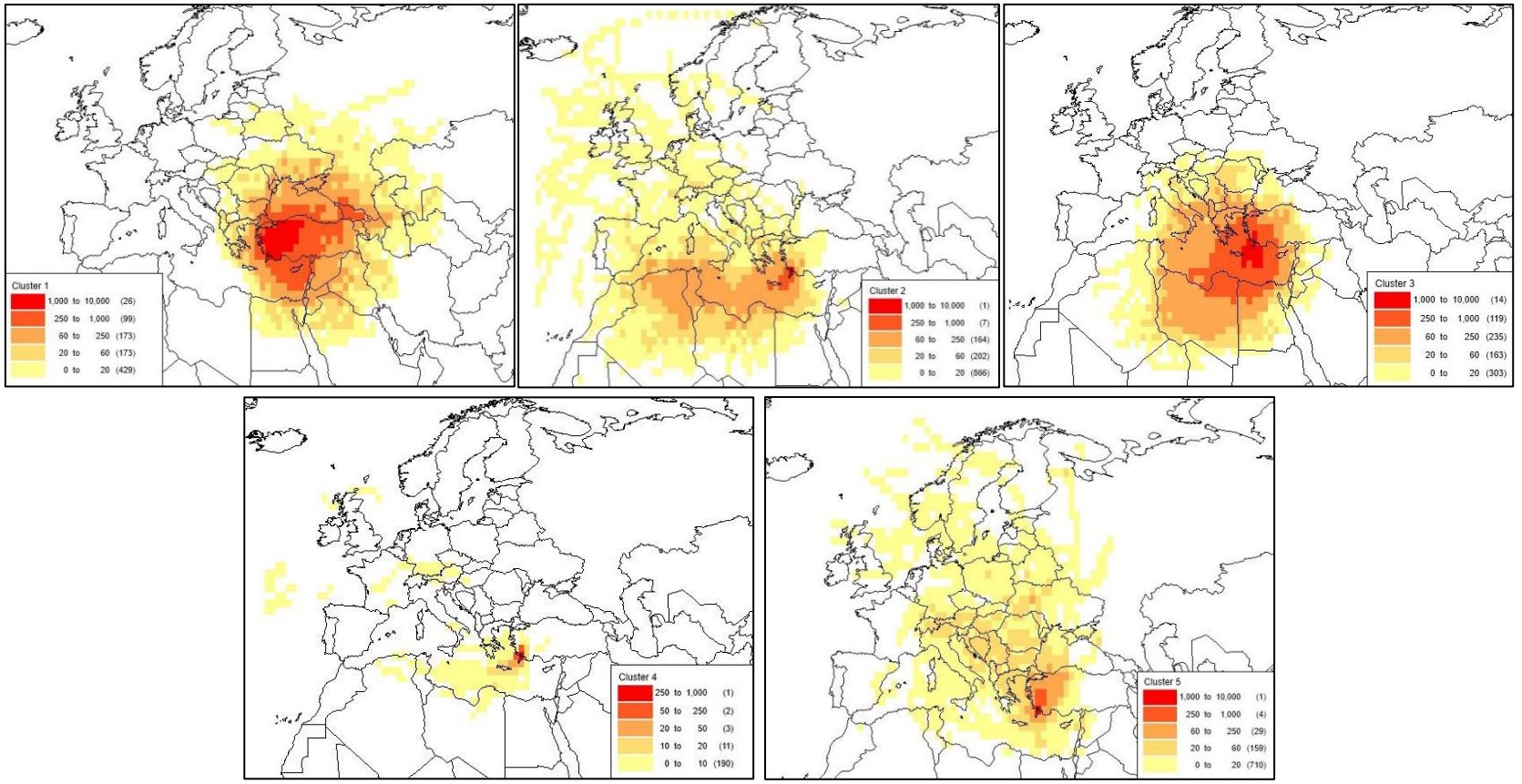

Figure 4.13 Residence Times of Air Parcels below 500 m for each Cluster

Cluster 1 represents flow from NE sector. Since Balkan countries, Eastern European Countries and some of the industrialized western European countries are in this sector, one can expect these trajectories carry pollution to Eastern Mediterranean basin. Trajectories in cluster 1 accounts for approximately 34% (approximately 4700 trajectories) of all computed trajectories. Distributions of low-lying segments demonstrate that Sources from which emissions can be transported to our site with trajectories in this cluster are relatively local. Western part of Turkey Balkan countries, countries in the Middle East and northern bank of the Black Sea are impact areas for cluster 1.

Please note that transport of pollutants from a certain grid depends on (1) frequency of air mass transport from that grid and (2) magnitude of emissions in that grid. High residence times of low-lying segments shown in Figure 4.13 for five clusters indicate that frequency of air mass transport at $z < 500$ m are frequent from these grids, but it does not include any information about emissions in those girds. However, since grids with high residence times of low-lying segments for cluster 1 are all industrialized regions, (Western Turkey, Ukraine, Israel, Balkan countries) and it accounts for 36% of all trajectories, this cluster can be the most important one in terms of pollution transport to Eastern Mediterranean atmosphere.

Cluster 2 includes trajectories originating from west and having moderate length. Primary impact areas for this cluster can be in France, Italy and Greece. Since trajectories in clusters are not on the cluster centroid all the time and shows a distribution around the centroids, other source areas in Europe also can contribute to pollution transport by trajectories in this cluster. Residence times of trajectory segments with $z < 500$ m in Figure 4.13 demonstrate that grids with long residence time of low-lying segments of cluster 2 trajectories are on the Mediterranean Sea itself and grids on the north Africa, particularly Tunisia and Algeria. This distribution of residence times suggests that cluster 2 can bring litophilic and marine species to our station, but its contribution to pollution transport to Marmaris area is probably not very likely.

Cluster 3 consisted of very short trajectories. Its centroid is toward west, but it is very short. The short nature of trajectories in this cluster also reflects to residence times of low segments. Cluster 3 has high residence times of low-lying segments near the sampling location. High residence times are observed on the Mediterranean Sea itself, Crete, Aegean part of Turkey, Libya, Egypt and southern parts of Greece. Cluster 3 is an important contributor to rain water chemistry at Marmaris as it includes approximately 24% of all trajectories.

Cluster 4 is an interesting one. It only includes very long trajectories, representing unusually fast-moving air masses. These air masses, in five days (length of our trajectory calculations), travel from North America (US and Canada) to our receptor. It is shown that these air masses can bring emissions from boreal forest fires in Canada to Europe (Forster, et al., 2001; Schreier, et al., 2014; Sigler, et al., 2003). Similar clusters having long trajectories starting at North America was also observed as a component in Eastern and Western Black Sea Aerosols (Genç Tokgöz & Tuncel, 2015; Balcılar, et al., 2018). It is not easy to differentiate pollution levels coming from North America, because these trajectories crosses Europe before they are intercepted at our station. They probably pick up pollutants emitted from source areas in Europe on their way to Eastern Mediterranean. There are no grids with high residence times of trajectory segments with $z < 500$ m., indicating that these are high trajectories, which advect to surface near the station. Cluster 4 accounts for approximately 5% (700 trajectories) of the computed trajectories.

Cluster 5 can be named as “European” cluster. It represent transport from NW sector. Most of the trajectories associated with this cluster are on European they spent more time on Eastern European countries. Trajectories in this cluster accounts for 16% (approximately 2300 trajectories) of total trajectories. Residence times of low segments are high in western Turkey and distributed uniformly in Balkan countries and central European countries. Residence times are relatively small in distant countries (countries on the Atlantic coast).

Median concentrations of measured ions in each cluster are given in Table 4.3. Hydrogen ion concentration does not change significantly between clusters. Please note that H^+ ion concentration depends not only on the concentrations of acidifying ions (SO_4^{2-} and NO_3^-), but also on concentrations of bases in rainwater ($CaCO_3$ and NH_3), particularly $CaCO_3$ in this work. This means H^+ concentration in clusters depends on relative abundances of acidifying and neutralizing species in that cluster. When all these factors are combined H^+ ion concentrations do not change much among clusters. Although concentrations of SO_4^{2-} and NO_3^- ions, which accounts for all free H^+ ion are not same in all clusters, pH of rainwater does not show a parallel distribution.

All ions measured in this study have higher concentrations in cluster 4. This is interesting because, as discussed previously in this manuscript, cluster 4 includes very long trajectories starting from North America. As pointed before, it is not easy to associate these high concentrations to long-range transport from USA or Canada, because these same trajectories cross whole Europe before they reach to Eastern Mediterranean basin. Consequently, high concentrations of pollution-derived ions in this cluster can originate from distant sources beyond the Atlantic Ocean or in Europe. It should be noted that although concentrations of pollution-derived ions are high in cluster 4, it does not mean that contribution of cluster 4 to rainwater chemistry in Eastern Mediterranean is the highest, because cluster 4 accounts for only 5% of the total number of trajectories, indicating that frequency of air mass movement from these source areas, which results in high concentrations of ions in cluster 4, to Eastern Mediterranean region is not frequent.

There are also few other patterns observed in clusters other than cluster 4. Concentrations of sea salt elements, namely Na^+ and Cl^- are higher in clusters 2 and 3, probably because trajectories included in these clusters spent more time over the Mediterranean Sea, than trajectories in other clusters. This can be seen in Figure 4.13, where residence times of low-lying trajectory segments are shown. Ions with anthropogenic origin, namely SO_4^{2-}, NO_3^- and NH_4^+, have slightly higher median concentrations in cluster 1. This is not surprising, because trajectories in cluster 1

brings pollutants from western parts of Turkey, Balkan countries, Ukraine and Black Sea coast of Russia, which are well-documented source regions in this region.

Table 4.3 Median Concentrations of Measured Species (mg/L)

	Cluster 1	**Cluster 2**	**Cluster 3**	**Cluster 4**	**Cluster 5**
H^+	0.001	0.0008	0.001	0.0008	0.001
SO_4^{2-}	1.786	1.618	1.363	2.830	1.554
NO_3^-	0.992	0.632	0.600	1.048	0.555
Cl^-	0.770	3.042	1.335	4.981	1.261
NH_4^+	0.189	0.130	0.130	0.201	0.105
Ca^{2+}	0.929	0.858	0.672	1.510	0.716
Mg^{2+}	0.222	0.368	0.212	0.497	0.254
K^+	0.094	0.121	0.094	0.210	0.130
Na^+	0.666	2.148	1.120	2.460	0.736

4.3. Ionic Composition of Wet Deposition

4.3.1. Ion Balance

The scatterplot of Σanions vs Σcations is given in Figure 4.14. Average Σanion -to-Σcation ratio at our station is 0.72 ± 0.57 (median 0.65), indicating approximately 30% deficiency in anions, compared to total cation equivalent concentration. The deficiency is due to HCO_3^- ion, which was not measured in this study. Similar deficiency in anion concentration in most of the rainwater studies in the Eastern Mediterranean region (Al-Momani, et al., 1998; Işıkdemir, 2006).

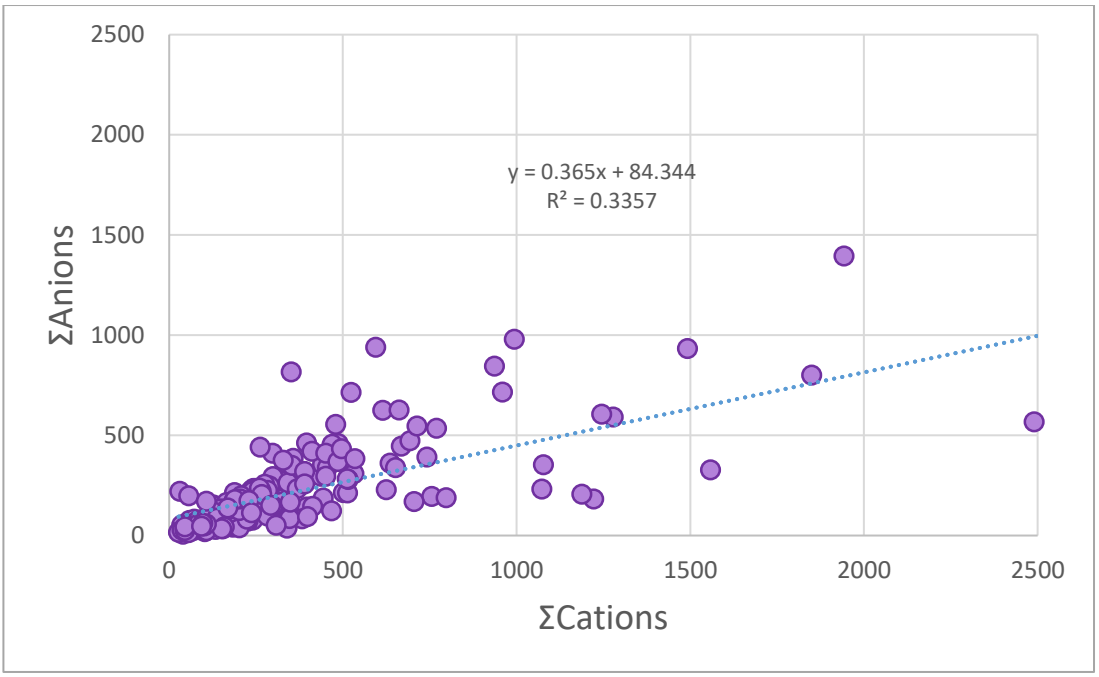

Figure 4.14 Scatterplot of Equivalent ΣCations to Equivalent Σanions

4.3.2. Contributions of Ions to Total Ion Mass

Mass contributions of the ions measured in this work to total ionic mass is given in Figure 4.15. From the pie chart, it is seen that the ions that contributes most to the total ion mass are Cl^- (25%), SO_4^{2-} (22%), Na^+ (18%), Ca^{2+} (14%) and NO_3^- (11%). These four ions account for 90% of total ion mass. Sulfate and NO_3^- ions, which are secondary inorganic anions, accounts for a large fraction of ionic mass in most studies (Al-Khashman, 2009; Huang, et al., 2010; Arsene, et al., 2007). High contribution of Na^+, and Cl^- ions to Σion mass is due to proximity of the station to the Mediterranean coast (approximately 10 km).

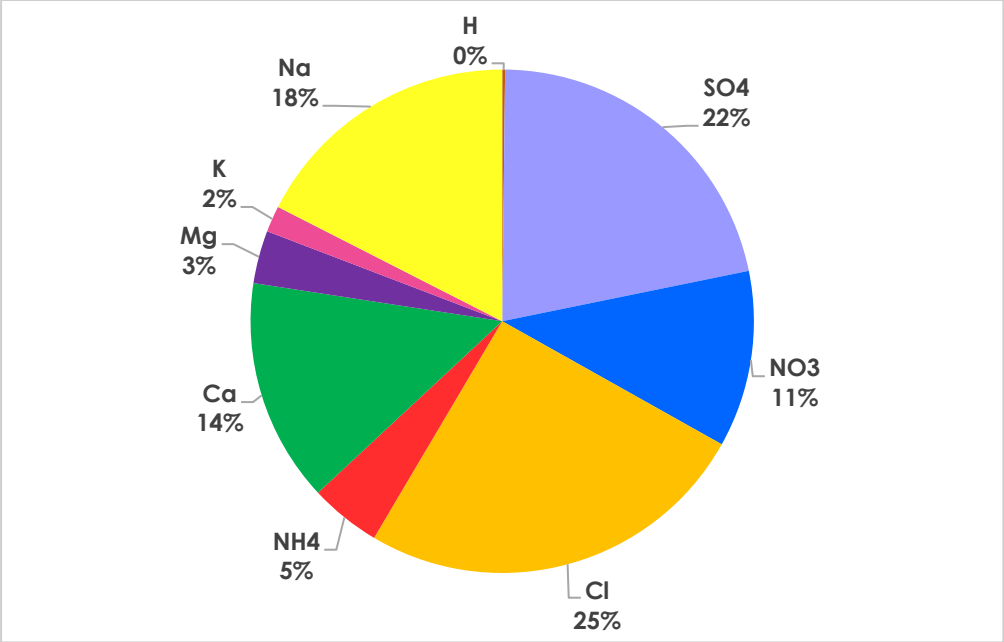

Figure 4.15 Contribution of Ions Measured in This Work to Total Ion Mass

Since our station is under strong influence of sea salt, some of the ions, which are known as "crustal" can have a significant contribution from sea salt in this work. To find out sea salt contribution to measured concentrations of ions, we calculated sea salt fractions of ions using the following relation (Equation 4.3):

$$X_{seasalt} = X_{sample} - \left(\frac{Na_{sample} * X_{seasalt}}{Na_{seasalt}}\right) \quad (4.3)$$

Where $X_{seasalt}$ is the seassalt contribution to the concentration of an specie X

X_{sample} is the concentration measured for the specie X

$X_{seasalt}$ / Na_{sample} is a ratio of specie to Na ion

Na_{sample} is concentration measured for sodium ion

All units in the formula are mg L^{-1}.

Based on this computation, 21% of the measured SO_4^{2-} concentration, 44% of the measured K^+ concentration, 6% of the measured Ca^{2+} concentration and 70% of the measured Mg^{2+} concentration originate from sea salt.

Long-term (interannual) variation in contribution of ions to total ion mass between 2011 and 2016 are given in Figure 4.16. The most striking point in the figure is approximately 10% decrease in contribution of SO_4^{2-} ion (from 35% in 2011 to 23% in 2016), which indicates the success of actions taken to reduce SO_2 emissions in Turkey and in Europe as a whole.

Contributions of other ions (both anthropogenic and natural) did not change significantly during sampling period. The only exception to this is the increase observed in Na contribution from 11% in 2011 to 19% in 2016. This increase probably an artifact to compensate the decrease in SO_4^{2-} contribution.

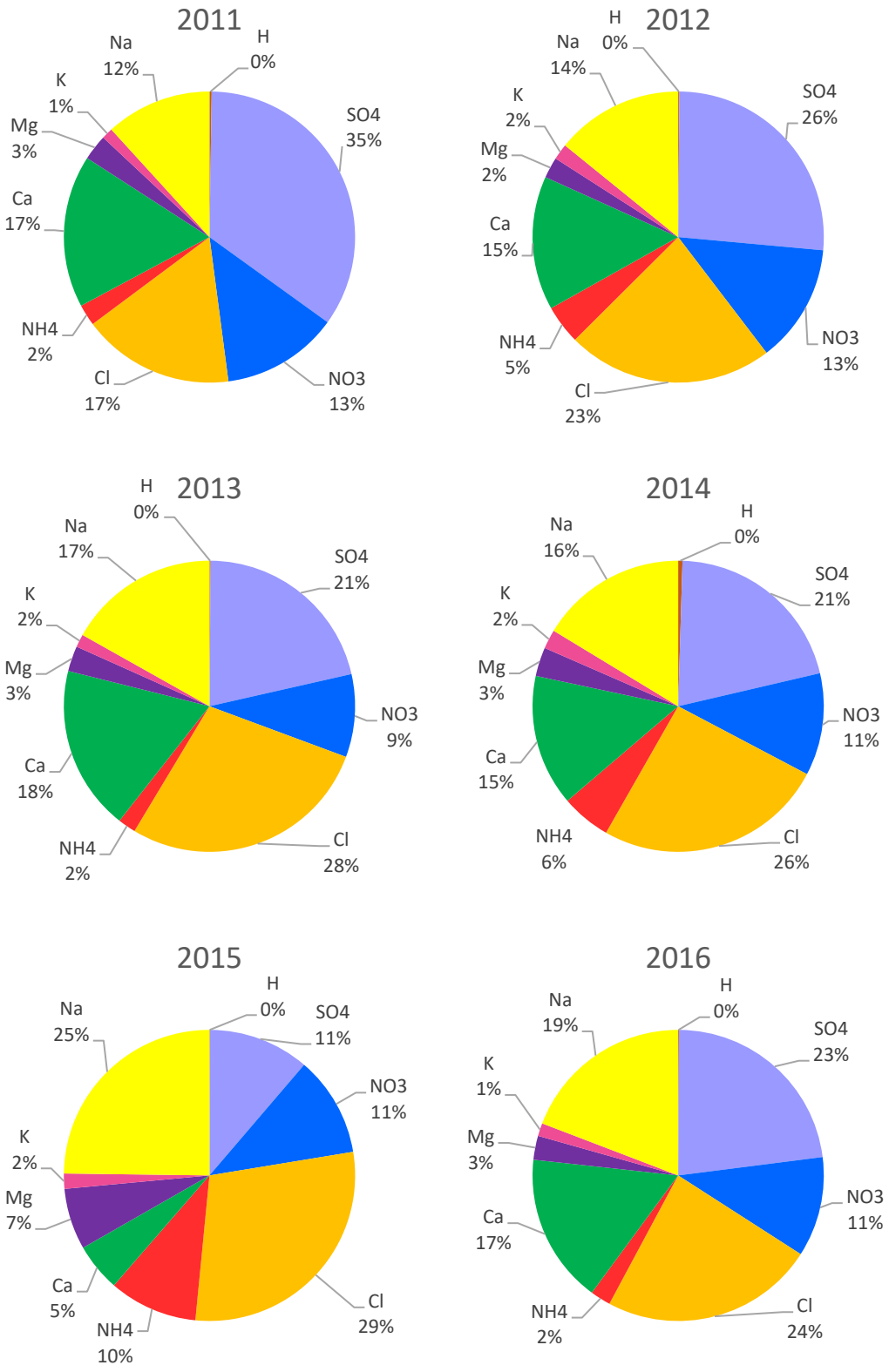

Figure 4.16 Variation of Ionic Contribution to Total Ionic Mass in Time

Seasonal changes in the contribution of ions to the total ion mass is given in Figure 4.17. Contributions of anthropogenic ions, SO_4^{2-} and NO_3^-, do not change significantly from one season to another. Contributions of ions, which originate from the sea, namely Na^+ and Cl^- are higher in winter months, due to increased production of sea salt with stronger winds and longer windy periods winter season. On the contrary, crustal ions Ca^{2+}, Mg^{2+} and K^+, have higher contributions to total ion mass during summer months; due to easier resuspension of dry soil in summer. In winter, soil is mostly wet (mud), hence resuspension of the soil particles to the atmosphere is more difficult.

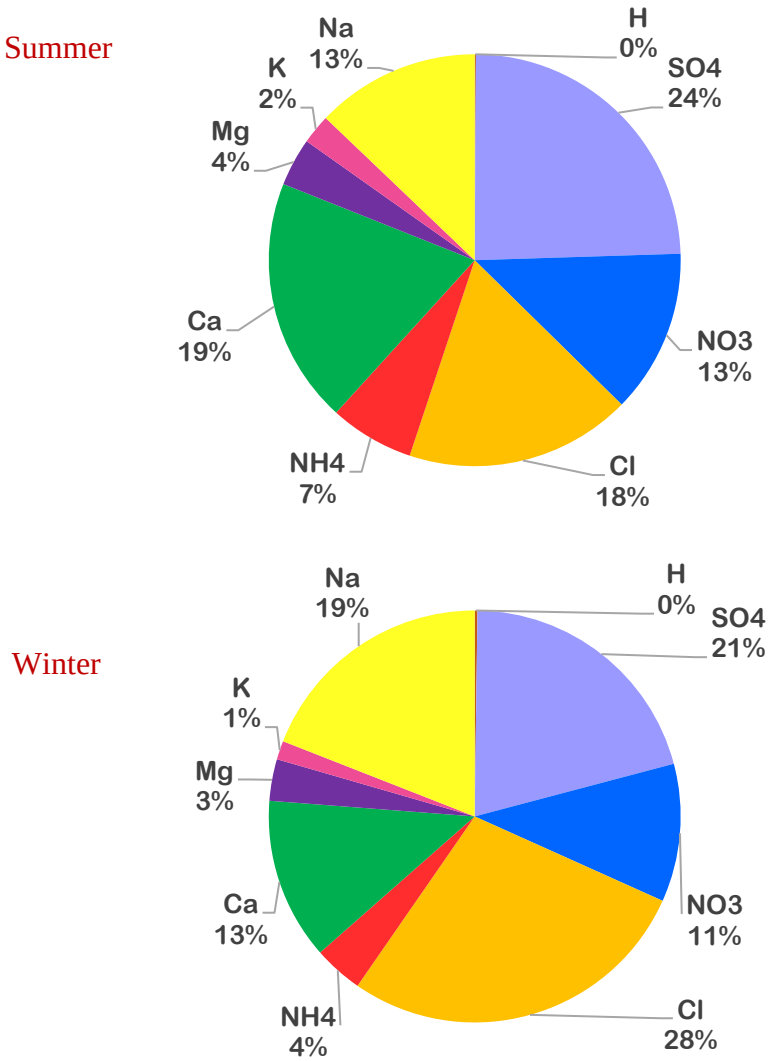

Figure 4.17 Seasonal Variation in Ionic Contributions to Total Ion Mass

4.4. Acidity of Wet Deposition

As pointed out in earlier sections, SO_4^{2-} and NO_3^- measured in Eastern Mediterranean rainwater is among the highest measured in entire Europe, suggesting that pH should be low as these the ions are the main source of acidity in wet deposition. However, high pH of rainwater in Eastern Mediterranean atmosphere is also well documented in literature (Al-Momani, et al., 1995; Özsoy, et al., 2008). This apparent dilemma is due to extensive neutralization of acidity in rainwater and will be discussed in this section.

4.4.1. pH of Rainwater

Annual, summer and winter frequency distribution of pH are given in Figure 4.18. The pH values measured during the study varies between 3.7 and 7.9 with a median value of 6.0. Since pH of a very clean rainwater varies between 5.0 and 5.6 due to dissolution of CO_2 and presence of natural SO_2 in atmosphere, only, rain with pH < 5.0 is considered as acid rain (Jacob, 1999). Although relatively low pH values, such as 3.7, were measured in some of the rainwater samples, only 17% of rain samples have pH < 5 and can be considered as "acid rain". Remaining 83% of all samples collected at Marmaris station had pH > 5.0 and cannot be considered as "acid rain". This general pattern can also be seen in pH frequency histograms given in Figure 4.18. Approximately 40% of pH data occurs between 5.5 and 6.5, 70% of data occurs between pH 5 and 7, on an annual basis. There are some differences between summer and winter histograms as well. There is a shift in frequency of occurrences toward higher pH's in summer. Approximately 44% of pH data occurs between pH's 5.5 and 6.5 in winter histogram, whereas 55% of pH data is between pH 6 and pH 7 in summer, indicating more extensive neutralization during summer season.

Monthly variation in pH values are given in Figure 4.19. There is a clear pattern of higher pH values in summer. Observed seasonal behavior is also due to more extensive neutralization of acidity in summer season, because SO_4^{2-} and NO_3^- concentrations are higher during summer season and if free acidity originates from H_2SO_4 and HNO_3, H^+ ion concentration should also be higher in summer.

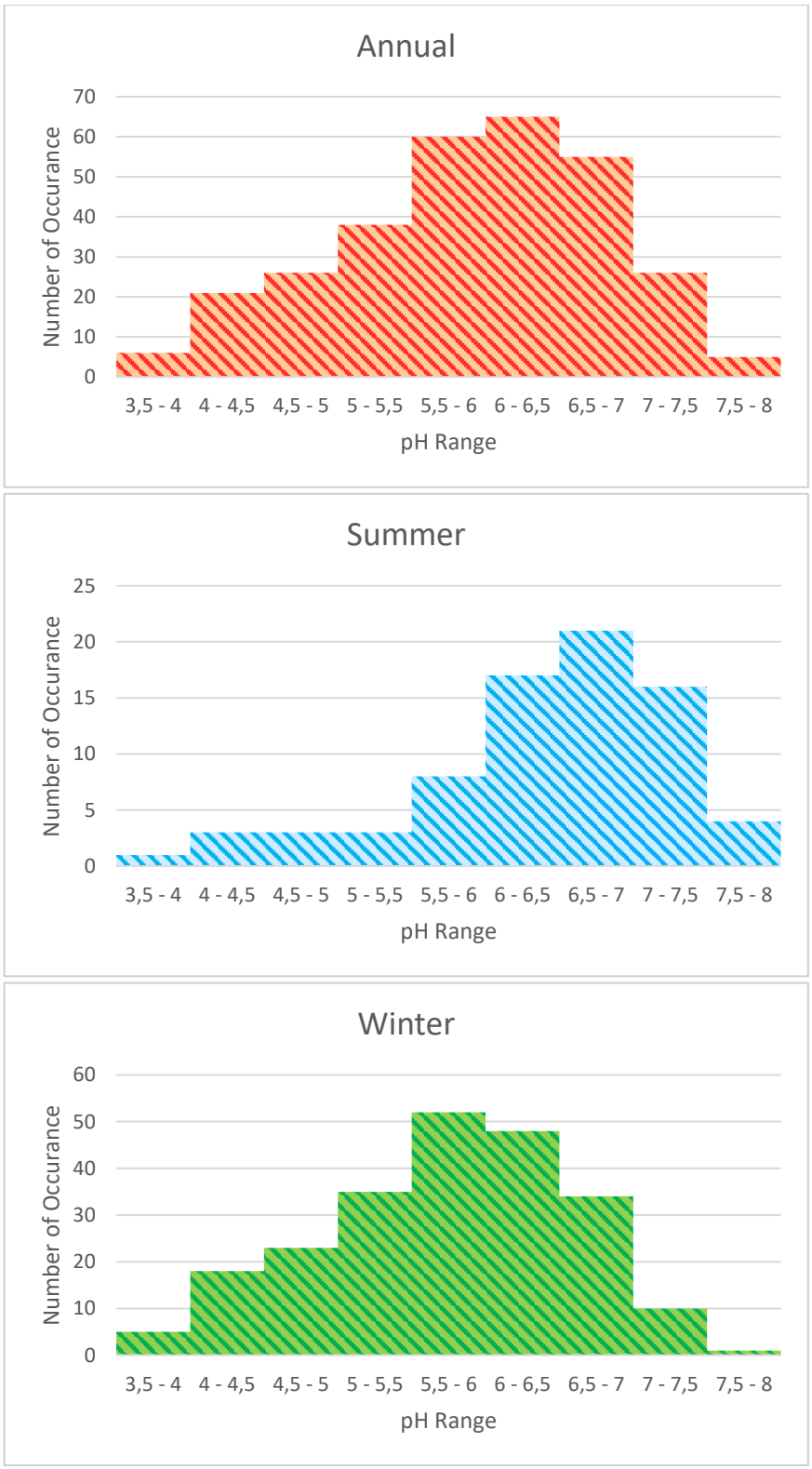

Figure 4.18 pH Frequency Distributions in Marmaris Rainwater

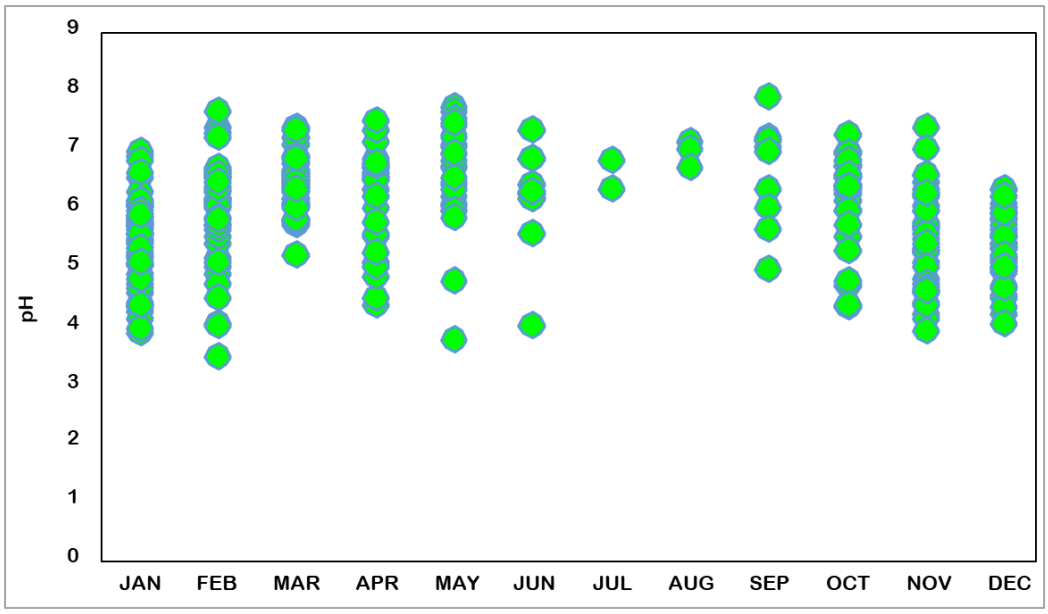

Figure 4.19 Monthly Variation of Rainwater pH at Marmaris

4.4.2. Neutralization of Rainwater

All pH measurements in Marmaris rainwater, which were discussed in previous paragraphs demonstrate two basic facts; (1) SO_4^{2-} and NO_3^- concentrations are high Marmaris rainwater, but (2) H^+ ion concentration, which is expected to be correlated with these two anions is very low. These two facts suggest that majority of H^+ concentration in rain is neutralized by bases that are available in Marmaris atmosphere.

Seasonality of the neutralization process was tested by calculating monthly median equivalent ratio of $H^+/(SO_4^{2-}+NO_3^-)$. If the free acidity (H^+ ions) that comes from H_2SO_4 and HNO_3 is not neutralized the ratio is expected to be unity. As H^+ ions are neutralized, the ratio deviates from unity and it becomes zero when all H^+ are neutralized. Monthly median $H^+/(SO_4^{2-}+NO_3^-)$ ratios are depicted in Figure 4.20. The figure highlights two important points: (1) more than 85% of hydrogen ions in Marmaris rainwater is neutralized throughout the year, (2) neutralization is more complete during summer season. The ratio is approximately 0.12 in January and December, indicating that 88% of acidity is neutralized in these months, but there is almost no free hydrogen ion in rainwater from May through September.

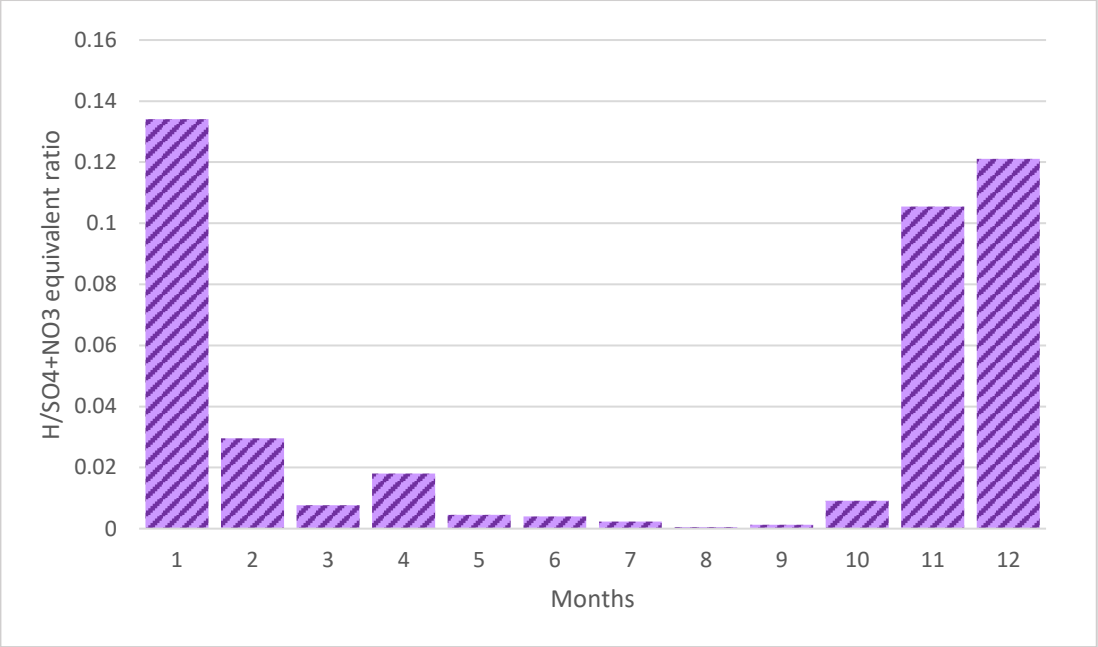

Figure 4.20 Seasonal Variation of $(H^+)/([SO_4^{2-}] + [NO_3^-])$ Ratio

The next question that should be answered is, "what neutralizes acidity in rainwater"? There are two bases that can neutralize acidity in rain water, namely, NH_3 and $CaCO_3$. Main sources of NH_3 in atmosphere is fertilizer applications in agriculture (Pan, et al., 2018; Personne, et al., 2015) and animal grazing (Behera, et al., 2013). Dominant source of $CaCO_3$ is the soil. Since soil in the Mediterranean region (not only along Turkish coast, but throughout the Mediterranean basin) is highly enriched with $CaCO_3$ (Federoff & Courty, 2013; Aydınalp & Cresser, 2008), $CaCO_3$ is the likely base which is responsible from high pH in Eastern Mediterranean rainwater. This can also be seen in Figure 4.21, where hydrogen ion concentration is regressed against Ca^{2+} and NH_4^+ ions. Stronger correlation between hydrogen ion and Ca^{2+} is clear in the figure.

High pH of rainwater is not unique for this work. It is observed in most rainwater studies performed in the Eastern Mediterranean region (Al-Momani, et al., 1995; Alagha & Tuncel, 2003; Morales-Baquero, et al., 2013; Özsoy, 2003).

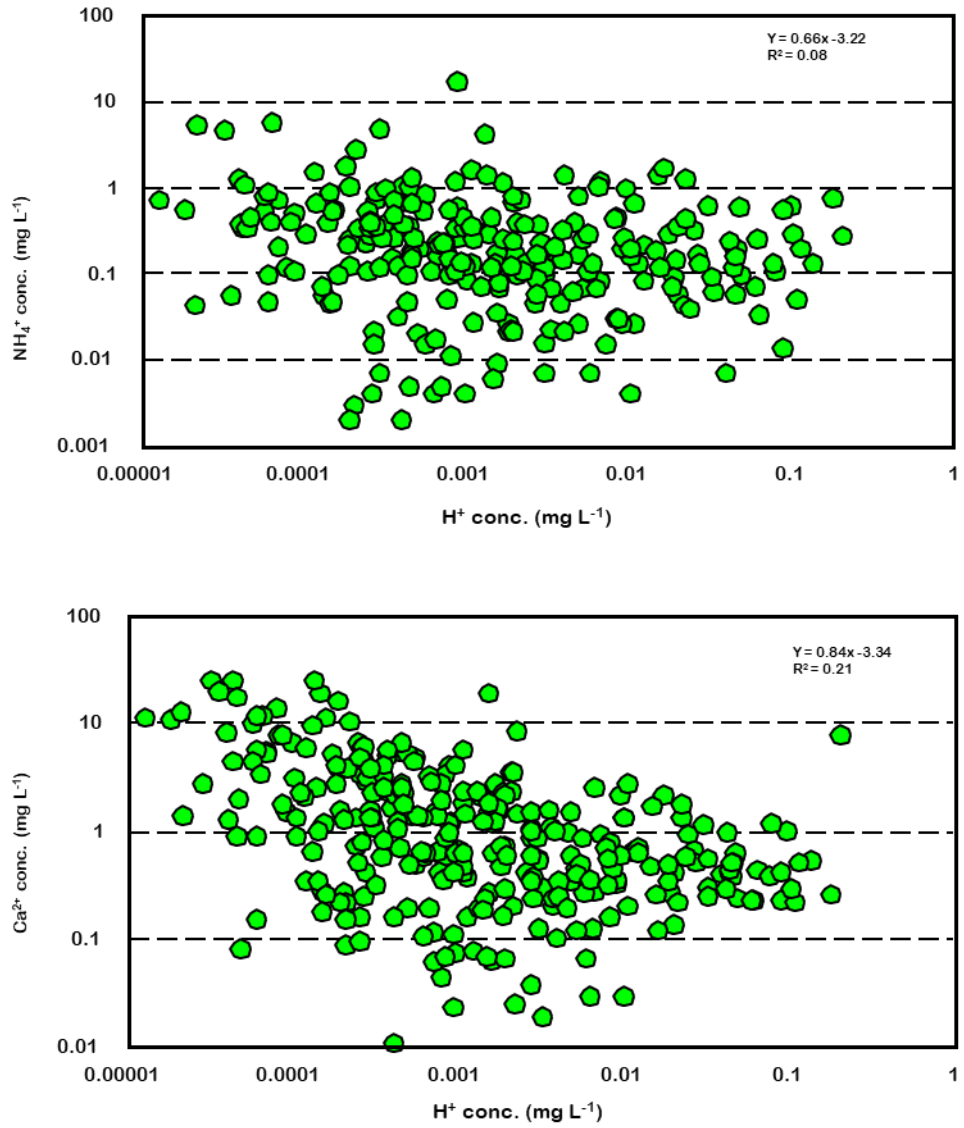

Figure 4.21 Relation between H^+ ion vs. NH_4^+ and Ca^{2+} ions

4.5. Temporal Variations

Seasonal variations in pollutant concentrations refer to short term episodes, diurnal variations, weekend-weekday variations, seasonal variations and interannual variations. These information can be very informative to determine factors controlling variability in concentrations of pollutants in urban atmosphere. However, in rural atmosphere seasonal variations and interannual variations are the only types of temporal variations that can be discussed.

4.5.1. Seasonal Variations in Ion Concentrations

Seasonal variations in concentrations of ions is generally due to variations in meteorology, such as higher mixing height in summer, or seasonal variations in transport patterns. Selection of geographical seasons may not be the best selection, because it can mask some of the factors that controls seasonal variability in ion concentrations. In this study seasons are selected based on rainfall data, because variations in concentrations of ions and other particulate pollutants in rainwater and aerosol is governed by variations in rainfall. Monthly rainfall at Marmaris Station is depicted in Figure 4.22. Rainfall data, consisting of monthly averages between 1926 and 2007 were obtained from Marmaris Meteorological station. Based on this pattern winter was selected as January, February, March, October, November and December, whereas summer included April, May, June, July, August and September months. With this division, approximately 14% of the annual rainfall, which is 1194 mm, occurs in our summer and 86% of annual rainfall occurs in winter, which is typical for the Eastern Mediterranean region.

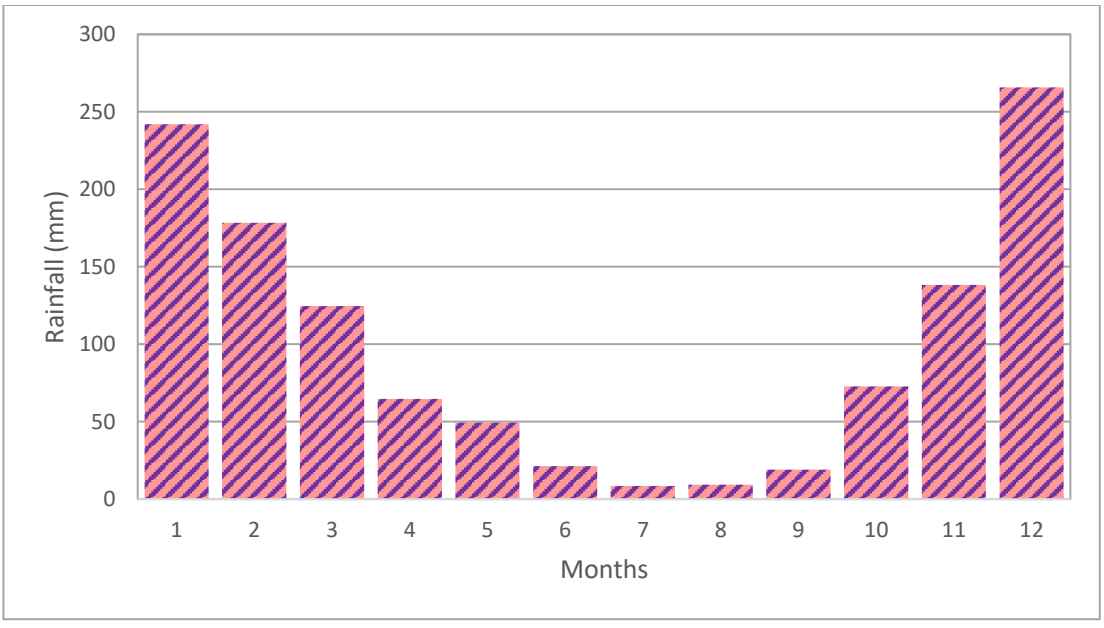

Figure 4.22 Monthly variation rainfall (mm) at Marmaris Meteorology Station

Monthly median concentrations of ions are given in Figure 4.23 and Figure 4.24. Ions depict two different patterns, which is determined by four different factors. Concentrations of SO_4^{2-}, NO_3^- and NH_4^+ in rainwater is clearly high during summer season. Summer to winter median ratios of these ions are 1.8, 2.3 and 2.7 for NH_4^+, SO_4^{2-} and NO_3^-, respectively.

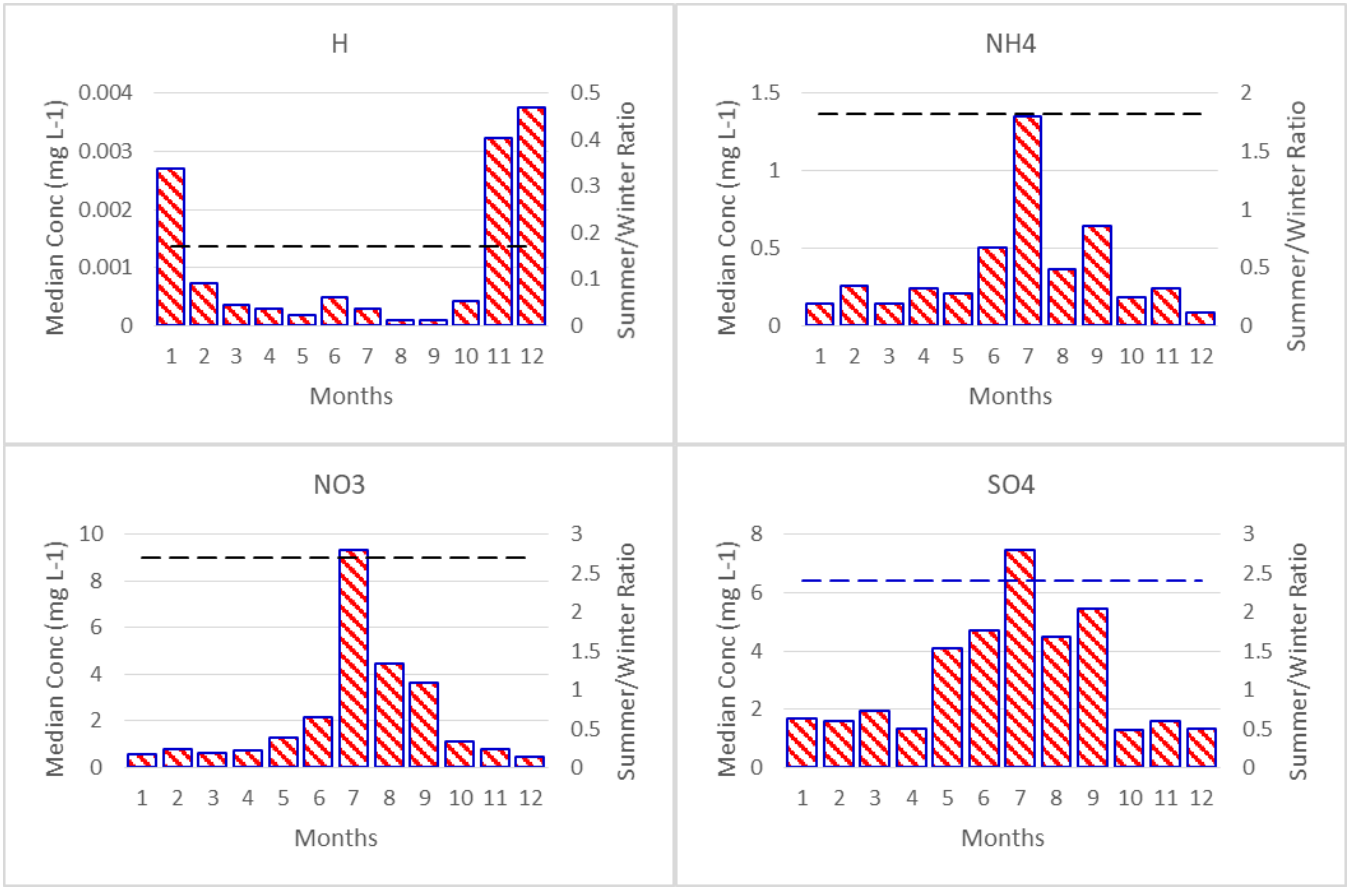

Figure 4.23 Monthly Variation of Ion Concentrations and Summer to Winter Concentration Ratio of Anthropogenic Ions

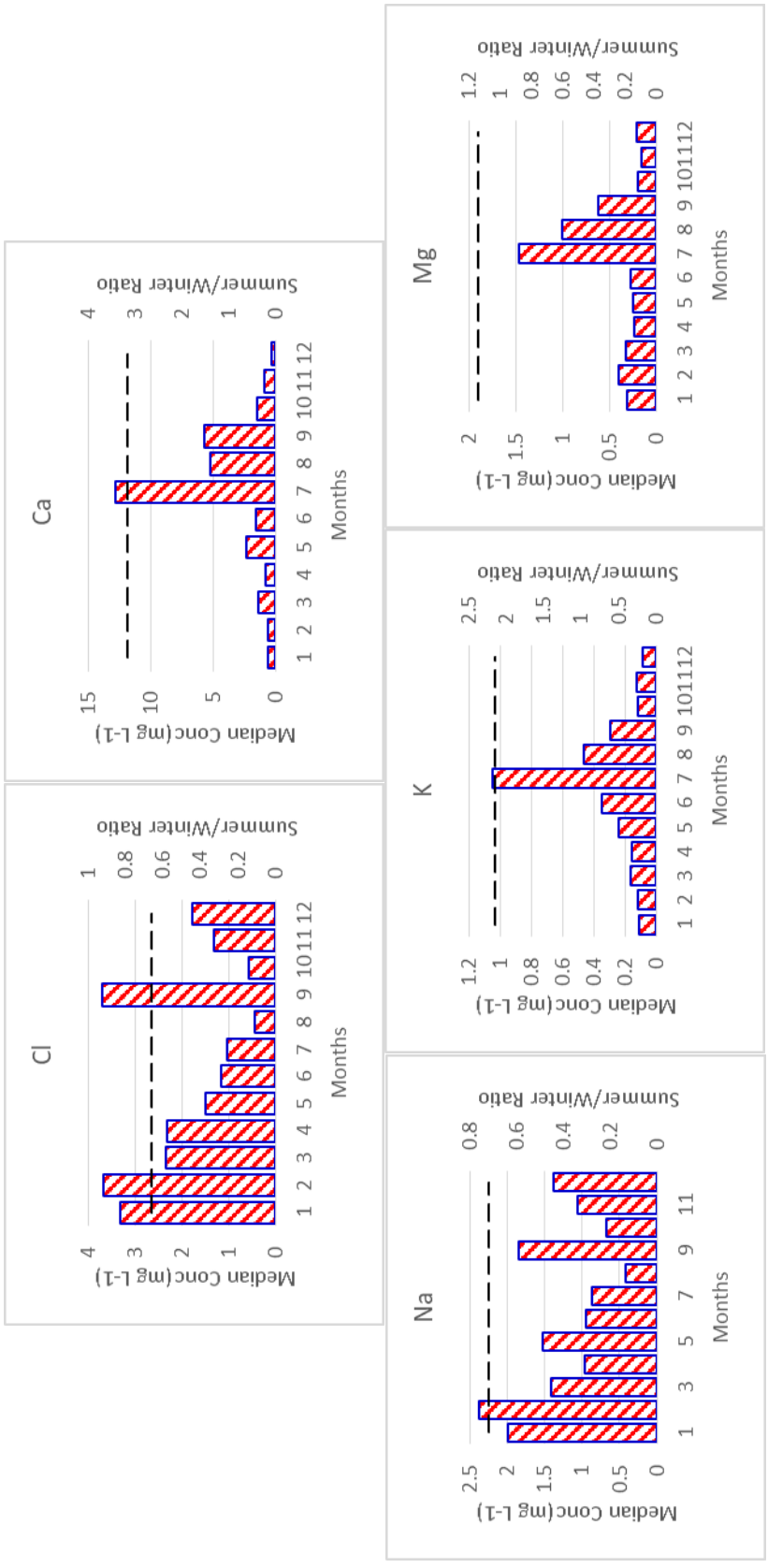

Figure 4.24 Monthly Variation of Ion Concentrations and Summer to Winter Concentration Ratio of Natural Ions

Higher concentrations of these ions, particularly SO_4^{2-} and NO_3^-, in atmosphere during summer months is attributed to faster gas-phase oxidation of SO_2 and NO_2 by more vigorous photochemical activity in summer (Güllü, et al., 1998; Bardouki, et al., 2003; Mihalopoulos, et al., 1997). More effective wet scavenging of particles and ions associated with them during their long-range transport to Eastern Mediterranean atmosphere in winter also contribute to observed higher concentrations of SO_4^{2-}, NO_3^- and NH_4^+ in summer precipitation (Kubilay & Saydam, 1995; Al-Momani et al., 1998; Güllü et al., 2005; Öztürk et al., 2012). For NH_4^+ ion, in addition to faster oxidation in summer and more effective scavenging from atmosphere in winter, enhanced evaporation of NH_3 from applied fertilizers in summer and its subsequent oxidation to NH_4^+ also contribute to its higher summer concentrations (Güllü et al., 1998).

Concentrations of Na^+ and Cl^-, on the other hand, are higher in winter. This is not surprising, because both Na^+ and Cl^- are good indicators of marine aerosol, which forms by bubble-bursting at the sea surface. Sea salt particle that are highly enriched in Na^+ and Cl^- are formed in large quantities by increased storm activity in winter. Higher concentrations of Na^+ and Cl^- in winter aerosol and precipitation samples in not new in this work and reported frequently in literature (Güllü et al., 1998; 2005; Al-Momani et al., 1998; Öztürk et al., 2012)

Like ions with anthropogenic sources, crustal ions, including Ca^{2+}, Mg^{2+} and K^+ have also higher concentrations during summer seasons, but for a different reason. Concentrations of soil related elements and ions in atmosphere depend on efficiency of resuspension of soil particles, which is season dependent. Soil particles cannot become airborne easily in winter, as the surface soil is permanently mud or ice covered. No matter how strong winds are, it is difficult to get the soil particles airborne. However, in summer surface is dry and soil particles can become airborne even with moderate wind speeds. Since Ca^{2+}, Mg^{2+} and K^+ are associated with soil particles, their concentrations are expected to be high in summer.

Hydrogen ion concentrations are much higher in winter and very low in summer. This seasonal pattern is governed entirely by season-dependent neutralization of acidity, which is a local process. High $CaCO_3$ content of soil in in Mediterranean region and how it neutralizes acidity in rain water was discussed in the previous section. Higher atmospheric loading of crustal material (and $CaCO_3$) in summer months results in more extensive neutralization and very low H^+ concentration during summer.

Summer-to-winter concentration ratios of ions measured in this work is depicted in Figure 4.25. Summer-to-winter ratios computed for anthropogenic (SO_4^{2-}, NO_3^- and NH_4^+) and crustal (Ca^{2+}, Mg^{2+}, K^+) ions are > 1.0 and those for sea salt (Na^+, Cl^-) ions and H^+ are < 1.0. Reasons for these patterns were discussed in previous paragraphs. Although summer-to-winter ratio > 1.0 for SO_4^{2-}, NO_3^-, NH_4^+, Mg^{2+}, K^+ and Ca^{2+}, the ratio is not the same for all of them. The highest ratio was computed for Ca^{2+}, which is followed by NO_3^- and SO_4^{2-}.

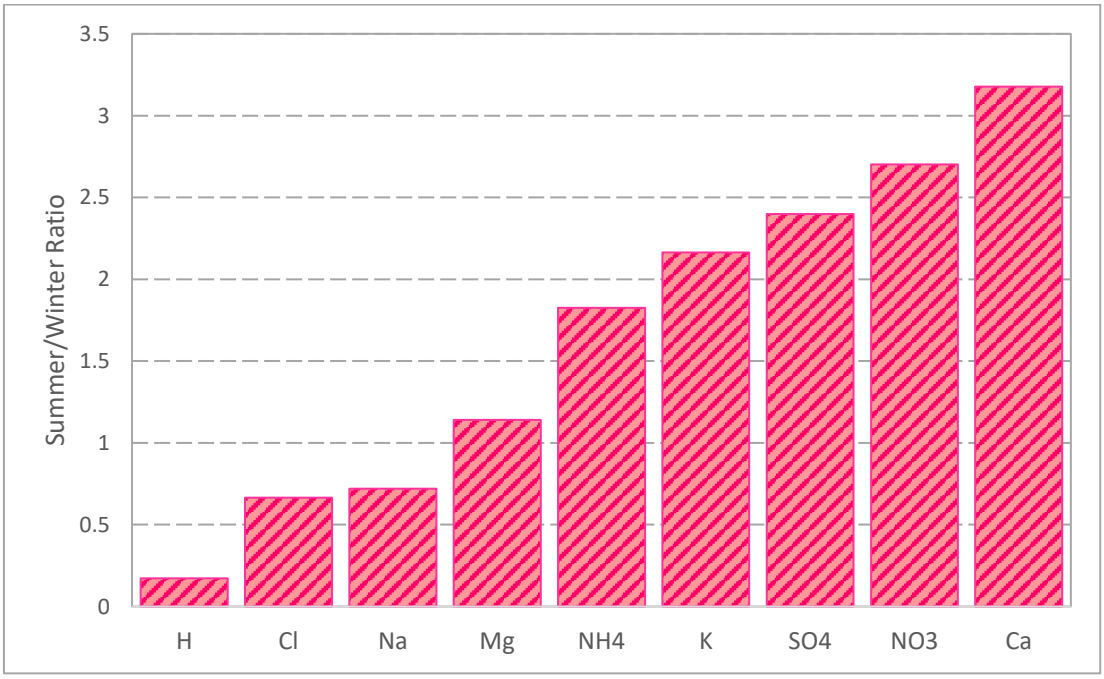

Figure 4.25 Summer-to-Winter Concentration ratios of Ions in Marmaris Rainwater

It is expected to see higher summer-to-winter ratios for crustal elements, as their generation rate is a very different between summer and winter. PM10 concentrations measured at a station operated by the Ministry of Environment and Municipality (MoEM) at Ören, which is approximately 30 km from Marmaris station are 224 μg m^{-3} in summer and 39 μg m^{-3} in winter. This corresponds to summer-to-winter concentration ratio of 5.6. The Summer/Winter ratios of crustal ions in precipitation are lower than this ratio measured in aerosol. Summer-to-winter ratio of Ca^{2+}, K^{+} and Mg^{2+} are 4.9, 2.9 and 2.1, respectively.

Smaller Summer/Winter ratio that had been observed in the collected precipitation samples compared to similar ratio found in atmospheric particles is probably due to sea-salt contribution to concentrations of Ca^{2+}, K^{+} and Mg^{2+}. It was calculated in Section 4.3.2 that 70% of Mg^{2+}, 44% of K^{+} and 6% of Ca^{2+} can be accounted for by sea salt particles at our station. Since sea-salt concentration in atmosphere is higher during winter season, higher sea salt contribution to concentrations of these ions in winter results in lower S/W ratios. Ordering of Summer/Winter ratios of these ions also supports this hypothesis. Sea salt contribution is the highest for Mg^{2+}, then to K^{+} and the least to Ca^{2+} (Al-Momani et al., 1998; Güllü et al., 1998; 2005). Since sea salt contribution to Ca^{2+} is smaller than its contribution to Mg^{2+} and K^{+} concentrations, Summer/Winter ratio for this ion is similar to the summer-to-winter ratio observed in PM_{10} particles.

4.5.2. Interannual Variations in Ion Concentrations

Interannual variations in concentrations of ions, which demonstrate long-term trends, is useful to assess results of actions taken to improve air quality. Although there are tests to determine statistical significance of observed trends (such as Mann-Kendall test), data generated in this study is not long enough for such trend analysis (generally data longer than 10 years is needed). In this work we investigated visual increasing and decreasing trends in concentrations of ions without testing its statistical significance.

Box-and whisker plots that are prepared for ions with anthropogenic, marine and crustal sources are depicted in Figure 4.26 and Figure 4.27. Different trends were observed in concentrations of different ions. Among ions with anthropogenic sources, concentrations of SO_4^{2-}, NO_3^- and H^+ decreased between 2011 and 2015, then slightly increased in 2016. How significant is the increase in 2016 is not clear, but decrease between 2011 and 2015 is consistent with decreasing trend in their concentrations in European rainwater and aerosol. There is no obvious decreasing or increasing pattern in NH_4^+ concentrations, which is given in Figure 25d. Statistical significance of small increases measured in 2014, 2015 and 2016 is not clear.

Concentrations of ions with crustal source, namely Ca^{2+} and K^+, show trends that are similar to anthropogenic ions. A decrease in their concentrations between 2011 and 2015, then a small increase in 2016 can be seen in Figures 26 (c) and (d). It is interesting to note that a similar decreasing trend in concentrations of crustal element (Al, Fe, Ca, K) was also observed in aerosol samples collected at a station that is approximately 20 km to the west of Antalya (Öztürk et al., 2012). The decrease was attributed to reduced frequency of Saharan Dust transport. The decrease in dust transport to Mediterranean region is reported by other researchers as well (Mahowald, et al., 2010; Ganor, et al., 2010). However, doubling of dust transport to Eastern Mediterranean region is also reported (Floutsi, et al., 2016).

Concentrations of marine ions, namely Na^+ and Cl^- gradually increase between 2011 and 2016. This trend observed in concentrations of both Na^+ and Cl^- suggests an increasing trend in storm activity during study period. However, there is no literature information that support or oppose this observation.

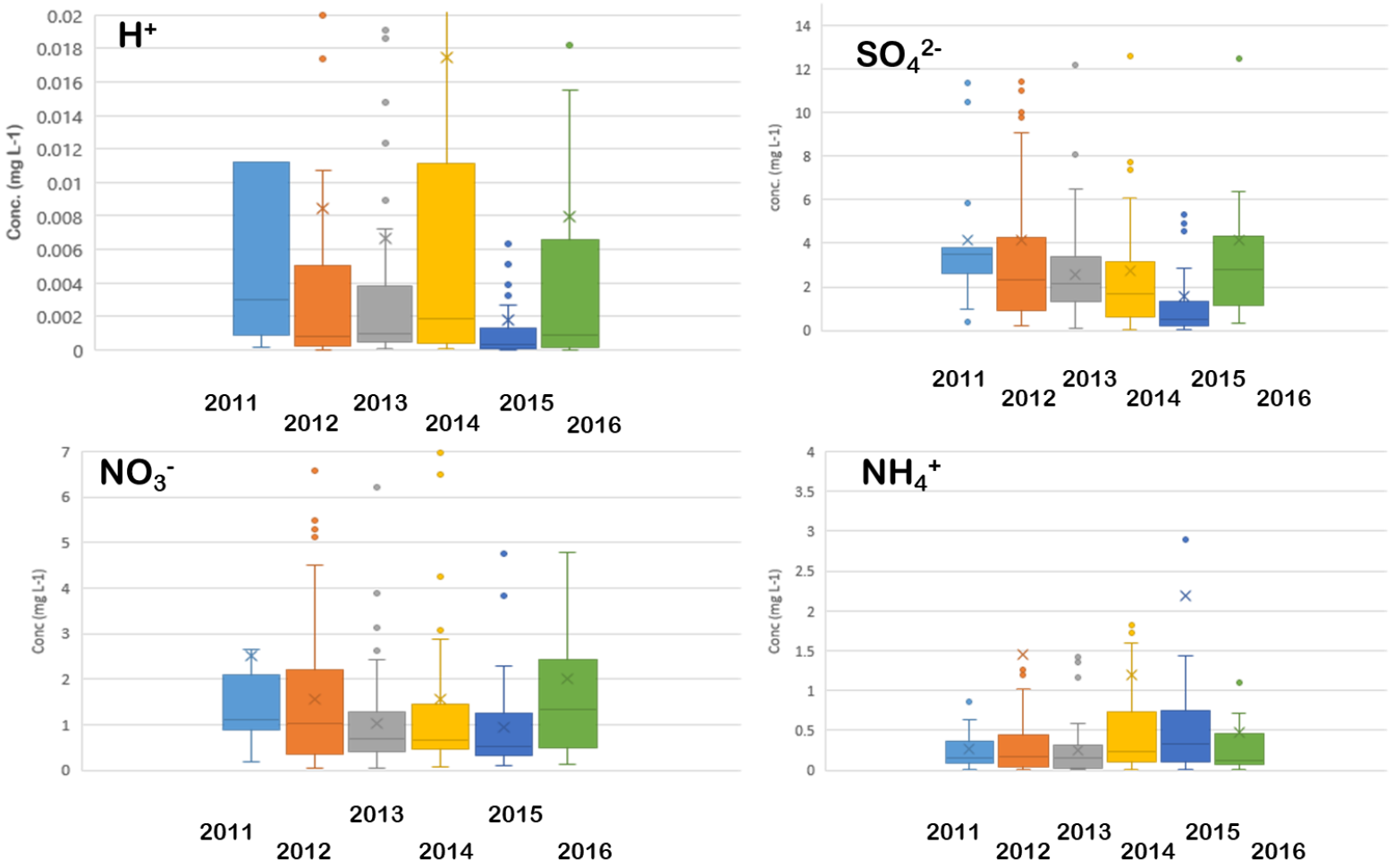

Figure 4.26 Interannual Variation in Concentrations of Pollution Derived ions in Marmaris Rainwater

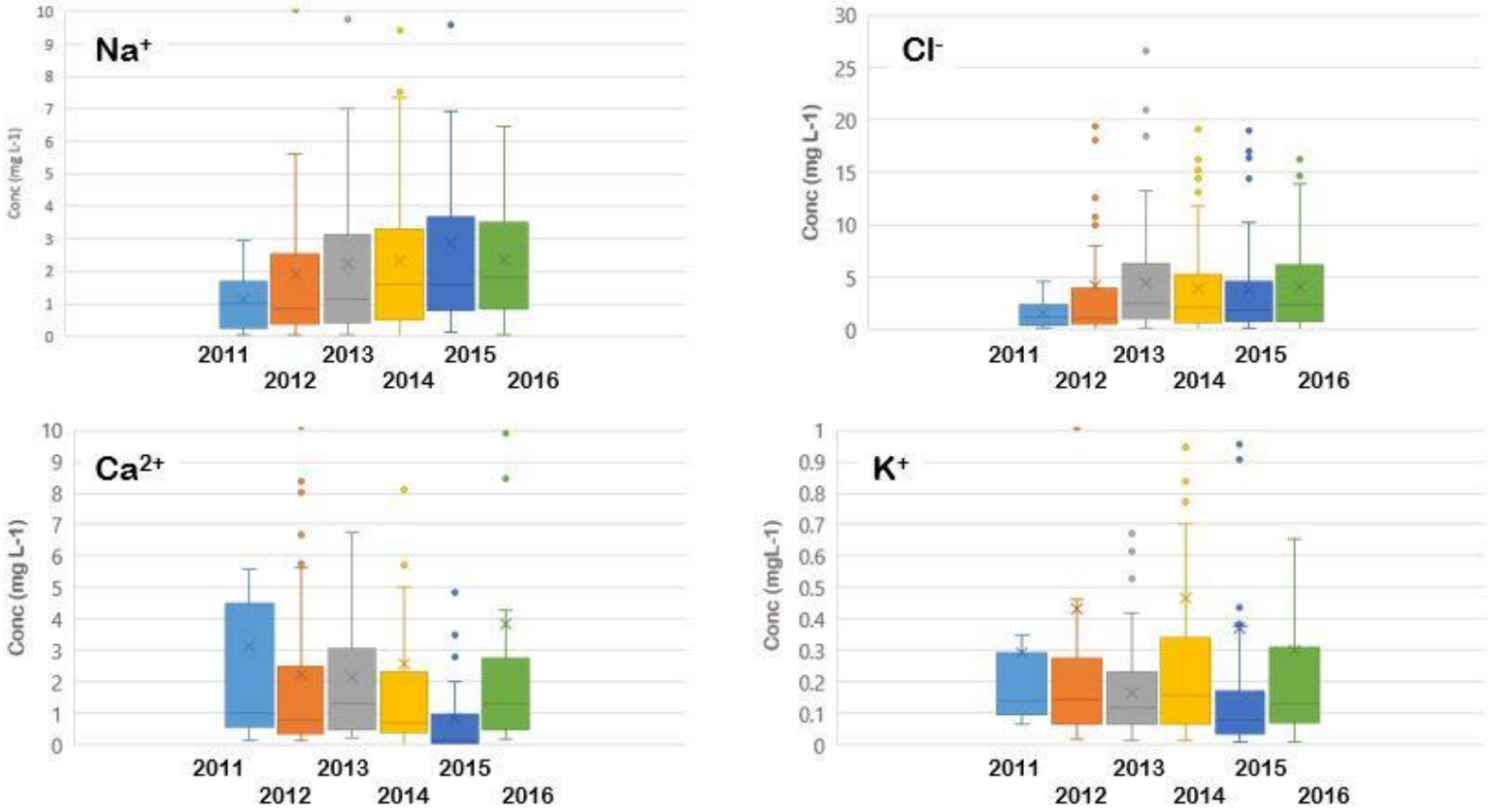

Figure 4.27 Interannual Variation in Concentrations of Crustal and Sea Salt Ions in Marmaris Rainwater

4.6. Positive Matrix Factorization

One of the rationale of measuring ionic composition of rainwater at Marmaris is to find out source regions in and out of Turkey that affect our country and Eastern Mediterranean in general. This can be answered in two steps using different statistical tools. In the first step, types of sources that affect composition of rainwater at Marmaris was determined using positive matrix factorization, which is a multivariate statistical tool. In the second step locations of sources, which came out in the first step, was found by applying "potential source contribution function" (PSCF), which is a method in trajectory statistics.

Positive matrix factorization (PMF) is newer version of factor analysis (FA) and principal component analysis (PCA), which are two widely used statistical tools in receptor modeling. Despite these well-known multivariate tools, PMF found wide use, because it has two important advantages over the other two methods. First advantage is the quantitative nature of PMF, whereas results obtained from FA and PCA are qualitative. The second advantage is that samples are not rejected from PMF due to missing data, FA and PCA, on the other hand, require complete data sets.

Input to PMF consists of two sets of information, namely data file, which contains measurement results and uncertainty file, which includes uncertainty information about each datum. Based on these two information PMF assigns categories to each specie with respect to their signal-to-noise ratios (S/N). Ions are classified as "Bad", "Weak" of "Strong"; where "Bad" is the specie with S/N below 0.5. "Weak" species have S/N ratio between 0.5 and 1.0 and "Strong" category refers to the species with S/N greater than 1.0.

Species categorized as "Bad" are removed entirely from analysis. Uncertainties of weak species are increased so that they do not contribute to the "fit", but contributions of factors to these "weak" species are calculated and they are included to output. Contribution of weak species to "fit" is avoided by multiplying their uncertainties by three. "Strong" species are included in PMF run without modifying their uncertainties. These "strong" parameters are used in the fit. The S/N values and categories of the

species measured in this study are given in Table 4.4. All of the ions measured in this study are categorized as “strong” in PMF analysis.

Table 4.4 Categories and Signal-to-noise Ratios of the Ions

Species	Category	S/N
SO_4^{2-}	Strong	9.6
NO_3^-	Strong	9.2
Cl^-	Strong	8.7
NH_4^+	Strong	3.2
Ca^{2+}	Strong	8.4
Mg^{2+}	Strong	9.2
K^+	Strong	6.0
Na^+	Strong	9.6

In PMF analysis, selection of proper number of factors is an important point and unfortunately left to user. Unlike in FA and PCA there is no rule that defines the number of factors that should be retained. However, there are some guidelines, which can assist in selecting factors to be retained. First and the most important guideline is the minimization of the “object function” Q. For each run with different factors, the PMF software calculates a Q_{robust} value, which should be compared with $Q_{theoretical}$, which is a function of number of parameters used in the fit and number of factors. The difference between these two Q values should be minimized by changing number of factors. Number of factors that corresponds to minimum ΔQ is the factors that should be extracted in PMF exercise. The second very important criteria in deciding factor-number is that factors extracted should have physical meaning. There are few other criteria to select factors, such as scaling residuals, but these two are the most important ones.

After running PMF between four-to-seven factors and optimizing each run, solution with four factors was accepted. The object function Q_{robust} calculated by the software for 4 factors was 1565 and $Q_{theoretical}$ calculated using the Equation 4.4 for same

number of factors was 1176. Higher number of factors had smaller ΔQ but additional factors did not make sense or they formed by splitting one of the existing factors

$$Q_{theoretical} = (k * m) - t(k + m) \quad (4.4)$$

Please note that resolution of PMF analysis depends strongly on number of samples and number of parameters included in the fit. In this study, number of samples was sufficient and did not cause a resolution problem. However, number of parameters analyzed in this study (nine ions) was too small for a successful PMF. Four factors found in this work does not mean there is only four source types (or components) in rainwater. It means ions can resolve these four sources. If more parameters, such as trace elements, carbon fractions or particulate organics, were measured, larger number of factors, each representing a different source type, could be extracted.

Factor 1

Diagnostic figures for factor 1, which includes Factor loadings, percent contribution of factor 1 on measured concentrations of ions and monthly median values of factor scores are given in Figure 4.28. Factor 1 accounts for all of the measured NH_4^+ concentration, approximately 41% of the measured NO_3^- concentration and 22% of the measured K^+ concentration. High concentrations of NH_4^+ was reported both in particles (Güllü et al., 1998; 2005; Öztürk et al., 2012) and rainwater (Al-Momani et al., 1995; 1998) in the eastern Mediterranean region and attributed to oxidation of NH_3 emitted from fertilizer application in the region. Higher factor 1 scores during summer months support fertilizer source, because fertilizers are applied in spring and evaporation of NH_3 is expected to be maximum in summer due to high temperature. Factor 1 also accounts for 22% of the measured K^+ concentration. Potassium has three important sources in the atmosphere, namely, crustal, sea salt and biomass burning (Sullivan, et al., 2019; Sun, et al., 2019; Tunno, et al., 2019). Presence of K^+ in the same factor with NH_4^+ indicates a mixing of biomass burning particles with NH_3 emitted from fields, or may indicate higher NH_3 emission rates during forest fires. Both of these hypotheses are highly speculative at this point, because there is no

supporting literature. Based on these arguments, factor 1 is identified as fertilizer factor.

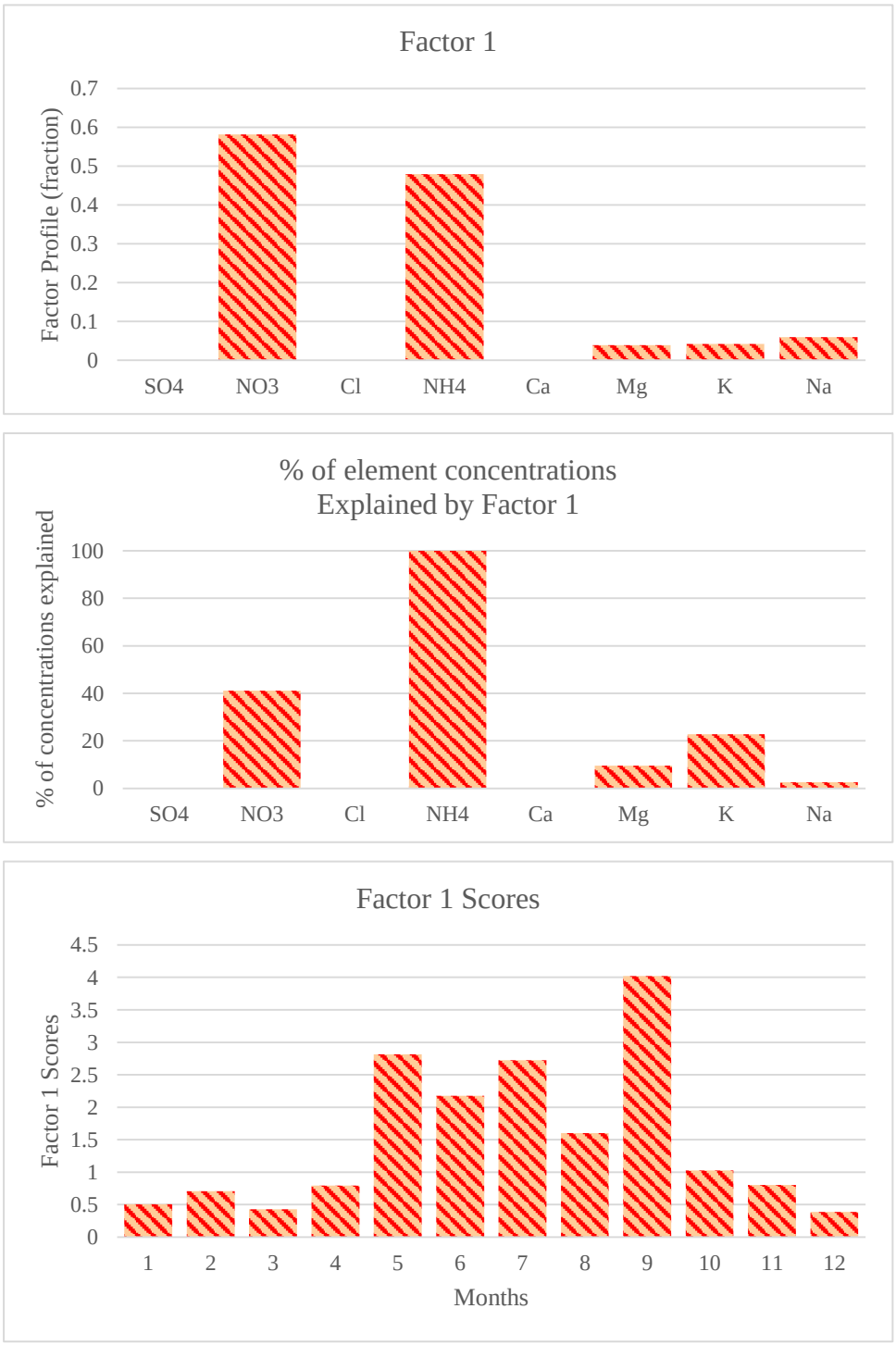

Figure 4.28 Factor 1 diagnostics: (a) factor loadings, (b) fractions of ion concentrations explained by factor 1 and (c) monthly variations of factor scores

Factor 2

Diagnostic figures for factor 2 are given in Figure 4.29. Factor 2 is a very clear crustal factor. It accounts for almost 87% of measured Ca concentration, 23% of measured concentrations of Mg^{2+} and 37% of measured K^{+}.

It can be seen in Figure 4.29 (c) that Factor 2 scores are high during summer and low in winter. This supports crustal source for factor 2, because resuspension of surface soil is easier during summer season when the soil is dry, as discussed previously Section 4.5.

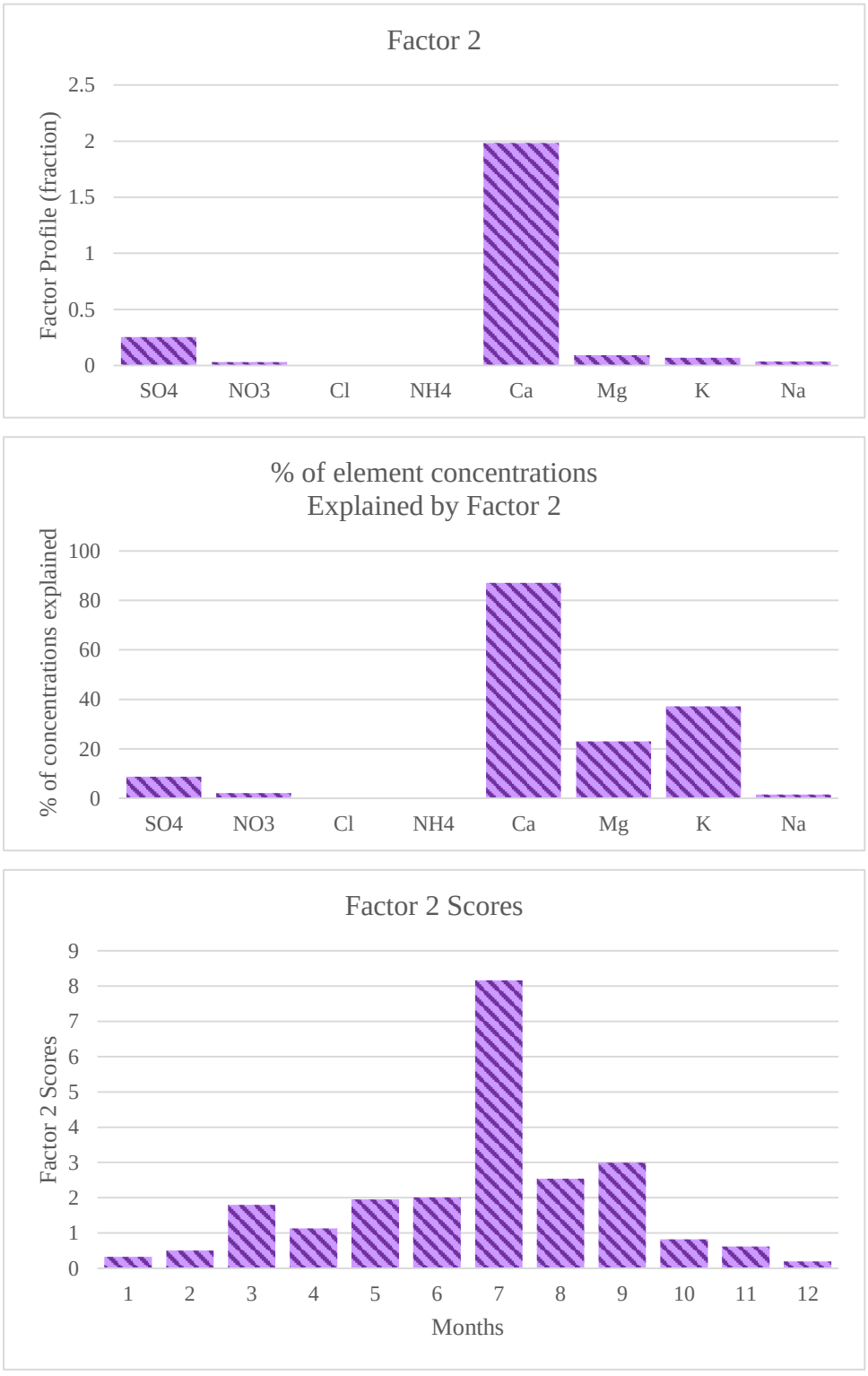

Figure 4.29 Factor 2 diagnostics: (a) factor loadings, (b) fractions of ion concentrations explained by factor 1 and (c) monthly variations of factor scores

Factor 3

Diagnostic figures for factor 3 are given in Figure 4.30. Factor 3 is dominated by SO_4^{2-} and NO_3^- . It accounts for 82% of measured SO_4^{2-} and 56% of the measured NO_3^- concentrations. Factor scores depicted a well-defined seasonal pattern with higher scores in summer. Factor 3 is a typical combustion factor, which was seen in most of the previous aerosol and rainwater studies in the Eastern Mediterranean region. Factor 3 is identified as long range transport-combustion factor. It represent rain that brings pollutants from distant sources. Emissions from power plants located at different parts of our study domain are the main component in this factor.

Distribution of PSCF values calculated using Factor 3 scores are given in Figure 4.31. Main industrial source regions affecting ionic composition of rain water at Marmaris are İstanbul and Thrace area, Western Black Sea coast of Turkey, regions in Azerbaijan and Dagestan Republic, South eastern part of Ukraine, Jordan - Saudi Arabia border. There are also some minor source areas in Balkans and along African Coast. Source areas at the inner parts of Africa can be due to too few segments in those grids, which are in the outskirts of the study area. Although we applied the weighting approach developed by Zhao and Hopke (2006), it does not completely eliminate the limitation of PSCF, when there are few segments in a grid. Western parts of Turkey, Balkan Countries Eastern parts of Ukraine, Black Sea coast of Russia appears as primary sources regions in most of the aerosol and rainwater studies performed in our group (Balcılar et al., 2014; Öztürk et al., 2012; Al-Momani et al., 1998; Alagha et al., 2003; Tokgöz et al., 2015). Since effect of these source regions were consistently identified in both Mediterranean and Black Sea regions of Turkey, they can be identified as important foreign sources contributing to atmospheric composition in our country.

Another important point to note in the figure is that most of the major cities in the region, including Rome, Athens, Istanbul, Ankara, Cairo appears as source areas. This observation suggests that factor 3 is not an exclusively industrial factor. It also represent anthropogenic emissions from highly-populated urban areas.

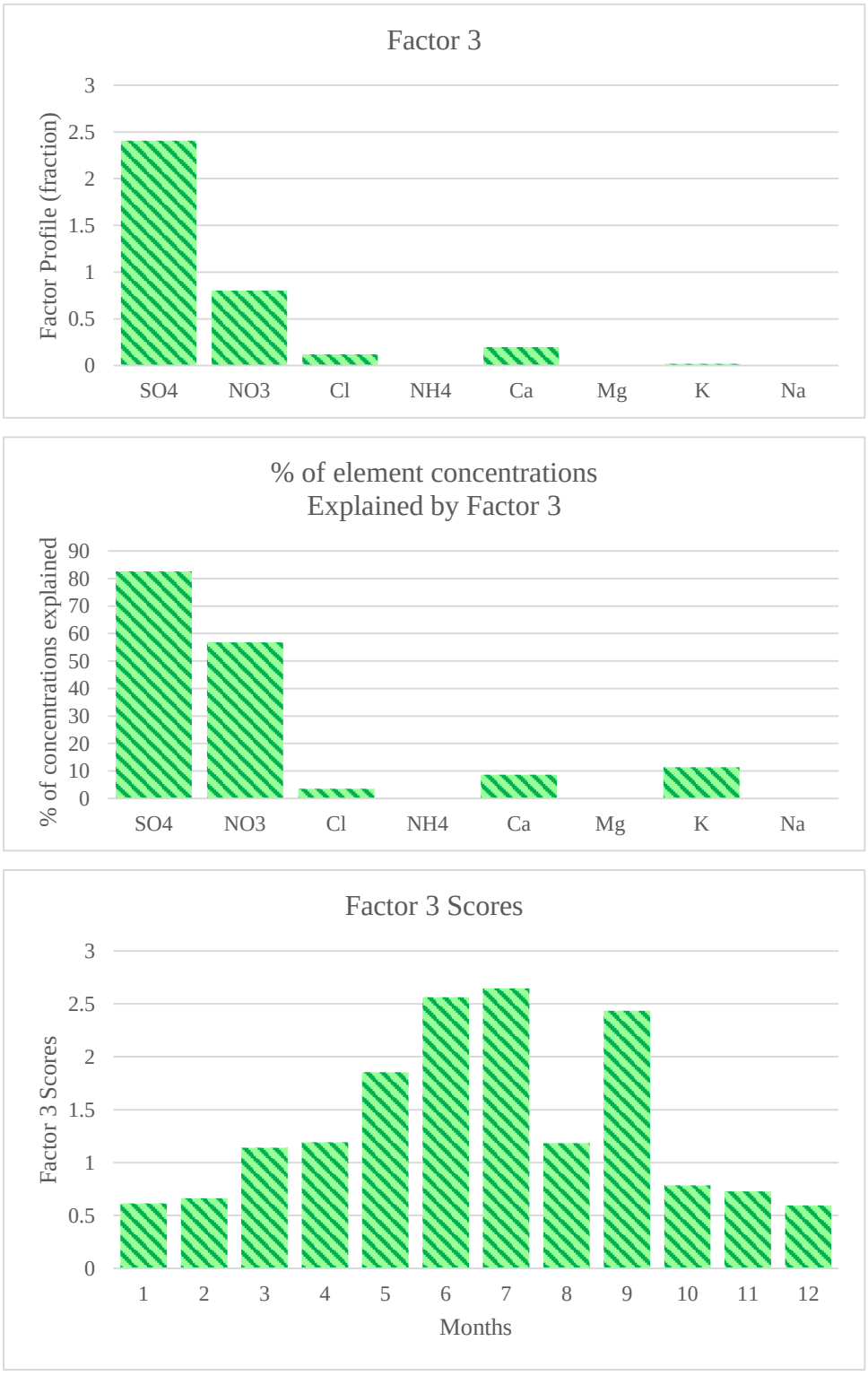

Figure 4.30 Factor 3 diagnostics: (a) factor loadings, (b) fractions of ion concentrations explained by factor 3 and (c) monthly variations of factor scores

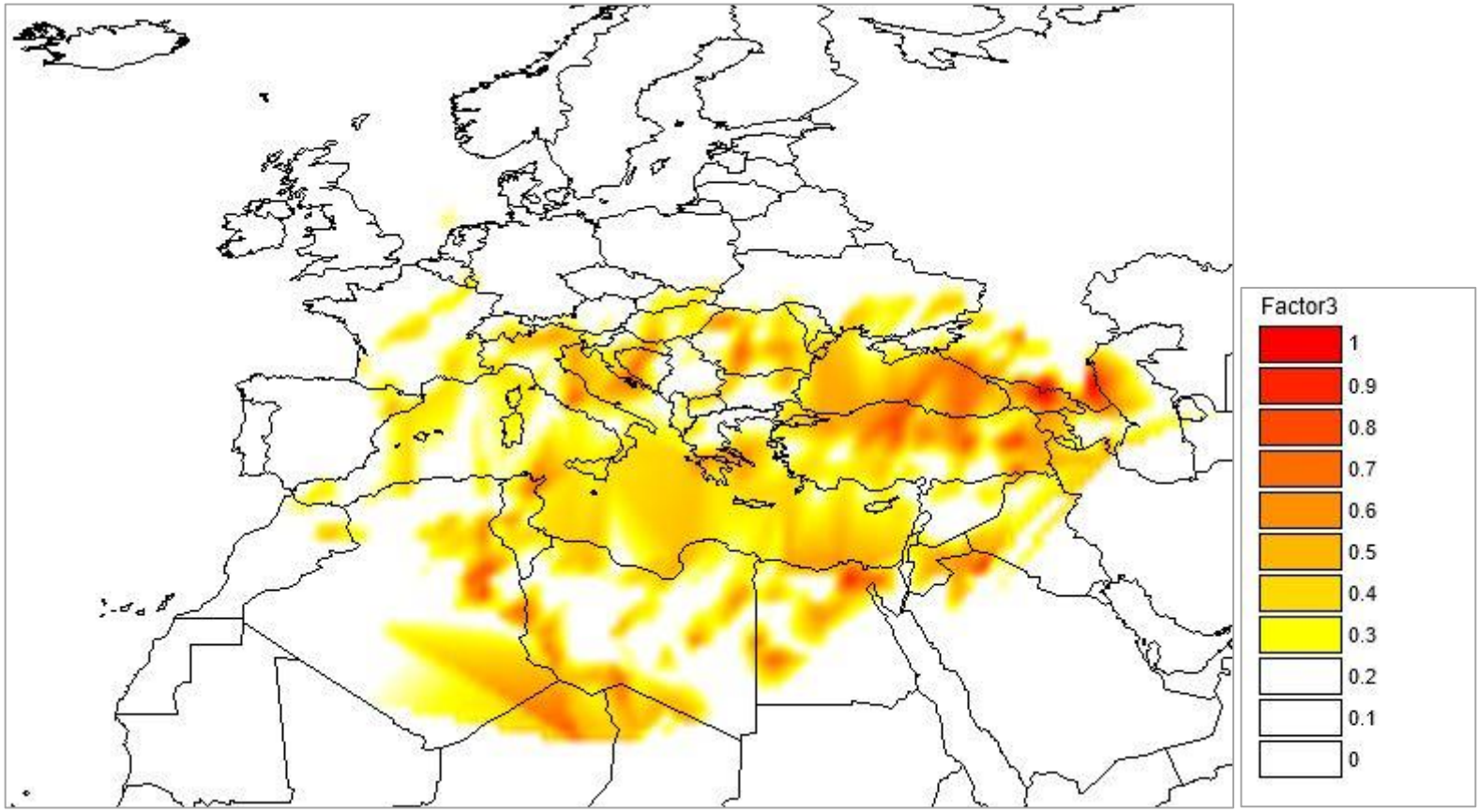

Figure 4.31 Factor 3 potential source regions. Distribution of PSCF values computed using Factor 2 sc ores. Trajectories that correspond to highest 40% of Factor 3 scores were taken as polluted trajectories

Factor 4

Diagnostic figures for Factor 4 are given in Figure 4.32. Factor 4 is a clear marine factor. This factor explains of 95 % of the Na^+ and 96 % of Cl^- concentrations, which are the most abundant species in sea water (accounting for 36% and 55% of total suspended solids in rain water, respectively). Factor 4 also accounts for 9% of SO_4^{2-} concentrations, 67% of Mg^{2+} concentrations and 28% of K^+ concentration. These ions are major components of sea water. Sulfate, Mg, K and Ca accounts for 8%, 3.7%, 2.4% and 1.2% of total dissolved solids in sea water respectively (Ault, et al., 2013; Lowenstein, et al., 2005).

Factor scores are higher in winter months, which is expected from sea salt. Sea salt particles are generated by bubble bursting at the sea surface, a process that strongly depend on wind speed over the sea (Brooks & Thorton, 2018; Song, et al., 2019). Higher scores in winter is due to stronger and more frequent storm activity in Northeastern Mediterranean in winter season.

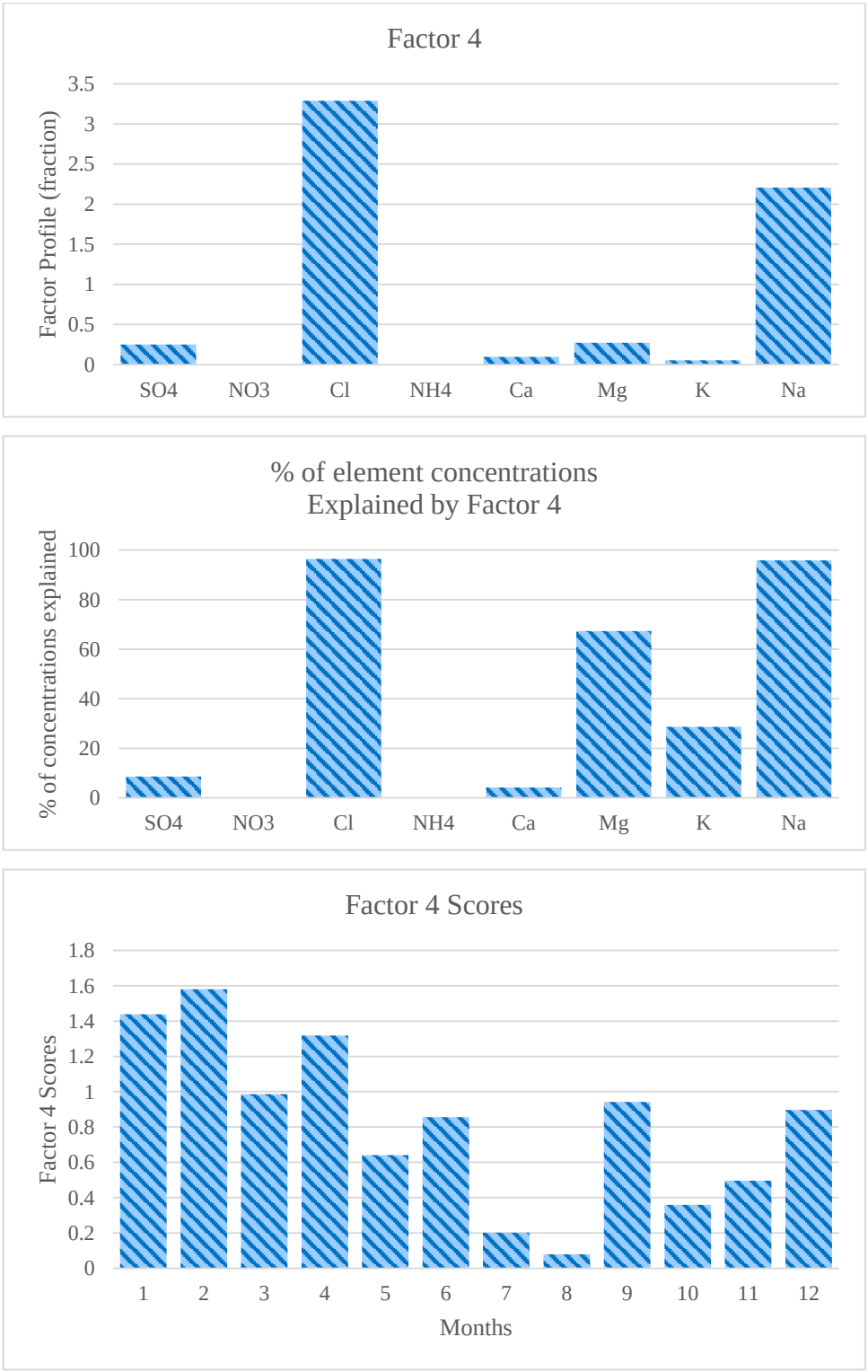

Figure 4.32 Factor 4 diagnostics: (a) factor loadings, (b) fractions of ion concentrations explained by factor 4 and (c) monthly variations of factor 4 scores

4.7. Deposition Fluxes

Wet deposition fluxes of ions can be viewed from two perspective. First it is a mean of cleaning atmosphere. However, it is also a mechanism of transport of pollutants from atmosphere to surface and has a potential to contaminate receptor ecosystem components. Several examples do exists that clearly demonstrate damage caused by wet deposition of pollutants on lakes or forests. Acid rain is the best documented example.

Wet deposition fluxes of ions measured in this study were calculated by multiplying measured concentrations of ions (mg L^{-1}) with rainfall for that event (mm or L m^{-2}) and correcting for surface area of the bucket. Since wet deposition fluxes of ions depend strongly on the rainfall, higher fluxes during winter months, when approximately 80% of the annual rainfall occur, is expected. Monthly variation of SO_4^{2-} deposition flux is given in Figure 4.33 as an example. Although SO_4^{2-} concentration is higher during summer season, its deposition flux is orders of magnitude lower during summer, demonstrating strong dependence of wet deposition fluxes on rainfall. However, relation between rainfall and SO_4^{2-} wet deposition flux is not as straightforward as expected, because although one expects to see a strong correlation between rainfall and ion fluxes, which are calculated by multiplying concentration with rainfall, the relation is not as strong as expected. This is shown in Figure 4.34 where SO_4^{2-} wet flux is plotted against rainfall per event. Although there is a statistically significant [$P(r,n) < 0.05$] correlation between flux and rainfall, it is not a strong correlation. This is due to inverse relation between ion concentrations and rainfall, which is shown for NO_3^- in Figure 4.35 as an example. A decreasing trend can be seen in NO_3^- concentrations with rainfall. The trend is not statistically significant with 5% confidence, not because there is no relation between two parameters, but because relation is not linear. Such non-linear inverse relation between concentrations of elements or ions with rainfall are frequently reported in literature and attributed to dilution of species (Lin, et al., 2017; Canovas, et al., 2012; Matsumoto, et al., 2005; Al-Momani, et al. 1998). All these indicate that relation

between ion flux and rainfall is not very simple, and although a statistically significant correlation between them do exist, it is not as strong as initially expected.

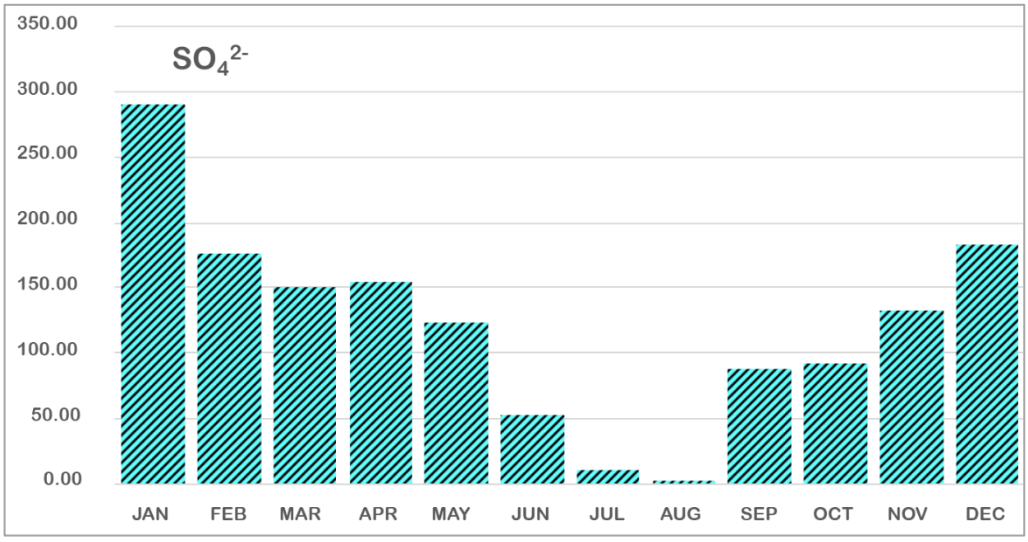

Figure 4.33 Monthly Variation in SO_4^{2-} Wet Deposition Flux

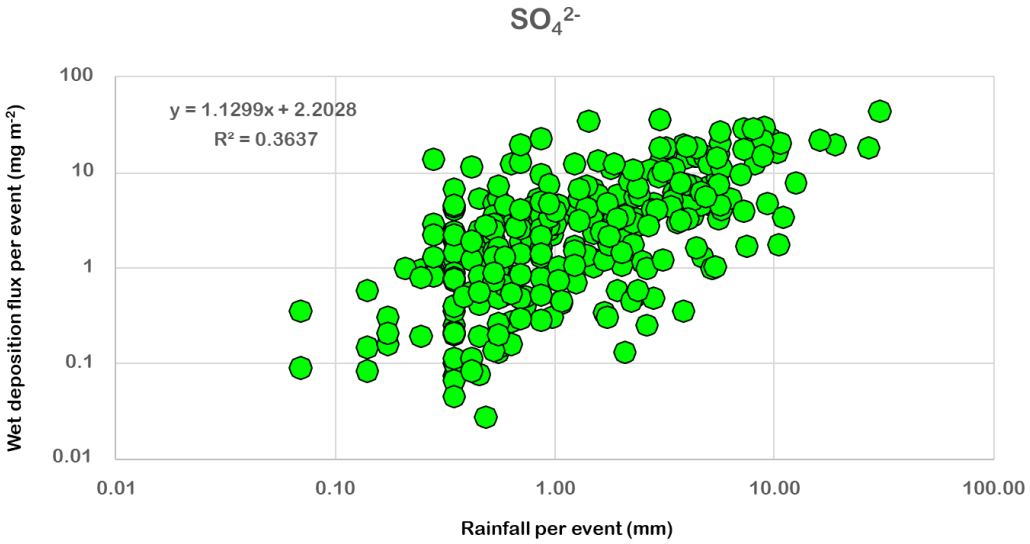

Figure 4.34 Relation Between SO_4^{2-} Wet Deposition Flux and Rainfall

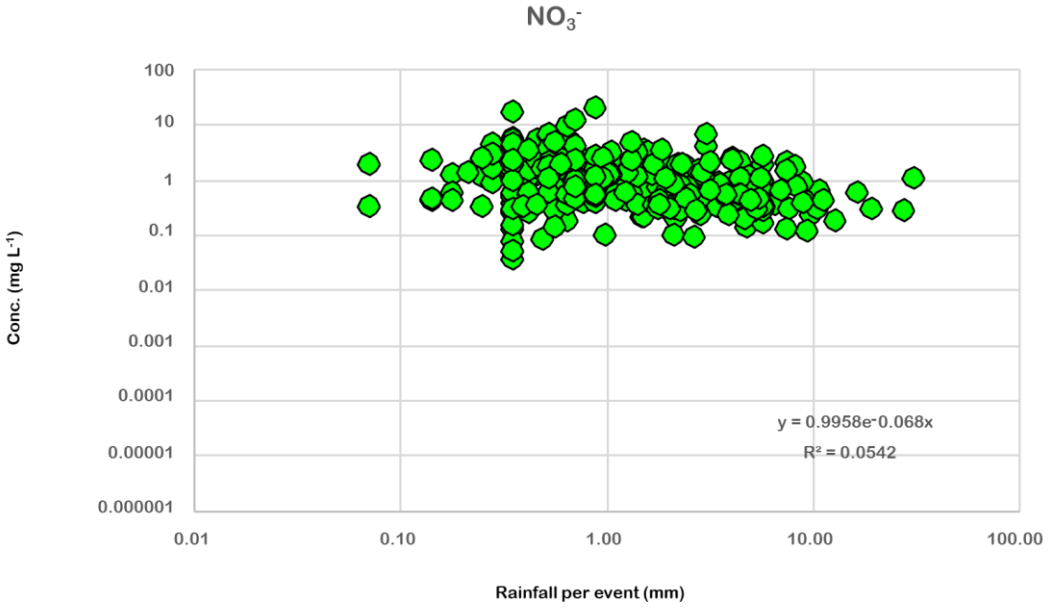

Figure 4.35 Relation Between Concentrations of Ions and Rainfall

Interannual variability in deposition fluxes of ions with anthropogenic origin are given in Figure 4.36. Hydrogen deposition flux does not show a clear, well-defined variation between 2011 and 2016. This was not unusual, because variation of H^+ concentration from one year to another depends not only on the concentrations of acidic species, namely $H_2SO_4^{2-}$ and HNO_3^- but also depends on concentrations of bases, namely $CaCO_3$ and NH_3, particularly $CaCO_3$.

Deposition fluxes of SO_4^{2-} and NO_3^- decrease between 2012 and 2016. Wet deposition fluxes of all ions are low in the year 2011, because rain sampling at Marmaris station started in June 2011. Since annual fluxes were generated by adding fluxes for each event, 2011 fluxes turned low, because half of the events (before June 2011) were not included in flux calculations. Statistical significance of these decreasing trends were not tested, because data is not long-enough for trend analysis. But decreasing SO_4^{2-} and NO_3^- fluxes are obvious. This is due to decreasing concentrations of these ions from 2010 to 2016, as discussed previously in this manuscript.

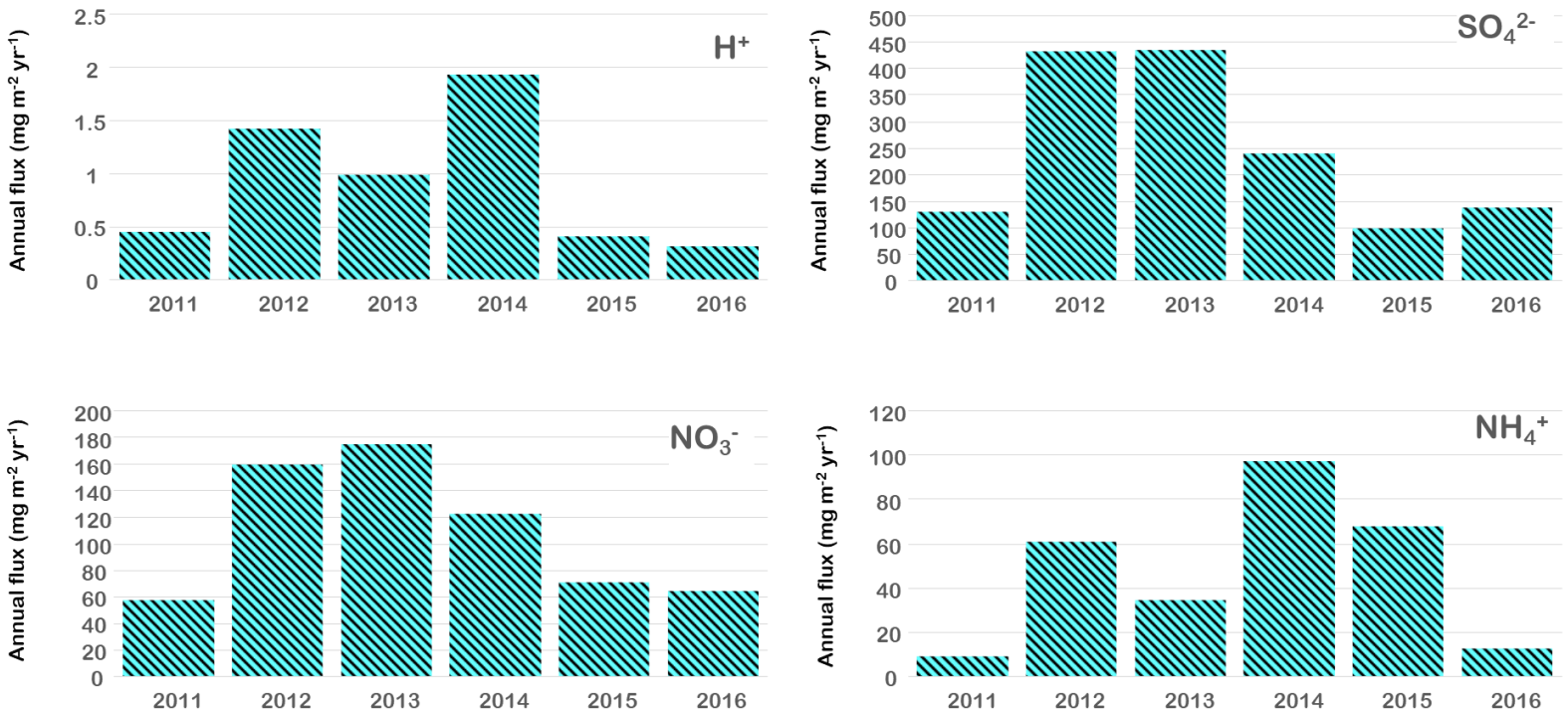

Figure 4.36 Inter-annual variation in wet deposition fluxed of anthropogenic ions

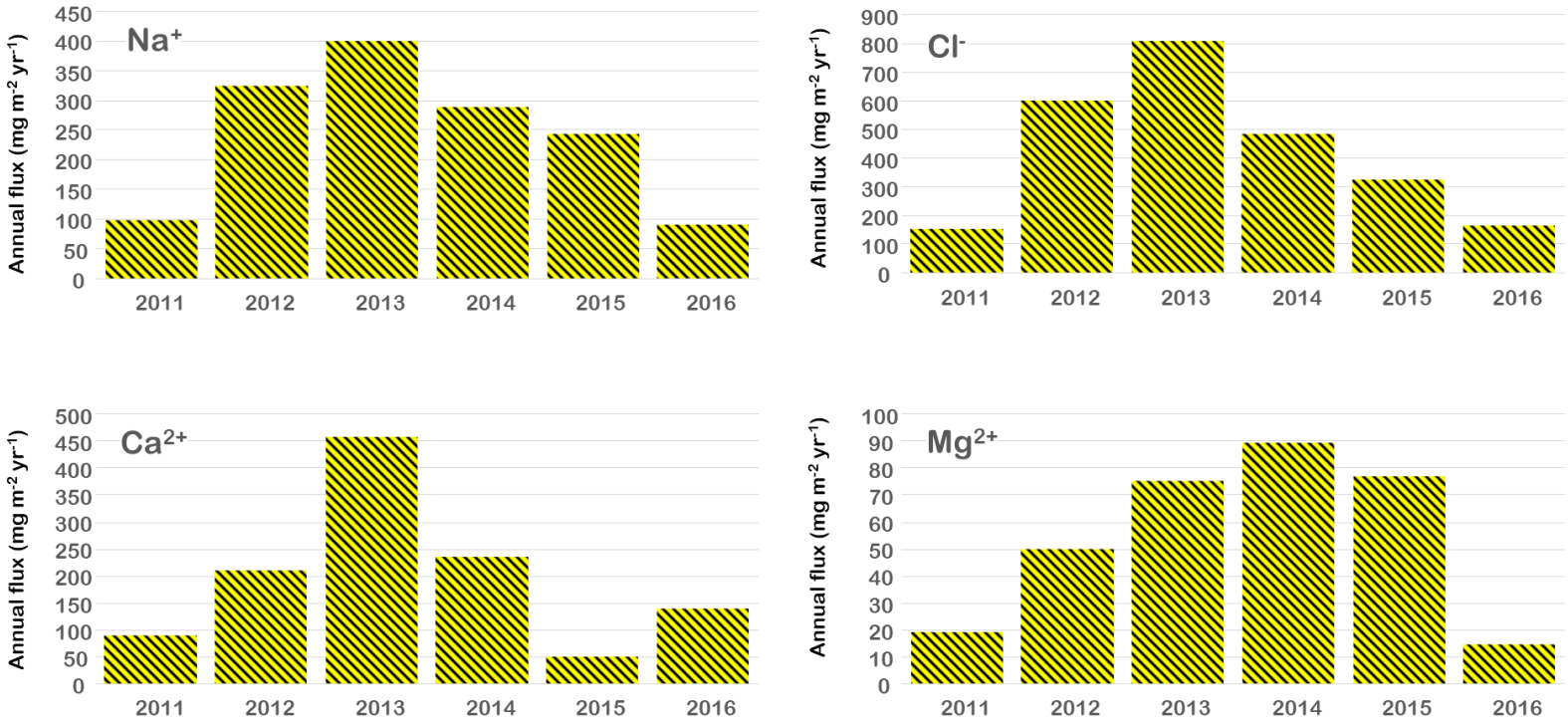

Figure 4.37 Inter-annual variation in wet deposition fluxed of marine and crustal ions

Unlike flux variations in SO_4^{2-} and NO_3^-, NH_4^+ wet deposition flux does not show well defined trend between 2012 and 2016. This is probably because main source of NH_4^+ at Marmaris is the fertilizer applications in the region, which did not change much in last 10 years.

Interannual variation in wet deposition fluxes of crustal and marine ions are depicted in Figure 4.37. Sea salt ions, namely Na^+ and Cl^- show a pattern that is very similar to anthropogenic ions. Their fluxes decrease between 2013 and 2016. This pattern is possible only if annual average wind speed decrease in time, but such decrease is wind speed is not reported in literature. Crustal elements Ca^{2+} and Mg^{2+}, on the other hand did not show a consistent and well-defined pattern as expected.

Wet deposition fluxes of anthropogenic and crustal ions are compared with corresponding fluxes in EMEP network in Figure 4.38 and Figure 4.39, respectively. Unlike concentrations of ions, fluxes measured at Marmaris station is not high compared to fluxes measured in the rest of the EMEP network. For example, SO_4^{2-} concentration is the highest among all EMEP stations, but SO_4^{2-} flux is not. This is due to smaller annual rainfall in the Mediterranean region, which strongly affects wet deposition fluxes of ions. This pattern is not specific for anthropogenic ions but is valid for crustal and marine ions as well.

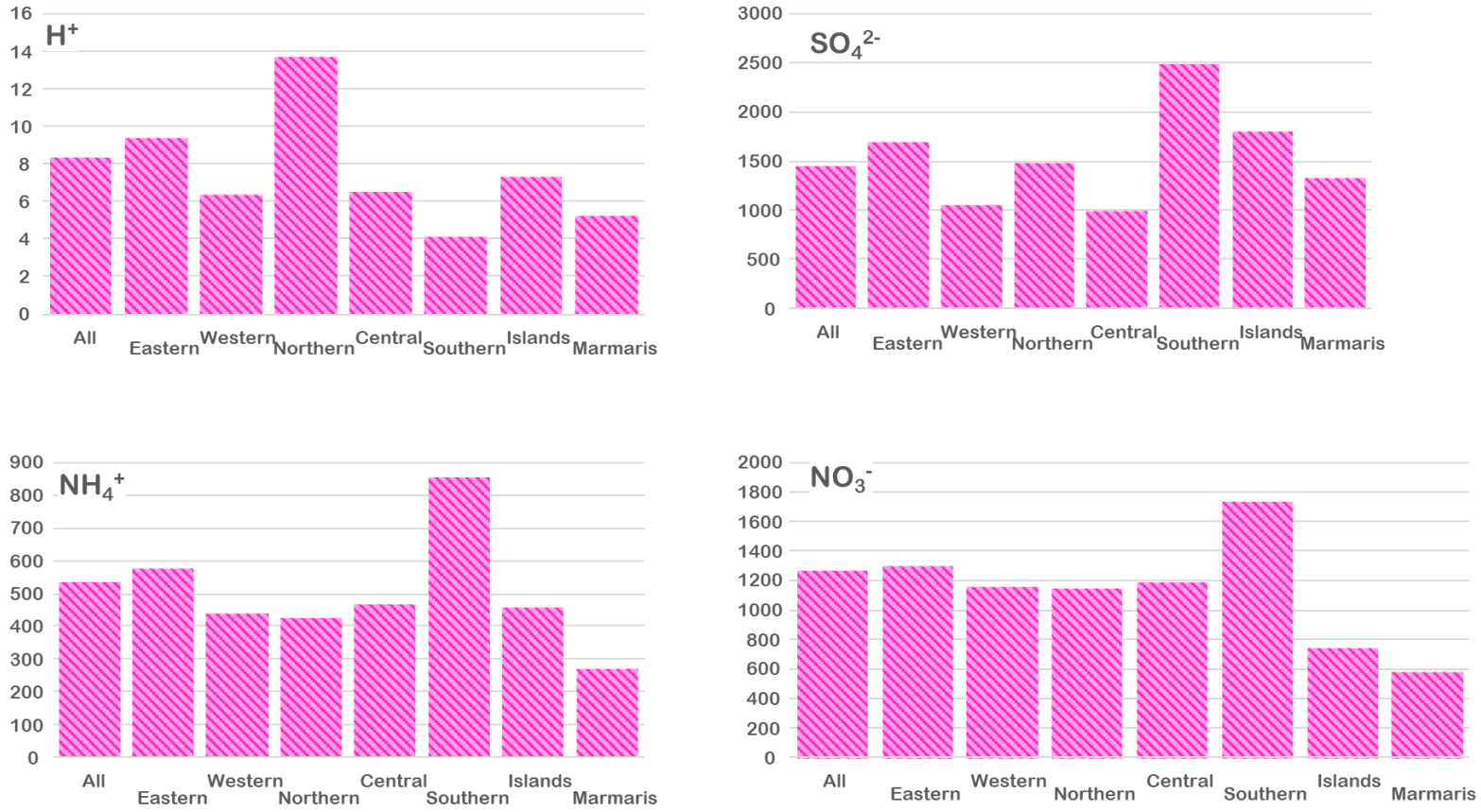

Figure 4.38 Comparison of wet deposition fluxes of Pollution-derived ions measured in this study with corresponding fluxes in EMEP network

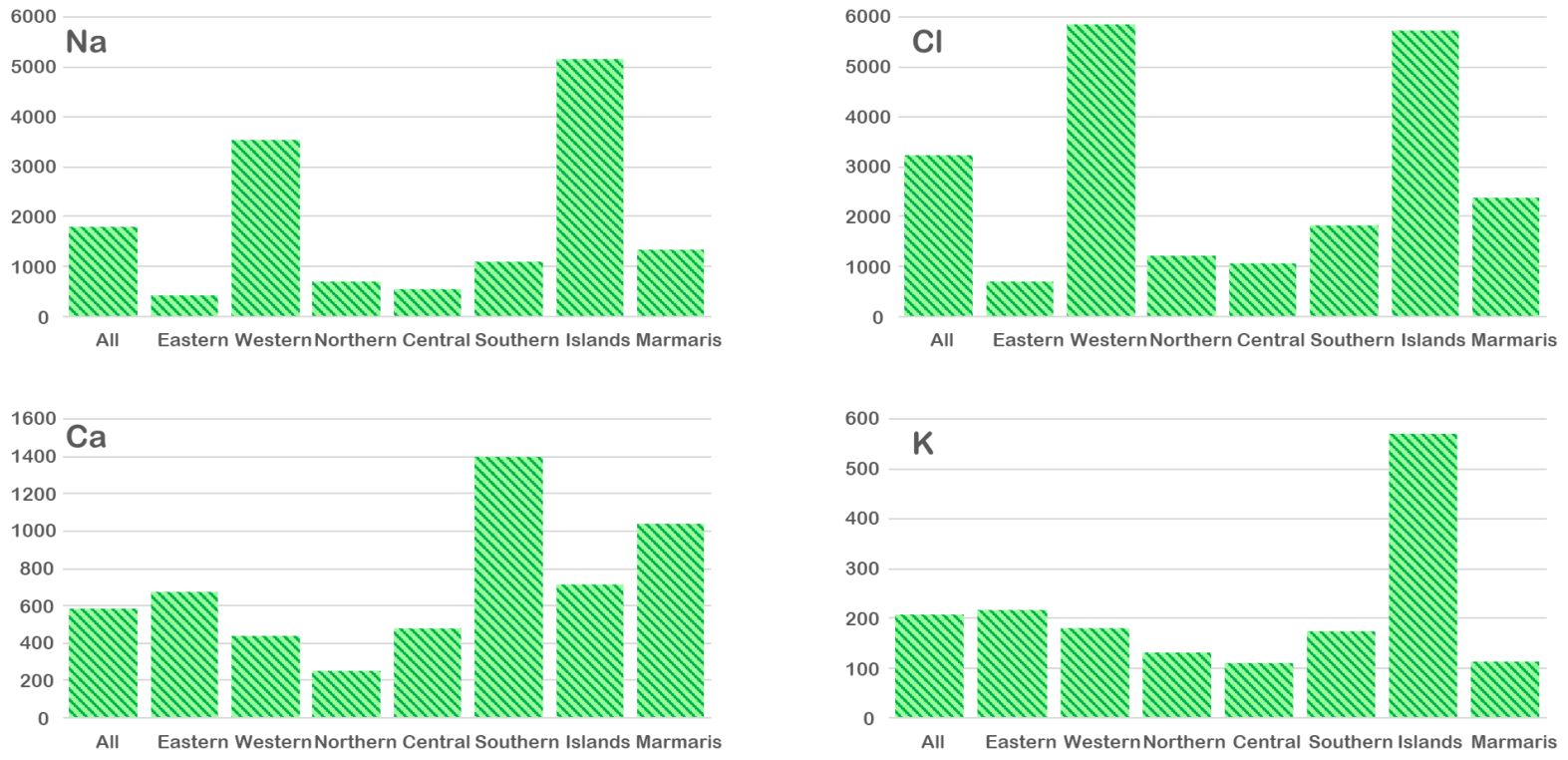

Figure 4.39 Comparison of wet deposition fluxes of marine and crustal ions measured in this study with corresponding fluxes in EMEP network

Another important point in wet deposition fluxes of ions is their episodic nature. Percentage of rain events that account for 90% of ion deposition is depicted in Figure 4.40. Hydrogen ion is the most episodic parameter. Approximately 20% of events accounted for 90% of H^+ deposition. For the remaining ions 90% of their deposition fluxes are accounted by 35% - 55% of rain events. Episodic nature of wet deposition fluxes of ions is due to episodic nature of the rainfall. At Marmaris station 53% of rain events account for 90% of annual deposition. However, more episodic nature of H^+ ion cannot be explained only by episodic nature of rainfall. Two factors play an important role in episodic nature of H^+ wet deposition. One of them is, like all other ions, episodic nature of rainfall. The second factor is the neutralization of free H^+ ion, which is dependent on $CaCO_3$ (represented by Ca^{2+} in our data set). Since Ca^{2+} concentration and flux are also episodic, Hydrogen flux, and concentration becomes more episodic than other ions.

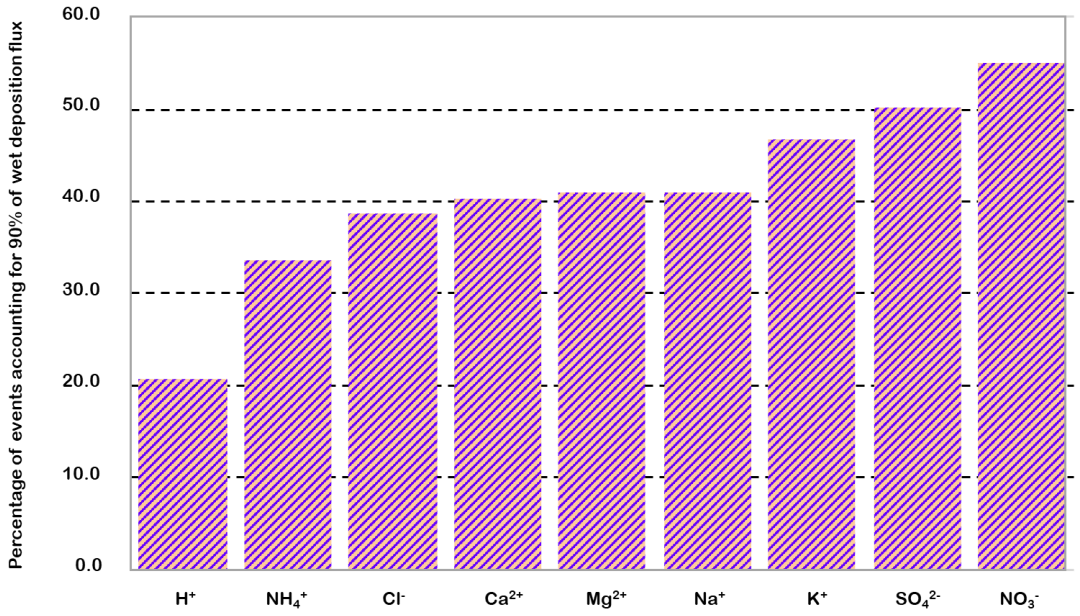

Figure 4.40 Episodic nature of wet deposition fluxes: Percentage of rain events accounting for 90% of wet deposition fluxes of ions

CHAPTER 5

CONCLUSION AND RECOMMENDATIONS

In this study, major ions (H^+, SO_4^{2-}, NO_3^-, Cl^-, NH_4^+, Ca^{2+}, Mg^{2+}, K^+, and Na^+) had been measured in the Marmaris Station of MGM with ion chromatography between the period 2011 and 2016. A total of 302 measurement days are present in the data set which were analyzed for this study.

General characteristics of the data were measured, volume weighted average, mean standard deviation, median values and ranges for all ions are calculated. Also by using software Statgraphics distributions of the ions were visualized and same software gave the information that the distributions are log-normal and right skewed.

Residence times of the air parcels reaching to the station is studied. Back trajectories that had been calculated for a thirteen-year period were used to determine the residence times for three different altitudes. The areas air masses spent time most before reaching the station is western part of Turkey and the Balkans. The difference of residence times with respect to dry and wet season was also calculated; in dry season, summer, northern areas are more dominant, however southern areas, especially North Africa, is dominant in winter, wet season. Dividing the study domain into eight wind sectors as N, NE, E, SE, S, SW, W and NW; N and NE sectors were dominant for summer months; E, SE, S and SW sectors had more segments in winter months. Which means that in summer months pollutants from N and NE, whereas in winter pollutants transported from E, SE, S and SW are more dominant. As a part of the flow climatology, cluster analysis was made on the station showed that, trajectories can be grouped as 5 clusters.

Contributions of the ions to the total ion mass was calculated and it is observed that the ion with most contribution is Cl^- in overall, followed by SO_4^{2-} and Na^+. Contributions of the ions were examined seasonally; contributions of the

anthropogenic sourced secondary ions, SO_4^{2-} and NO_3^-, do not change depending on the season, contributions of sea salt sourced Na^+ and Cl^-, are higher in winter months; on the contrary, crustal ions Ca^{2+}, Mg^{2+} and K^+, have higher contributions in summer months.

Temporal variation of the rainfall for the station was analyzed and dividing the winter as October to March and summer as April to September; it was measured that approximately 14% of the annual rainfall occurs in our summer and 86% of annual rainfall occurs in winter, which is typical for the Eastern Mediterranean region.

As for the temporal variations of the ions; higher concentrations of ions, particularly SO_4^{2-} and NO_3^- were observed in atmosphere during summer months, which is attributed to both faster gas-phase oxidation of SO_2 and NO_2 by more vigorous photochemical activity due to enhanced solar flux in summer. Concentrations of Na^+ and Cl^-, were higher in winter, because both ions are indicators of marine aerosol, which forms by bubble-bursting at the sea surface. Crustal ions, including Ca^{2+}, Mg^{2+} and K^+ have higher concentrations during summer seasons, due to the amount of suspended soil in the air, which is more likely to occur in summer months since the soil is drier. H^+ ion concentrations were much higher in winter and very low in summer, pattern is governed entirely by season-dependent neutralization of acidity.

Rainwater samples were exposed to both natural and anthropogenic pollutants while travelling to the station. In order to determine the sources and source locations of the ions, Positive Matrix Factorization and Potential Source Contribution Function models were used. The PMF model revealed four factors, which were identified as two anthropogenic, one marine and one crustal factors. Potential source regions for the anthropogenic components in rainwater were identified as to be western Ukraine, Western Black Sea coast of the Turkey, Balkan Countries, North Africa and Georgia.

In this study, major ion composition of rain water is analyzed. Trace element concentrations are not included in this work; so in future works, including trace elements in addition to this data, will give more detailed and precise results, especially in positive matrix factorization.

Since there are only nine ion concentration in PMF, obtained results are not completely reliable. In future works, trace element and organic compound concentrations, which are more specific source markers, should be included in the PMF analysis. Including these data may result as more factor numbers with specific marker species.

Also, in order to determine the statistical changes in temporal variations, longer sampling should be done. Thus tests such as Mann-Kendall Test can be applied to the data set, which will be statistically more accurate for long-term trends.

REFERENCES

Acid Deposition Monitoring Network in East Asia. (2000). *Quality Assurance/Quality Control (QA/QC) Program for Wet Deposition Monitoring in East Asia.* Asia Center for AirPollution Research.

Alagha, O., & Tuncel, G. (2003). Evaluation of Air Quality over the Black Sea: Major Ionic Composition of Rainwater. *Water, Air and Soil Pollution: Focus*, 89-98.

Al-Khashman, O. A. (2005). Ionic composition of wet precipitation in the Petra Region, Jordan. *Atmospheric Research*, 1-12.

Al-Khashman, O. A. (2005). Study of chemical composition in wet atmospheric precipitation in Eshidiya area, Jordan. *Atmospheric Environment*, 6175-6183.

Al-Khashman, O. A. (2009). Chemical characteristics of rainwater collected at a western site of Jordan. *Atmospheric Research*, 53–61.

Al-Momani, I. F., Aygun, S., & Tuncel, G. (1998). Wet deposition of major ions and trace elements in the eastern Mediterranean basin. *Journal of Geophysical Research*, 8287-8299.

Al-Momani, I. F., Tuncel, S., Eler, Ü., Örtel, E., Sirin, G., & Tuncel, G. (1995). Major ion composition of wet and dry deposition in the eastern Mediterranean basin. *The Science of the Total Environment*, 75-85.

Anil, I., Alagha, O., & Karaca, F. (2017). Effects of transport patterns on chemical composition of sequential rain samples: Trajectory clustering and principle component analysis approach. *Air Quality, Atmosphere and Health*, 1193-1206.

Arsene, C., Olariu, R. I., & Mihalopoulos, N. (2007). Chemical composition of rainwater in the northeastern Romania, Iasi region (2003–2006). *Atmospheric Environment*, 9452-9467.

Ault, A. P., Moffet, R. C., Baltrusaitis, J., Collins, D. B., Ruppel, M. J., Caudra-Rodriguez, L. A., & Grassian, V. H. (2013). Size-dependent changes in sea spray aerosol composition and properties with differen seawater conditions. *Environmental Science and Technology*, 5603-5612.

Ayaklı, G. (2014, February). Chemical Composition of Precipitation in Different Parts of Turkey. *M. Sc. Thesis*. Ankara: Middle East Technical University.

Aydınalp, C., & Cresser, M. S. (2008). Red soils under Mediterranean type climate: Their properties use and productivity. *Bulgarian Journal of Agricultural Science*, 576-582.

Balcılar, İ., Zararsız, A., Kalaycı, Y., Doğan, G., & Tuncel, G. (2018). Temporal variatioins of Eastern Black Sea aerosol. *Global NEST Journal*, 115-121.

Bardouki, H., Liakakou, H., Economou, C., Sciare, J., Smolik, J., Zdimal, V., Eleftheriadis, K., Lazaridis, M., Dye, C., Mihaloloulos, N. (2003). Chemical composition of size-resolved atmospheric aerosols in the eastern Mediterranean during summer and winter. *Atmospheric Environment*, 195-208.

Behera, S. N., Shharma, M., Aneja, V. P., & Balasubramanian, R. (2013). Ammonia in the atmosphere: A review on emission sources, atmospheric chemistry and deposition on terrestrial bodies. *Environmental Science and Pollution Research*, 8092-8131.

Belis, C. A., Larsen, B. R., Amato, F., El Haddad, I., Favez, O., Harrison, R. M., Hopke, P., Nava, S., Paatero, P., Prevot, A., Quass, U., Vecch, R., Viana, M. (2014). *European Guide on Air Pollution Source Apportionment with Receptor Models.* Ispra: Joint Research Centre of the European Commission.

Blondel, J., Aronson, J., Bodiou, J.-Y., & Boeuf, G. (2010). *The Mediterranean Region: Biological Diversity in Space and Time.* New York: Oxford University Press.

Bottenberg, C., Schanus, L., Kluss, R., & Kuball, C. (2006). The Mediterranean Climate.

Brankov, E., Rao, S. T., & Porter, P. S. (1998). A Trajectory-clustering-correlation methodology for examining the long-range transport of air pollutants. *Atmospheric Environment*, 1525-1534.

Bricker, O. P., & Rice, K. C. (1993). Acid Rain. *Annual Review of Earth and Planetary Sciences*, 151-174.

Brooks, S. D., & Thorton, D. C. (2018). Marine aerosols and clouds. *Annual Review of Marine Science*, 289-313.

Bruno, F., Cocchi, D., & Greco, F. (2011). Clustering compositional data trajectories: The case of particulate matter in the lower troposphere. *Environmetrics*, 975-984.

Burke, K. (2006). *Ion Chromatography*. Retrieved from New Mexico State University: https://web.nmsu.edu/~kburke/Instrumentation/IC.html

Canovas, C. R., Olias, M., Vazquez-Suñé, E., Ayora, C., & Nieto, J. M. (2012). nfluence of releases from a fresh water reservoir on the hydrochemistry of the Tinto River (SW Spain). *Science of The Total Environment*, 418-428.

Casiday, R., & Frey, R. (1998). *Acid Rain*. Retrieved from Washington University Department of Chemistry: http://www.chemistry.wustl.edu/~edudev/LabTutorials/Water/FreshWater/acidrain.html

Cheng, S., Wang, F., Li, J., Chen, D., Li, M., Zhou, Y., & Ren, Z. (2013). Application of trajectory clustering and source apportionment methods for investigating

trans-boundary atmospheric PM10 pollution. *Aerosol and Air Quality Research*, 333-342.

Chmielewski, A. G. (2011). *Monitoring, Control and Effects of Air Pollution.* Rijeka: InTech.

Colls, J. (2002). *Air Pollution.* Spoon Press.

Committee on Public Works. (1975). *Air Quality and Stationary Source Emission Control.* Washington: U.S. Government Printing Office.

Dayan, U., Ricaud, P., Zbinden, R., & Dulac, F. (2017). Atmospheric pollution over the eastern Mediterranean during summer – a review. *Atmospheric Chemistry*, 13233-13263.

Dorling, S. R., Davies, T. D., & Pierce, C. E. (1992). Cluster analysis: A technique for estimating the synoptic meteorological controls on air and precipitation chemistry—Method and applications. *Atmospheric Environment*, 2575-2581.

Draxler, R. R., & Hess, G. D. (1997). *Description of the HYSPLIT_4 modelling system.* Silver Spring: NOAA Technical Memorandum NOAA Air Resources Laboratory.

Draxler, R. R., & Hess, G. D. (1998). An overview of the HYSPLIT_4 modelling system for trajectories. *Australian Meteorological Magazine*, 295-308.

Emami, F., & Hopke, P. K. (2017). Effect of adding variables on rotational ambiguity in positive matrix factorization solutions. *Chemometrics and Intelligent Laboratory Systems*, 198-202.

EMEP. (2017, November). *EMEP acidifying/eutrophying compounds*. Retrieved from EMEP: https://projects.nilu.no//ccc/emepdata.html

Erel, Y., Kalderon-Asael, B., Dayan, U., & Sandler, A. (2007). European atmospheric pollution imported by cooler air masses to the eastern mediterranean during the summer. *Environmental Science and Technology*, 5198-5203.

Federoff, N., & Courty, M. A. (2013). Revisiting the genesis of red Mediterranean soils. *Turkish Journal of Earth Sciences*, 359-375.

Fisher, R. A., & Yates, F. (1963). *Statistical tables for biological, agricultural and medical research.* Edinburgh: Oliver & Boyd.

Floutsi, A. A., Korras-Carraca, M. B., Matsoukas, C., Hatzianastassiou, N., & Biskos, G. (2016). Climatology and trends of aerosol optical depth over Mediterranean basin during the last 12 years (2002-2014) based on Collection 006 MODIS-Aqua data. *Science of the Total Environment*, 551-552.

Forster, C., Wandinger, U., Wotawa, G., James, P., Mattis, I., Althausen, D., & Stohl, A. (2001). Transport of boreal forest fire emissions from Canada to Europe. *Journal of Geophysical Research: Atmospheres*, 22887-22906.

Ganor, E., Osetinsky, I., Stupp, A., & Alpert, P. (2010). Increasing trend of African dust, over 49 years, in the eastern Mediterranean. *Journal of Geophysical Research: Atmospheres*.

Genç Tokgöz, D. (2013, February). Temporal Variation in Aerosol Composition at Northwestern Turkey. *Ph. D Thesis*. Ankara: Middle East Technical University.

Genç Tokgöz, D. D., & Tuncel, G. (2015). Ionic composition of aerosols in northwestern Turkey. *International Journal of Global Warming*, 161-172.

Ghanem, M., Shalash, I., & Al-Rimmawi, H. (2010). Hydrochemical Characteristics of Rainwater in Ramallah District. *Asian Journal of Earth Sciences*.

Giardina, M., & Buffa, P. (2018). A new approach for model dry deposition velocity particles. *Atmospheric Environment*, 11-22.

Güllü, G. H., Ölmez, İ., Aygün, S., & Tuncel, G. (1998). Atmospheric trace element concentrations over the eastern Mediterranean Sea: Factors affecting temporal variability. *Journal of Geophysical Research*, 21943-21954.

Güllü, G., Doğan, G., & Tuncel, G. (2005). Atmospheric trace element and major ion concentrations over the eastern Mediterranean Sea: Identification of anthropogenic source regions. *Atmospheric Environment*, 6376-6387.

Hacısalihoğlu, G., Eliyakut, F., Ölmez, I., & Balkas, T. I. (1992). Chemical composition of particles in the black sea atmosphere. *Atmosphric Environment*, 3201-3218.

Hartley, Jr, E. M. (1973). *Sulfur Dioxide Reactions with Aqueous Solutions of Manganase at High Temperature and with Ammonia in the Gas Phase, PhD Thesis.* Georgia: Georgia Institute of Technology.

Hopke, P. K. (2000). *A Guide to Positive Matrix Factorization.* New York: U.S. Environmental Protection Agency.

Hopke, P. K. (2009). Air Quality and Ecological Impacts: Relating Sources to Effects. *Developments in Environmental Science*.

Huang, X.-F., Li, X., He, L.-Y., Feng, N., Hu, M., Niu, Y.-W., & Zeng, L.-W. (2010). 5-Year study of rainwater chemistry in a coastal mega-city in South China. *Atmospheric Research*, 185-193.

Im, U., Christodoulaki, S., Violaki, K., Zarmpas, P., Kocak, M., Daskalakis, N., & Kanakidou, M. (2013). Atmospheric deposition of nitrogen and sulfur over southern Europe with focus on the Mediterranean and the Black Sea. *Athmospheric Environment*, 660-670.

Işıkdemir, Ö. (2006, January). Investigation of 8-Year-Long Composition Record in the Eastern Mediterranean Precipitation. *M. Sc. Thesis*. Ankara: Middle East Technical University.

Jacob, D. (1999). *Introduction to Atmospheric Chemistry*. Princeton: Princeton University Press.

Karagulian, F., Belis, C. A., Dora, C. F., Prüss-Ustün, A. M., Bonjour, S., Adair-Rohani, H., & Amann, M. (2015). Contributions to cities' ambient particulate

matter (PM): A systematic review of local source contributions at global level. *Atmospheric Environment*, 475-483.

Kaya, G., & Tuncel, G. (1997). Trace element and major ion composition of wet and dry depositon in Ankara, Turkey. *Atmospheric Environment*, 3985-3998.

Koulouri, E., Saarikoski, S., Theodosi, C., Markaki, Z., Gerasopoulos, E., Kouvarakis, G., Makela, T., Hillamo, R., Mihalopoulos, N. (2008). Chemical composition and sources of fine and coarse aerosol particles in the Eastern Mediterranean. *Atmospheric Environment*, 6542-6550.

Kumar, D. B., & Verma, S. (2016). Potential emission flux to aerosol pollutants over Bengal Gangetic plain through combined trajectory clustering and aerosol source fields analysis. *Atmospheric Reserch*, 415-425.

Lee, E., Chan, C. K., & Paatero, P. (1999). Application of positive matrix factorization in source apportionment of particulate pollutants in Hong Kong. *Atmospheric Environment*, 3201-3212.

Lestari, P., & Mauliadi, Y. D. (2009). Source apportionment of particulate matter at urban mixed site in Indonesia using PMF. *Atmospheric Environment*, 1760-1770.

Liang, J. (2013). *Chemical Modeling for Air Resources: Fundamentals, Applications, and Corroborative Analysis.* Academic Press.

Lin, J., Qi, J., Xie, D., & Meng, X. (2017). The concentrations and wet depositions fluxes of inorganic ions in oceanic precipitation-study on precipitation over the China Sea and northwest Pacific Ocean. *Zhongguo Huanjing Kexue/China Environmental Science*, 1706-1715.

Lionello, P. (2012). *The Climate of Mediterranean Region: From the Past to the Future.* London: Elsevier.

Lionello, P., Malanotte-Rizzoli, P., Boscolo, R., Alpert, P., Artale, V., Li, L., Lutherbacher, J., May, W., Trigo, R., Tsimplis, M., Ulbrich, U., Xoplaki, E.

(2006). The Mediterranean Climate: An Overview of the Main Characteristics and Issues. *Developments in Earth & Environmental Sciences*, 1-26.

Lowenstein, T. K., Timofeeff, M. N., Kovalevych, V. M., & Horita, J. (2005). The major-ion composition of permian seawater. *Geochimica Et Cosmochimica Acta*, 1701-1719.

Lu, Z., Liu, Q., Xiong, Y., Huang, F., Zhou, J., & Schauer, J. J. (2018). A hybrid source apportionment strategy using positive matrix factorization (PMF) and molecular marker chemical mass balance (MM-CMB) models. *Environmental Pollution*, 39-51.

Lu, Z., Streets, D. G., de Foy, B., Lamsal, L. N., Duncan, B. N., & Xing, J. (2015). Emissions of nitrogen oxides from US urban areas: estimation from Ozone Monitoring Instrument retrievals for 2005 - 2014. *Atmospheric Chemistry and Physics*, 10367-10383.

Luria, M., Peleg, M., Sharf, G., Tov-Alper, D. S., Spitz, N., Ami, Y. B., Lifschitz, B., Yitzchaki, A., Seter, I. (1996). Atmospheric sulfur over the east Mediterranean region. *Journal of Geophysical Research: Atmospheres*, 25917-25930.

Mahowald, N. M., Kloster, S., Engelstaedter, S., Moore, J. K., Mukhopadhyay, S., McConnell, J. R., Albani, S., Doney, S. C., Bhattacharya, A., Lawrence, D. M., Lindsay K., Mayewski, P. A., Neff, J., Rothenberg, D., Thomas, E., Thorton, P. E., Zender, C. S. (2010). Observed 20th century desert dust variability: Impact on climateand biogeochemistry. *Atmospheric Chemistry and Phsics*, 10875-10893.

Matsumoto, K., Kawai, S., & Igawa, M. (2005). Dominant factors controlling concentrations of aldehydes in rain, fog, dew water, and in the gas phase. *Atmospheric Environment*, 7321-7329.

MGM. (2017). *Resmi İstatistikler*. Retrieved from Meteoroloji Genel Müdürlüğü: https://www.mgm.gov.tr/veridegerlendirme/il-ve-ilceler-istatistik.aspx?k=A&m=MUGLA

Mihalopoulos, N., Stephanou, E., Kanakidou, M., Pilitsidis, S., & Bousquet, P. (1997). Tropospheric aerosol ionic composition in the Eastern Mediterranean region. *Tellus*, 314-326.

Morales-Baquero, R., Pulido-Vilenna, E., & Reche, I. (2013). Chemical signature of Saharan dust on dry and wet atmospheric deposition in the south-western Mediterranean region. *Tellus*.

Nastos, P. T., Alexakis, D., Kanellopoulou, H. A., & Kelepertsis, A. E. (2007). Chemical composition of wet deposition in a Mediterranean site Athens, Greece related to the origin of air masses. *Journal of Atmospheric Chemistry*, 167-179.

Norris, G., Duvall, R., Brown, S., & Bai, S. (2014). *EPA Positive Matrix Factorization (PMF) 5.0 Fundamentals and User Guide.* Washington D.C.: U.S. Environmental Protection Agency.

Ogen, Y., Neumann, C., Chabrillat, S., Goldshleger, N., & Dor, E. B. (2018). Evaluating the detection limit of organic matter using point and imaging spectroscopy. *Geoderma*, 100-109.

Özsoy, T. (2003). Atmospheric wet deposition of soluable macro nutrients in Cilician basin, north-eastern Mediterranean sea. *Journal of Environmental Monitoring*, 971-976.

Özsoy, T., Türker, P., & Örnektekin, S. (2008). Precipitation Chemistry as an Indicator of Urban Air Quality in Mersin, North-Eastern Mediterranean Region. *Water Air Soil Pollution*, 69-83.

Pan, Y., Tian, S., Liu, D., Fang, Y., Zhu, X., Gao, M., & Wang, Y. (2018). Source apportionment of aerosol ammonium in an ammonia rich atmosphere: An isotropic study of summer clean hazy days in urban Beijing. *Journal of Geophysical Research*, 5681-5689.

Personne, E., Tardy, F., Génermont, S., Decuq, C., Gueudet, J., Mascher, N., & Loubet, B. (2015). Investigating sources and sinks for ammonia exchanges between the atmosphere and a wheat canopy following slurry application with trailing hose. *Agricultural and Forest Meteorology*, 11-23.

Petroselli, C., Crocchianti, S., Moroni, B., Castellini, S., Selvaggi, R., Nava, S., Calzolai, G., Lucarelli, F., Cappelletti, D. (2018). Disentangling the major source areas for an intense aerosol advection in the Central Mediterranean on the basis of Potential Source Contribution Function modeling of chemical and size distribution measurements. *Atmospheric Research*, 67-77.

Pitchford, M. L., Tombach, I., Barna, M., Gebhart, K. A., Green, M. C., Knipping, E., Kumar, N., Malm, W. C., Pun, B., Schichtel, B. A., Seigneur, C. (2004). *Big Bend Regional Aerosol and Visibility Observational Study*. Fort Collins: Colorado State University.

Reff, A., Eberly, S. I., & Bhave, P. V. (2007). Receptor Modeling of Ambient Particulate Matter Data Using Positive Matrix Factorization: Review of Existing Methods. *Air & Waste Management Association*, 146-154.

Rodhe, H., Dentener, F., & Schulz, M. (2002). The Global Distribution of Acidifying Wet Deposition. *Environmental Science & Technology*, 4382-4388.

Rose, K. A. (2006). *Source Allocation and Visibility Impairment in Two Class I Areas with Positive Matrix Factorization.* U.S Environmental Protection Agency.

Schauer, J. J., Rogge, W. F., Hildemann, L. M., Mazurek, M. A., & Cass, G. R. (1996). Source apportionment of airborne particulate matter using organic compounds as tracers. *Atmospheric Environment*, 3837-3855.

Schreier, S. F., Richter, A., Schepaschenko, D., Shvidenko, A., Hilboll, A., & Burrows, J. P. (2014). Differences in satellite-derived NOx emission factors between Eurasian and North American boreal forest fires. *Atmospheric Environment*, 55-65.

Seinfeld, J. H., & Pandis, S. N. (1997). *Atmospheric Chemistry and Physics: From Air Pollution to Climate Change.* Wiley-Interscience.

Sicard, P., Coddeville, P., Sauvage, S., & Galloo, J.-C. (2007). Trends in Chemical Composition of Wet Only Precipitation at Rural French Monitoring Stations Over the 1990-2003 Period. *Water Air Soil Pollution: Focus*, 49-58.

Sigler, J. M., Lee, X., & Munger, W. (2003). Emission and long-range transport of gaseous mercury from a large-scale Canadian boreal forest fire. *Environmental Science and Technology*, 4343-4347.

Smith, S. J., van Aardenne, J., Klimont, Z., Andres, R. J., Volke, A., & Delgado Arias, S. (2011). Anthropogeniz sulfur dioxide emissions: 1850 - 2005. *Atmospheric Chemistry and Physics*, 1101-1116.

Song, S., Shon, Z., Choi, Y., Son, Y., Kang, M., Han, S., & Bae, M. (2019). Global trend analysis in primary and secondary of marine aerosol optical depth 2000-2015. *Chemosphere*, 417-427.

Stohl, A. (1998). Computation, accuracy and applications of trajectories—A review and bibliography. *Atmospheric Environment*, 947-966.

Stohl, A., Eckhardt, S., Forster, C., James, P., Spictinger, N., & Seibert, P. (2002). A replacement for simple back trajectory calculations in the interpretation of atmospheric trace substance measurements. *Atmospheric Environment*, 4635-4648.

Stute, M. (2009, September 22). *Ion Chromatograph to detect major anions in precipitation (snow), groundwaters and drinking waters from New York.* Retrieved from Lamont-Doherty Earth Observatory, Columbia University Earth Institute: https://www.ldeo.columbia.edu/~martins/eda/Ic_lec.html

Sullivan, A. P., Guo, H., Schroder, J. C., Campuzano-Jost, P., Jimenez, J. L., Campos, T., & Weber, R. J. (2019). Biomass burning markers and reesidential burning

in the winter aircraft campaign. *Journal of Geophysical Research: Atmospheres*, 1846-1861.

Sun, J., Shen, Z., Zhang, Y., Zhang, Q., Lei, Y., Huang, Y., & Li, X. (2019). Characterization of PM 2.5 source profiles from typical biomass burning of maize straw, wood branch, and their processed products (briquette and charcoal) in China. *Atmospheric Environment*, 36-45.

Tiwari, S., Chate, D. M., Bisht, D. S., Srivastava, M. K., & Padmanabhamurty, B. (2012). Rainwater chemistry in the North Western Himalayan Region, India. *Atmospheric Research*, 128-138.

Toyota, K., Dastoor, A. P., & Ryzhkov, A. (2016). Parameterization of gaseous dry deposition in atmospheric chemistry models: Sensitivity to aerodynamic resistance formulations under statically stable conditions. *Atmospheric Environment*, 409-422.

Tunno, B., Longley, I., Somervell, E., Edwards, S., Olivares, G., Gray, S., & Clougherty, J. E. (2019). Separating spatial patterns in pollution attributable to woodsmoke ad other sources, during daytime and nighttime hours, in Christchuch, New Zealand. *Environmental Research*, 228-238.

U.S. Geological Survey Techniques of Water-Resources Investigation. (2006). Collection of Water Samples. In *National Field Manual for the Collection of Water-Quality Data.* Reston, VA: U.S. Geological Survey.

Vallero, D. (2008). *Fundamentals of Air Pollution.* San Diego: Elsevier.

van Leeuwen, E. P., Draaijers, G. P., & Erisman, J. W. (1996). Mapping wet deposition of acidifying components and base cations over Europe using measurements. *Atmospheric Environment*, 2495-2511.

Vazquez, A., Costoya, M., Pena, R. M., Garcia, S., & Herrero, C. (2003). A rainwater quality monitoring network: a preliminary study of the composition of rainwater in Galicia (NW Spain). *Chemosphere*, 375-386.

Vet, R., Artz, R. S., Carou, S., Shaw, M., Ro, C.-U., Aas, W., Baker, A., Bowersox, V. C., Dentener, F., Galy-Lacaux, C., Hou, A., Pienaart, J. J., Gillett, R., Forti, M. C., Gromov, S., Hara, H., Khodzeher, T., Mahowald, N. M., Nickovic, S., Rao, P. S. P., Reid, N. W. (2014). A global assessment of precipitation chemistry and deposition of sulfur, nitrogen, sea salt, base cations, acidity and pH, and phosphorus. *Atmospheric Environment*, 3-100.

Wang, Y.-Q. (2008). *TrajStat Help V1.2.* Maryland: National Oceanic and Atmospheric Administration.

Ward, J. H. (1963). Hierarchical Grouping to Optimize an Objective Function. *Journal of the American Statistical Association*, 239-244.

Watmough, S. A., Eimers, C., & Baker, S. (2016). Impediments to recovery from acid deposition. *Atmospheric Environment*, 15-27.

Wesely, M. L., & Hicks, B. B. (2000). A review of the current status of knowledge on dry deposition. *Atmospheric Environment*, 2261-2282.

Zhao, W., & Hopke, P. K. (2006). Source investigation for ambient PM 2.5 in Indianapolis. *Aerosol Science and Technology*, 898-909.

Zodiatis, G., Lardner, R., Lascaratos, A., Georgiou, G., Korres, G., & Syirimis, M. (2003). High resolution nested model for the Cyprus, NE Levantine Basin, eastern Mediterranean Sea: Implementation and climatological runs. *Annales Geophysicae*, 221-236.

APPENDIX A

CODES, NAMES AND LOCATIONS OF THE EMEP STATIONS

Code	Country	Station name	Latitude	Longitude	Altitude
AM01	Armenia	Amberd	40°23’04”N	044°15’38”E	2080.0m
AT02	Austria	Illmitz	47°46’00”N	016°46’00”E	117.0m
AT03	Austria	Achenkirch	47°33’00”N	011°43’00”E	960.0m
AT04	Austria	St. Koloman	47°39’00”N	013°12’00”E	851.0m
AT05	Austria	Vorhegg	46°40’40”N	012°58’20”E	1020.0m
AT48	Austria	Zoebelboden	47°50’19”N	014°26’29”E	899.0m
BA06	Bosnia Hercegovina	Ivan Sedlo	43°46’00”N	018°02’00”E	970.0m
BE01	Belgium	Offagne	49°52’40”N	005°12’13”E	430.0m
BY04	Belarus	Vysokoe	52°20’00”N	023°26’00”E	163.0m
CH01	Switzerland	Jungfraujoch	46°32’51”N	007°59’06”E	3578.0m
CH02	Switzerland	Payerne	46°48’47”N	006°56’41”E	489.0m
CH03	Switzerland	Tänikon	47°28’47”N	008°54’17”E	539.0m
CH04	Switzerland	Chaumont	47°02’59”N	006°58’46”E	1137.0m
CH05	Switzerland	Rigi	47°04’03”N	008°27’50”E	1031.0m
CZ01	Czech Republic	Svratouch	49°44’00”N	016°03’00”E	737.0m
CZ03	Czech Republic	Kosetice (NOAK)	49°34’24”N	015°04’49”E	535.0m
CZ05	Czech Republic	Churanov	49°04’00”N	013°36’00”E	1118.0m
DE01	Germany	Westerland	54°55’32”N	008°18’35”E	12.0m
DE02	Germany	Waldhof	52°48’08”N	010°45’34”E	74.0m
DE03	Germany	Schauinsland	47°54’53”N	007°54’31”E	1205.0m
DE04	Germany	Deuselbach	49°45’53”N	007°03’07”E	480.0m
DE05	Germany	Brotjacklriegel	48°49’10”N	013°13’09”E	1016.0m
DE06	Germany	Arkona	54°41’00”N	013°26’00”E	42.0m
DE07	Germany	Neuglobsow	53°10’00”N	013°02’00”E	62.0m
DE08	Germany	Schmücke	50°39’00”N	010°46’00”E	937.0m
DE09	Germany	Zingst	54°26’00”N	012°44’00”E	1.0m
DE44	Germany	Melpitz	51°31’49”N	012°56’02”E	86.0m
DK01	Denmark	Færøerne	62°01’48”N	007°04’00”W	210.0m
DK03	Denmark	Tange	56°21’00”N	009°36’00”E	13.0m
DK05	Denmark	Keldsnor	54°44’47”N	010°44’10”E	10.0m

Code	Country	Station name	Latitude	Longitude	Altitude
DK07	Denmark	Færøerne-Akraberg	61°24’00”N	006°40’00”W	90.0m
DK08	Denmark	Anholt	56°43’00”N	011°31’00”E	40.0m
DK12	Denmark	Risoe	55°41’37”N	012°05’09”E	3.0m
DK20	Denmark	Pedersker	55°01’01”N	014°56’45”E	5.0m
DK22	Denmark	Sepstrup Sande	56°04’59”N	009°25’15”E	60.0m
DK31	Denmark	Ulborg	56°17’26”N	008°25’39”E	10.0m
EE02	Estonia	Syrve	57°57’00”N	022°06’00”E	2.0m
EE09	Estonia	Lahemaa	59°30’00”N	025°54’00”E	32.0m
EE11	Estonia	Vilsandi	58°23’00”N	021°49’00”E	6.0m
ES01	Spain	San Pablo de los Montes	39°32’52”N	004°20’55”W	917.0m
ES02	Spain	La Cartuja	37°12’00”N	003°36’00”W	720.0m
ES03	Spain	Roquetas	40°49’14”N	000°29’29”E	44.0m
ES04	Spain	Logroño	42°27’28”N	002°30’11”W	445.0m
ES05	Spain	Noya	42°43’41”N	008°55’25”W	683.0m
ES06	Spain	Mahón	39°52’00”N	004°19’00”E	78.0m
ES07	Spain	Víznar	37°14’00”N	003°32’00”W	1265.0m
ES08	Spain	Niembro	43°26’32”N	004°51’01”W	134.0m
ES09	Spain	Campisabalos	41°16’52”N	003°08’34”W	1360.0m
ES10	Spain	Cabo de Creus	42°19’10”N	003°19’01”E	23.0m
ES11	Spain	Barcarrota	38°28’33”N	006°55’22”W	393.0m
ES12	Spain	Zarra	39°05’10”N	001°06’07”W	885.0m
ES13	Spain	Penausende	41°17’00”N	005°52’00”W	985.0m
ES14	Spain	Els Torms	41°24’00”N	000°43’00”E	470.0m
ES15	Spain	Risco Llamo	39°31’00”N	004°21’00”W	1241.0m
ES16	Spain	O Saviñao	43°13’52”N	007°41’59”W	506.0m
ES17	Spain	Doñana	37°01’50”N	006°19’55”W	5.0m
FI04	Finland	Ähtäri	62°32’00”N	024°13’18”E	162.0m
FI06	Finland	Kökar	59°55’00”N	020°55’00”E	10.0m
FI07	Finland	Virolahti	60°31’00”N	027°41’00”E	8.0m
FI09	Finland	Utö	59°46’45”N	021°22’38”E	7.0m
FI17	Finland	Virolahti II	60°31’36”N	027°41’10”E	4.0m
FI18	Finland	Virolahti III	60°31’48”N	027°40’03”E	4.0m
FI22	Finland	Oulanka	66°19’13”N	029°24’06”E	310.0m
FI36	Finland	Pallas (Matorova)	68°00’00”N	024°14’14”E	340.0m
FR01	France	Vert-le-Petit	48°32’00”N	002°22’00”E	64.0m
FR03	France	La Crouzille	46°08’00”N	001°23’00”E	497.0m
FR05	France	La Hague	49°37’00”N	001°50’00”W	133.0m

Code	Country	Station name	Latitude	Longitude	Altitude
FR06	France	Valduc	47°35’00”N	004°52’00”E	470.0m
FR07	France	Lodeve	43°42’00”N	003°20’00”E	252.0m
FR08	France	Donon	48°30’00”N	007°08’00”E	775.0m
FR09	France	Revin	49°54’00”N	004°38’00”E	390.0m
FR10	France	Morvan	47°16’00”N	004°05’00”E	620.0m
FR11	France	Bonnevaux	46°49’00”N	006°11’00”E	836.0m
FR12	France	Iraty	43°02’00”N	001°05’00”W	1300.0m
FR13	France	Peyrusse Vieille	43°37’00”N	000°11’00”E	200.0m
FR14	France	Montandon	47°18’00”N	006°50’00”E	836.0m
FR15	France	La Tardière	46°39’00”N	000°45’00”W	133.0m
FR16	France	Le Casset	45°00’00”N	006°28’00”E	1750.0m
FR17	France	Montfranc	45°48’00”N	002°04’00”E	810.0m
FR18	France	La Coulonche	48°38’00”N	000°27’00”W	309.0m
GB02	United Kingdom	Eskdalemuir	55°18’47”N	003°12’15”W	243.0m
GB03	United Kingdom	Goonhilly	50°03’00”N	005°11’00”W	108.0m
GB04	United Kingdom	Stoke Ferry	52°34’00”N	000°30’00”E	15.0m
GB05	United Kingdom	Ludlow	52°22’00”N	002°38’00”W	190.0m
GB06	United Kingdom	Lough Navar	54°26’35”N	007°52’12”W	126.0m
GB07	United Kingdom	Barcombe Mills	50°52’00”N	000°01’59”W	8.0m
GB13	United Kingdom	Yarner Wood	50°35’47”N	003°42’47”W	119.0m
GB14	United Kingdom	High Muffles	54°20’04”N	000°48’27”W	267.0m
GB15	United Kingdom	Strath Vaich Dam	57°44’04”N	004°46’28”W	270.0m
GB16	United Kingdom	Glen Dye	56°58’03”N	002°35’20”W	85.0m
GB36	United Kingdom	Harwell	51°34’23”N	001°19’00”W	137.0m
GB48	United Kingdom	Auchencorth Moss	55°47’32”N	003°14’34”W	260.0m
GR01	Greece	Aliartos	38°22’00”N	023°05’00”E	110.0m
HR02	Croatia	Puntijarka	45°54’00”N	015°58’00”E	988.0m
HR04	Croatia	Zavizan	44°49’00”N	014°59’00”E	1594.0m
HU01	Hungary	Kecskemét	46°58’00”N	019°35’00”E	125.0m
HU02	Hungary	K-puszta	46°58’00”N	019°35’00”E	125.0m
IE01	Ireland	Valentia Observatory	51°56’23”N	010°14’40”W	11.0m
IE02	Ireland	Turlough Hill	53°02’12”N	006°24’00”W	420.0m
IE03	Ireland	The Burren	53°00’00”N	009°06’00”W	90.0m
IE04	Ireland	Ridge of Capard	53°07’00”N	007°27’00”W	340.0m
IE05	Ireland	Oak Park	52°52’07”N	006°55’29”W	59.0m
IE06	Ireland	Malin Head	55°22’30”N	007°20’34”W	20.0m
IE07	Ireland	Glenveagh	55°03’07”N	007°56’24”W	44.0m

Code	Country	Station name	Latitude	Longitude	Altitude
IE09	Ireland	Johnstown Castle	52°17’56”N	006°30’39”W	62.0m
IS01	Iceland	Rjupnahed	64°05’00”N	021°51’00”W	120.0m
IS02	Iceland	Irafoss	64°05’00”N	021°01’00”W	66.0m
IS91	Iceland	Storhofdi	63°24’00”N	020°17’00”W	118.0m
IT01	Italy	Montelibretti	42°06’00”N	012°38’00”E	48.0m
IT02	Italy	Stelvio	46°21’00”N	010°23’00”E	1415.0m
IT03	Italy	Vallombrosa	43°44’00”N	011°33’00”E	1000.0m
IT04	Italy	Ispra	45°48’00”N	008°38’00”E	209.0m
IT05	Italy	Arabba	46°31’00”N	011°53’00”E	2030.0m
LT03	Lithuania	Nida	55°21’00”N	021°04’00”E	17.0m
LT15	Lithuania	Preila	55°22’34”N	021°01’50”E	5.0m
LV10	Latvia	Rucava	56°09’43”N	021°10’23”E	18.0m
LV16	Latvia	Zoseni	57°08’07”N	025°54’20”E	188.0m
MD12	Republic Of Moldova	Leova	46°30’00”N	028°16’00”E	156.0m
MD13	Republic Of Moldova	Leova II	46°29’18”N	028°17’01”E	166.0m
ME08	Montenegro	Zabljak	43°09’00”N	019°08’00”E	1450.0m
MK07	Macedonia	Lazaropole	41°32’10”N	020°41’38”E	1332.0m
NL02	The Netherlands	Witteveen	52°49’00”N	006°40’00”E	18.0m
NL05	The Netherlands	Rekken	52°06’00”N	006°43’00”E	25.0m
NL06	The Netherlands	Appelscha	52°57’00”N	006°18’00”E	10.0m
NL07	The Netherlands	Eibergen	52°05’00”N	006°34’00”E	20.0m
NL08	The Netherlands	Bilthoven	52°07’00”N	005°12’00”E	5.0m
NL09	The Netherlands	Kollumerwaard	53°20’02”N	006°16’38”E	1.0m
NL91	The Netherlands	De Zilk	52°18’00”N	004°30’00”E	4.0m
NO01	Norway	Birkenes	58°23’00”N	008°15’00”E	190.0m
NO08	Norway	Skreådalen	58°49’00”N	006°43’00”E	475.0m
NO15	Norway	Tustervatn	65°50’00”N	013°55’00”E	439.0m
NO30	Norway	Jergul	69°27’00”N	024°36’00”E	255.0m
NO35	Norway	Narbuvoll	62°21’00”N	011°40’00”E	768.0m
NO37	Norway	Bjørnøya	74°31’00”N	019°01’00”E	20.0m
NO39	Norway	Kårvatn	62°47’00”N	008°53’00”E	210.0m
NO41	Norway	Osen	61°15’00”N	011°47’00”E	440.0m
NO55	Norway	Karasjok	69°28’00”N	025°13’00”E	333.0m
NO56	Norway	Hurdal	60°22’21”N	011°04’41”E	300.0m
NO99	Norway	Lista	58°06’00”N	006°34’00”E	13.0m
PL01	Poland	Suwalki	54°08’00”N	022°57’00”E	184.0m
PL02	Poland	Jarczew	51°49’00”N	021°59’00”E	180.0m

Code	Country	Station name	Latitude	Longitude	Altitude
PL03	Poland	Sniezka	50°44’00”N	015°44’00”E	1603.0m
PL04	Poland	Leba	54°45’00”N	017°32’00”E	2.0m
PL05	Poland	Diabla Gora	54°09’00”N	022°04’00”E	157.0m
PT01	Portugal	Braganca	41°49’00”N	006°46’00”W	690.0m
PT02	Portugal	Faro	37°01’00”N	007°58’00”W	8.0m
PT03	Portugal	Viana do Castelo	41°42’00”N	008°48’00”W	16.0m
PT04	Portugal	Monte Velho	38°05’00”N	008°48’00”W	43.0m
RO01	Romania	Rarau	47°27’00”N	025°27’00”E	1536.0m
RO02	Romania	Stina de Vale	46°41’00”N	023°32’00”E	1111.0m
RO03	Romania	Semenic	45°07’00”N	025°58’00”E	1432.0m
RO04	Romania	Paring	45°23’00”N	023°28’00”E	1585.0m
RO05	Romania	Fundata	45°28’00”N	025°18’00”E	1371.0m
RO06	Romania	Turia	46°07’00”N	025°59’00”E	1008.0m
RS05	Serbia	Kamenicki vis	43°24’00”N	021°57’00”E	813.0m
RU01	Russia	Janiskoski	68°56’00”N	028°51’00”E	118.0m
RU08	Russia	Lesogorsky	61°00’00”N	028°58’00”E	39.0m
RU13	Russia	Pinega	64°42’00”N	043°24’00”E	28.0m
RU14	Russia	Pushkinskie Gory	57°00’00”N	028°54’00”E	103.0m
RU16	Russia	Shepeljovo	59°58’00”N	029°07’00”E	4.0m
RU18	Russia	Danki	54°54’00”N	037°48’00”E	150.0m
RU20	Russia	Lesnoy	56°31’48”N	032°56’24”E	340.0m
SE01	Sweden	Ekeröd	55°54’00”N	013°43’00”E	140.0m
SE02	Sweden	Rörvik	57°25’00”N	011°56’00”E	10.0m
SE03	Sweden	Velen	58°47’00”N	014°18’00”E	127.0m
SE05	Sweden	Bredkälen	63°51’00”N	015°20’00”E	404.0m
SE08	Sweden	Hoburgen	56°55’00”N	018°09’00”E	58.0m
SE11	Sweden	Vavihill	56°01’00”N	013°09’00”E	175.0m
SE12	Sweden	Aspvreten	58°48’00”N	017°23’00”E	20.0m
SE13	Sweden	Esrange	67°53’00”N	021°04’00”E	475.0m
SE14	Sweden	Råö	57°23’38”N	011°54’50”E	5.0m
SI01	Slovenia	Masun	45°39’00”N	014°22’00”E	1026.0m
SI08	Slovenia	Iskrba	45°34’00”N	014°52’00”E	520.0m
SK02	Slovakia	Chopok	48°56’00”N	019°35’00”E	2008.0m
SK04	Slovakia	Stará Lesná	49°09’00”N	020°17’00”E	808.0m
SK05	Slovakia	Liesek	49°22’00”N	019°41’00”E	892.0m
SK06	Slovakia	Starina	49°03’00”N	022°16’00”E	345.0m
SK07	Slovakia	Topolniky	47°57’36”N	017°51’38”E	113.0m

Code	Country	Station name	Latitude	Longitude	Altitude
TR01	Turkey	Cubuk II	40°30’00”N	033°00’00”E	1169.0m
UA05	Ukraine	Svityaz	51°31’00”N	023°53’00”E	164.0m
UA06	Ukraine	Rava-Russkaya	50°15’00”N	023°38’00”E	249.0m
UA07	Ukraine	Beregovo	48°15’00”N	022°41’00”E	112.0m